



MSc Thesis

A Study of the Thermal Behavior of Pea Protein Isolate for Food Applications

Mona Byberg Michelsen

Supervisor: Heloisa Nunes Bordallo

Co-supervisor: Ourania Gouseti

Submitted: May 19, 2023

Abstract

PEAS are a renewable feedstock and very attractive as a source of protein due to their wide availability, low cost, high digestibility etc. Pea protein provides an alternative to meat and dairy based protein sources which are less effective to produce, and importantly worse for the environment. Even so, the properties of pea proteins are still poorly understood. The thermal properties of a protein are amongst the most important for food applications, as thermal treatments, like cooking and pasteurization, are exceptionally common. In this work, we investigate the thermal properties and morphology of dry pea protein isolates (PPI). We use multi-modal thermal analysis to study moisture loss, denaturation, and degradation when heating the protein. Optical microscopy and X-ray scattering are employed in conjunction with thermal analysis to determine sample morphology and crystallinity. By performing all measurements on three different samples of the same pea protein isolate and duplicating each measurement we have demonstrated good repeatability of our results. A survey of pea proteins from three different manufacturers found moisture contents ranging from 3.58 % to 4.22 % when evaluated at 150 °C, and denaturation temperatures ranging from 124.7 °C to 133.1 °C. We have thereby demonstrated that the thermal properties of a PPI depend on its source. Thermal analysis of PPIs treated with a reducing agent (DTT) showed that increasing the concentration of DTT had a clear negative effect on the thermal stability of the samples, with at least some of this being attributed to the presence of DTT itself in the samples. By tracking the samples over the course of 20 days, we found that the samples evolved in a non-linear fashion over time. The process of freeze-drying the samples after reduction treatments was shown to contribute to the instability of samples over time.

Acknowledgements

This project would not have been possible without my two supervisors, Heloisa Nunes Bordallo and Ourania Gouseti. Their combined passion for pea proteins and thermal analysis is what started this project, and I am sure that they will continue it in the years to come. They have been patient and accommodating through each step of this project. Their involvement has truly made this a multi-disciplinary project, and that is all a young nano scientist can ask for. Thank you for allowing me to draw on your individual strengths.

I also want to thank my group members for bearing with me when I complain about the lab instruments, and for always being encouraging and keeping me going. A special thank you to Hery Mitsutake for always doing her best to answer my many questions, and for being accommodating and helpful in the lab, even when she was drowning in work herself.

Lastly, I want to thank my family for allowing me to ramble on about this project, before proceeding to talk sense into my head. You always know what I need to hear.

Contents

Abstract	ii
Acknowledgements	iii
1 Introduction	1
2 Pea protein functionality, production, and constituents	6
2.1 Peas as a plant-based protein source	6
2.2 Pea protein isolate and its constituents	7
2.3 Pea protein fractions	9
3 Experimental Methods	11
3.1 Differential scanning calorimetry	11
3.2 Thermogravimetric analysis with evolved gas analysis	12
3.3 Imaging	16
3.4 X-ray powder diffraction	17
3.5 Measurements and materials	18
4 Survey of sample heterogeneity and data reproducibility	23
4.1 Results	23
4.2 Discussion	31
5 Comparing different PPIs	33
5.1 Results	33
5.2 Discussion	38
6 PPI reduced with DTT	41
6.1 Results	42
6.2 Discussion	49
7 Conclusions	52
7.1 Future Perspectives	53
Bibliography	55
Appendix A: Microscopy, samples S1-S3	63

Appendix B: Mass Spectroscopy, samples SA-SC	66
Appendix C: Raman data, samples S1-S3	67
Appendix D: FTIR, treated samples	68
Appendix E: TGA of treated samples, all days	72
Appendix E: DSC of treated samples, all days	76
Appendix G: TGA-FTIR-MS of SA, 28-255 °C	78

1 Introduction

This project aims to further our understanding of the structure and thermal behavior of pea protein isolate. Pea (*pisum sativum*) proteins, along with other legume proteins, have a wide array of applications. These include material applications like bio-based plastics and bio-polymer films,^{1,2} as well as food applications like plant-based dairy and meat alternatives.^{3,4} With the temperature of our planet rising, it is critical that we work to reduce our production of greenhouse gasses and consumption of fossil fuels. In this regard, pea-based protein products are very attractive alternatives to animal proteins which have a higher environmental impact, as the legume is a renewable feedstock which is grown in most countries and easily harvested.⁵ Furthermore, it is inexpensive, hypoallergenic, highly nutritional, and rich in most essential amino acids. Despite the many benefits of pea proteins, not much is known about their thermal properties. This is especially important considering that heat treatments, like baking, pasteurization, or sterilization, are amongst the most common treatments of food products. By improving our knowledge of the thermal properties of pea protein, we can better design the pea-based food products of the future to have desirable properties in the store, the kitchen and at the dinner table.

Peas are a legume, meaning that they belong to the *Fabaceae* family which also includes lentils, chickpeas, and soybeans just to name a few. Compared to other plants, legumes have a high protein content. The pea contains around 25% protein, with some species and varieties being richer in protein than others.^{6,7} For comparison, most meats contain around 17-22 g protein per 100 g and chicken eggs around 12.5 g per 100 g.⁸ Other constituents of peas include starch, dietary fiber, and small amounts of fat. For this study, we focus in on pea protein isolates (PPI). These are peas which have undergone a series of processing steps including milling, chemical treatment, and physical separation to reach a protein concentration of around 80 %. Only few studies on the thermal properties of pea proteins exist. A 2018 study by Ricci et al.¹ compared the thermal properties of pea protein concentrates with purity degrees of 30-80 %. They showed a clear correlation between improved thermal stability and higher purity degrees. Proteins with purities above 60 % could be denatured without undergoing thermal degradation, making them more useful for various aggregation and polymerization purposes. In 2022, Rui Liu did a study on the thermal properties of pea protein isolates.⁹ Two samples, which were collected at different times but otherwise assumed to be identical, were studied. These samples were found to have very different properties. These properties include, but are not limited to, morphology, thermal denaturation, moisture contents, and thermal degradation. The results of these two studies raise the need for an in depth investigation of pea protein samples with high purity, where reproducibility of the data is ensured.

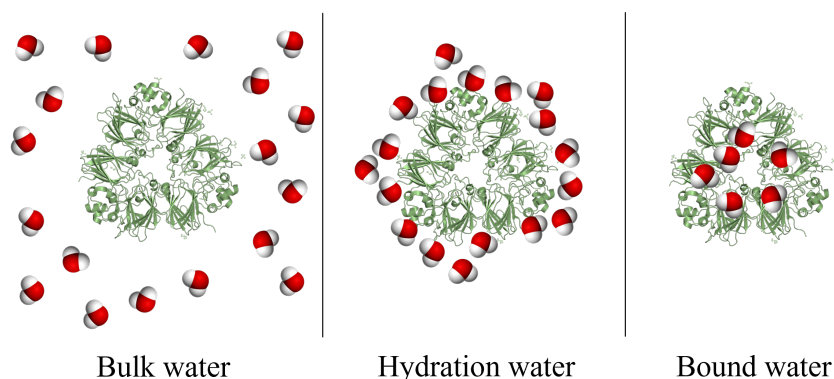


Figure 1: Representation of the three types of interactions between water and proteins: bulk water (no interaction), hydration water (surface interactions), and bound water (strong intermolecular interactions like hydrogen bonds).

A central molecule which can influence the thermal properties of proteins is water. Water is a small polar molecule, with a volume of 17.7 \AA^3 and a great ability to form hydrogen bonds.¹⁰ Hydrogen bonds occur when two electronegative atoms such as oxygen both compete to bind to the same hydrogen atom. The hydrogen atom formally remains covalently bound to one competitor, but interacts strongly with the other as well. The hydrogen bond is a strong non-covalent bond, and it plays an important role in forming and stabilizing the secondary, tertiary, and quaternary protein structure. Therefore, water molecules are often found within the protein structure as bound water.¹¹ Water can also be present in proteins as hydration water, which interacts with the surface of the proteins and help solubilize them, and bulk water which is found at a distance greater than the van der Waals interaction of the protein-water interface and is therefore free to move.¹² This is illustrated in Figure 1.

Water also plays an important role as a plasticizer. Plasticizers change the properties of a material by shielding inter- and intra-molecular interactions and reducing friction to facilitate translational movement.¹³ This creates a material which is more flexible and less brittle. In certain materials, such a change in mechanical properties can also be induced by heat. This is called thermal plasticization. The transition itself is called the glass transition, and the glass transition temperature, T_g , then describes the temperature at which the material switches between a glass-like and a rubbery state. The plasticizing effect of water can decrease the T_g with as much as 100K.¹⁴ This is of great importance, as it has been shown that whether a food is stored at temperature above or below the glass transition temperature, greatly affects its stability and shelf-life.^{14,15} Adding larger amounts of water can also lead to protein aggregation. Aggregation is one of the two steps

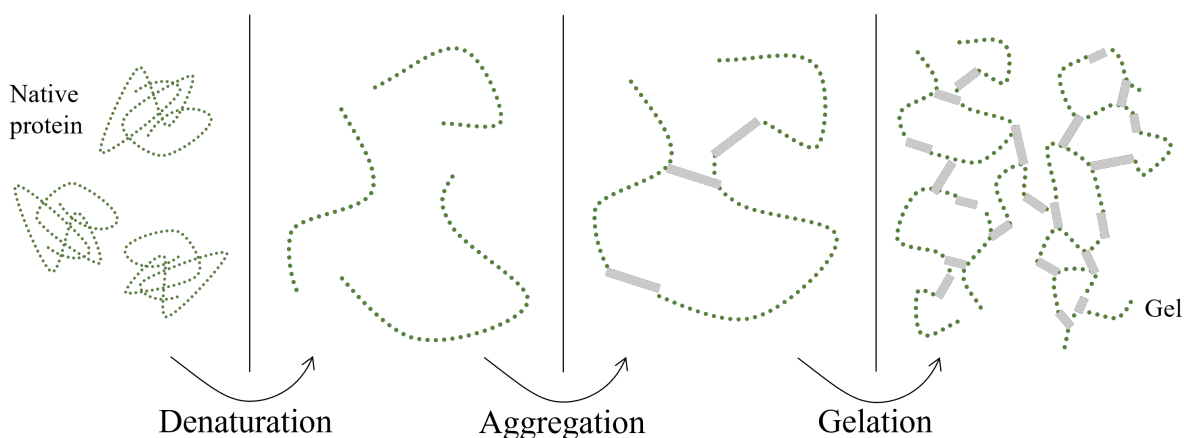


Figure 2: Representation of the processes leading to protein gelation. The proteins are unfolded through the denaturation process, which is often induced by heat. The unfolded proteins undergo aggregation by forming cross-linking inter-molecular bonds. In the last step, the individual aggregates link together to form the protein matrix that makes up the gel. Gelation can be induced by slowly cooling the proteins.

in gelation, the other being denaturation. Gelation is often described as one of the most important protein interactions for food applications, as it is used to control texture.^{14,16,17}

Pea proteins have in recent years been investigated as additives in food products. A study of sponge cakes made with wheat flour fortified with different concentrations of PPI showed that increasing PPI contents increased the crumb density and reduced air incorporation, but also increased the stability of the batter.¹⁸ Another study found that incorporating pea proteins in gluten- and egg-free pasta helps to improve the texture and hardness of the pasta.¹⁹ Other applications of pea proteins as a fortifying ingredient include beef patties, protein shakes, chicken nuggets and extruded snacks and cereals.³

From a food perspective, some of the most interesting characteristics of the protein are texture, color, taste, and gelling and emulsifying properties. Each can be affected in various ways through chemical or physical treatments during and after protein isolation. As an example, the Pisane™ C9* pea protein isolate used herein is extracted in aqueous solution with a fermentation step which beneficially affects properties like color, viscosity, mineral content, and sugar content of the final product.²⁰

The emulsification properties of pea proteins have been widely studied. Proteins can help stabilize oil droplets in aqueous environments due to their amphipathic nature. Pea proteins have been found to perform well compared to soy proteins which are widely applied as emulsifiers.²¹ Gelling and emulsifying properties can be altered through various

chemical, physical, and biological modifications. Varying the pH has been shown to have great impacts on the emulsifying properties of pea protein isolates, with the best performance at pH 3 and the worst performance close to the isoelectric point of the proteins at pH 5.²² Furthermore, heat treatment of pea proteins at 95 °C for 30 min has been shown to positively affect several factors important for emulsification.²³ The gelling properties of pea proteins have also been studied, e.g. for applications in fermented plant-based cheese where an optimal pea protein matrix with good gel hardness was obtained for gels produced with 10 % protein content and 10 % olive oil levels.²⁴

A possible chemical modification of pea proteins is the addition of a chemical reducing agent. Reducing agents like dithiothreitol (DTT) can be employed to break the disulfide bridges in proteins. This can have great effects on the functional properties of a protein. The addition of 10 mM DTT to a 15 % w/v whey protein concentrate solution has been shown to greatly increase the hardness of heat-induced whey protein gels.²⁵ Reduction (50 mM DTT) of soy proteins has been found to greatly impact extrusion, but not heat-induced gelation.²⁶ In red bean, red kidney bean and mung beans, DTT (20 mM) has been shown to weaken gel formation while not affecting thermal denaturation.²⁷ Reduction of pea protein isolates has only been studied to a very limited extent, and the thermal properties of reduced PPI are mostly unknown. In this project, we will therefore take a closer look at reduced PPI with different concentrations of DTT using thermal analysis.

To understand the thermal properties of pea protein isolates before and after reduction with DTT, we employ multi-modal thermal analysis (TA). TA is a powerful tool to study important processes like denaturation, dissociation, and aggregation, as well as how each of these are affected by heat treatment and moisture content. Here, we use a combination of thermogravimetric analysis (TGA) coupled with evolved gas analysis (Infrared spectroscopy and mass spectrometry), and differential scanning calorimetry (DSC) to deepen our understanding of the thermal properties of pea protein. TGA can be used to study moisture content and the release of water and other species during thermal degradation. By coupling to infrared spectroscopy and mass spectrometry, we gain insights into the nature of the mass loss observed through TGA, allowing us to determine the underlying thermal process. DSC is very useful for studying thermal denaturation of the proteins, as well as glass transitions and any other phase transitions which might occur. We also use X-ray powder diffraction (XRPD) to determine the crystallinity of the samples, and optical microscopy (OM) and to study the morphology of the proteins.

This work will begin in Chapter 2 by going into further detail about pea proteins and their isolates, applications, composition, and more. In Chapter 3, we will go over the

experimental methods. Here, we will also describe the samples and specific experimental settings in detail. Chapter 4 presents a data reproducibility survey of the PPIs, in which the degree of heterogeneity within the samples are determined. This will also serve as a general introduction to the thermal properties of PPIs. In Chapter 5, we compare PPIs from three different manufacturers to determine whether the thermal properties of all PPIs are the same. Chapter 6 is dedicated to studying the effects of the reducing agent DTT on PPIs, while also determining the stability of the treated samples over time by performing thermal analysis periodically over the course of 20 days. Finally, conclusions and perspectives to further work are presented in Chapter 7.

2 Pea protein functionality, production, and constituents

2.1 Peas as a plant-based protein source

There are many great ethical, environmental, and health reasons why humans should eat more protein from plant sources. Animal protein sources are more water-intensive, require more land area, inhibit biodiversity, and create more greenhouse gasses and pollution than plant protein sources. Animal products are therefore inefficient as a food source, and unsustainable for both the planet and the growing human population.²⁸ This is also reflected in both corporate and consumer trends. Plant-based protein is a growing business, and investments in plant-based companies has increased from 23 million USD in 2010 to 2100 million USD in 2020.²⁸ This is a more than 9000 % increase over a ten year period. Amongst consumers, dairy alternatives are the most popular plant-based food category, with plant-based milks taking up 16 % of the total category sales in 2021.²⁹

From a health-perspective, switching to plant-based proteins has both benefits and drawbacks. A plant-based diet is not inherently healthier than an omnivore diet. Instead, the variety and quality of the foods consumed is what defines the diet as healthy or unhealthy. When choosing a protein source, there are a variety of nutritional factors to consider, namely:³⁰

- **Amino acid (AA) profile.** Animal protein sources generally have a complete amino acid profile, meaning that they contain adequate amounts of all of the nine essential amino acids (EAA). These are AAs which humans cannot synthesize themselves and therefore need to consume through their diet. Plant protein sources generally do not have a complete AA profile. For instance, legumes have relatively low levels of sulfur-containing EAAs. However, cereals have good amounts of these AAs, but are low in the EAA lysine which legumes are rich in. Therefore, a complete AA profile is easily achievable by consuming more than a single plant-based protein.
- **Digestibility.** Before humans can benefit from the nutritional properties of the consumed protein, the protein chains need to be broken down into single amino acids or di- and tripeptides which can be absorbed in the bloodstream. This process is called digestion of proteins. Animal protein sources are generally completely digestible, but plant-based protein sources are not. There can be many different factors limiting digestibility, including the molecular structure of the protein, the

aggregation state, or anti-nutritional factors which inhibit the digestion process in various ways.

- **Protein quality.** The concept of protein quality is a summary of the AA profile and the digestibility of the protein. It considers the amount of each EAA which ends up in the blood stream after digestion. A common way to quantify protein quality is the DIAAS (Digestible Indispensable Amino Acid Score). The DIAAS is calculated for each EAA based on the amount (in mg) of the AA which is absorbed to the blood stream in the small intestine per gram of ingested protein, compared with an ideal reference protein. An overall score is given to the protein source based on the limiting AA, meaning the EAA with the lowest DIAAS. The score therefore gives a measure of how much of the protein source one would need to consume adequate amount of all EAAs. It is important to note that most humans consume protein from varied sources. If protein is consumed from sources with different limiting EAAs, less total protein is needed to consume enough EAAs.

Peas, like most legumes, have a near complete AA profile, with the exception of the sulfur-containing EAAs methionine and cysteine which are present in smaller amounts. As previously discussed, the AA profile of peas is well complemented by that of cereals like rice and wheat, as each contain the EAAs that the other lacks. Peas have a DIAAS of 66 % which is typical of legumes (the exception being soybeans with a score of 92 %).³⁰ Selected DIAAS values of legumes, cereals, and animal proteins can be found in Table 1. The quality score of pea protein is limited mostly by its digestibility. Peas contain different anti-nutritional factors which inhibit digestion. In contrast, most animal protein sources have DIAAS scores around or above 100 % with complete digestibility. The good news is that most of the anti-nutritional factors in legumes can be inactivated or destroyed through processing like extrusion or cooking. Pea protein isolates, like those investigated here, can therefore reach a digestibility of around 98 %, greatly improving the protein quality.³¹ From a nutrition perspective, peas therefore have the potential to be a very well rounded plant-based protein source.

2.2 Pea protein isolate and its constituents

Pea protein isolate is made from yellow field peas, and contain a higher concentration of protein than the native pea. To achieve a higher protein concentration, other components like fats and carbohydrates need to be removed. This can be done under either dry or wet conditions, yielding pea protein concentrates and isolates respectively. Pea protein concentrates are obtained through a combination of dry milling and air classification. After milling, the pea flour contains granules of starch which are 2-40 μm in diameter, and thereby larger than the 1-3 μm proteins. The pea flour can then be separated into

Table 1: Comparison of digestible indispensable amino acid scores (DIAAS) of selected legumes, cereals, and animal proteins with the limiting amino acid(s) given. Table adapted from McClements and Grossmann.³⁰

Protein source	DIAAS in %	Limiting amino acid(s)
<i>Legumes</i>		
Soy	92	Methionine + Cysteine
Pea	66	Methionine + Cysteine
Chickpea	69	Methionine + Cysteine
<i>Cereals</i>		
Rice	52	Lysine
Wheat	39	Lysine
<i>Animal protein</i>		
Beef	112	None
Egg	101	None
Whey	85	Histidine

a coarse starch-rich component and a fine protein-rich component (40-60 % protein).³² This process is energy-efficient and does not disrupt protein functionality, but is not as effective in isolating the pea proteins as wet processing.³³

PPIs are achieved by dissolving the pea flour in water and going through a series of different separation processes and chemical treatments. An example of wet processing with separation under acidic conditions is outlined in Figure 3, but alkaline separation is also very common. The procedure can be modified in many different ways, for example by adding hydrolyzing enzymes to the solution, including a fermentation step, or by employing ultrasound or microwaves to rupture the plant cell wall.³⁴ Each step of the protein isolation process has the possibility to affect smell, taste, and texture, as well as gelling, foaming and emulsifying properties in desirable or undesirable ways. Plant protein extraction is an active area of research, as new methods are needed to isolate proteins in a more effective and environmentally friendly way without negatively affecting protein functionality and properties.³⁵ The challenge lies in designing a protein product which has great taste and textural properties while optimizing its nutritional value.

Pea protein concentrates have purity degrees of up to 60%, whereas isolates can reach a purity of 95%.^{1,36} Here, we have chosen to work with a pea protein isolate (PPI) as this allows us more direct access to pea proteins. Even though PPIs contain 80-95 % protein, the remaining 5-20% is still made up of starch, fiber, fat and water. The samples are therefore complex as they contain various different components in unknown amounts.

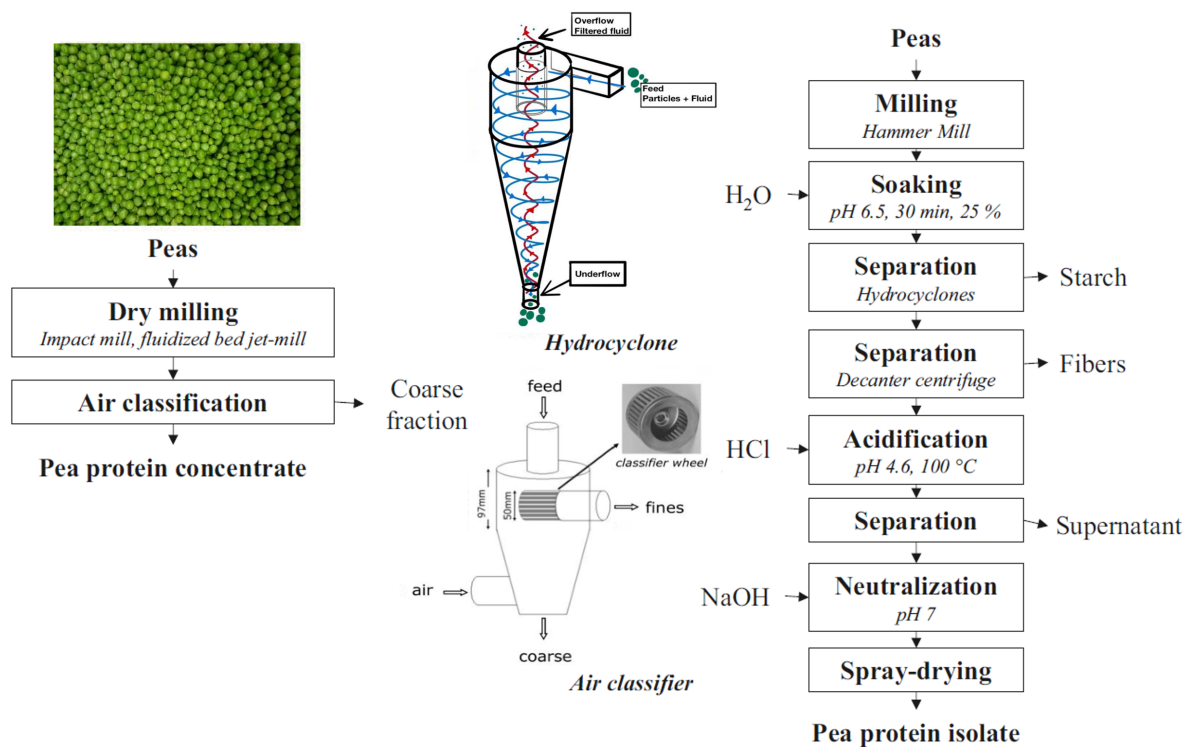


Figure 3: Schematic describing the steps involved in dry and wet processing of peas to obtain pea protein concentrate and isolate respectively. Examples of methods which can be used to perform these processing steps are also given. Figure adapted from McClements et al. 2022.³²

Moreover, the protein fraction is made up of an array of different types of proteins, each with distinct thermal properties.

2.3 Pea protein fractions

Peas contain many different types of protein, each with a specific purpose and function. Pea proteins are divided into four classes based on solubility, with the two main classes being globulins and albumins. Globulins are salt-soluble storage proteins, and albumins are water-soluble metabolic and enzymatic proteins. Both are globular proteins, meaning that they have a fixed sphere-like tertiary structure with limited flexibility.

Globulins represent the largest fraction of protein in peas, and can be subdivided into legumin, vicilin, and convicilin based on the sedimentation coefficients, S (Svedberg unit). The relative abundance of these proteins can vary with pea type and growing conditions, and especially the legumin/vicilin ratio is sensitive to these external factors, as well as the protein isolation method.⁶ The role of globulins is to store nutrients which can be

released during germination to facilitate plant growth.³⁷ Other classes of pea proteins include prolamins and gluteins. These are both storage proteins. An overview of the different protein fractions in peas can be found in Table 2.

Globulins not only represent the largest fraction of pea proteins, they are also the largest in molecular size. Legumin, the largest of the proteins, is a hexameric protein, meaning that it is comprised of six subunits: three so-called α -chains and three β -chains. The subunits are bound together with disulfide bridges, an S-S bond which form between cysteine residues.³⁸ Cysteine is a sulfur-containing amino acid. Pea proteins contain very few sulfur-containing amino acids, and therefore the disulfide bridges are few, but important for the protein structure and thereby functionality. If the disulfide bridges are broken, the protein will fall apart into its individual subunits.

Table 2: Overview of pea protein fractions divided into classes based on solubility and sedimentation coefficients (Svedberg unit). Table adapted from Lu et al.³⁷

Class	Content	Solubility	Protein	Svedberg unit	Molecular weight
Globulin	50-60%	Salt solution	Legumin	11S	320-410 kDa
			Vicilin	7S	150 kDa
			Convicilin	8S	180-210 kDa
Albumin	18-25%	Water solution	Albumin	2S	68.5 kDa
Prolamin	4-5%	Alcohol solution	Prolamin	n/a	n/a
Glutein	3-4%	Insoluble	Glutein	n/a	n/a

3 Experimental Methods

3.1 Differential scanning calorimetry

Differential scanning calorimetry (DSC) is a thermal analysis method. Here, we heat the sample while monitoring heat flow in and out of the sample. This allows us to track any endothermic or exothermic reaction/transition in the sample. This could for example be a chemical reaction, a crystal restructuring, or any phase transition. The heat flow is measured by placing the sample in a crucible. The sample crucible is measured relative to a reference crucible without the sample. The temperature of both crucibles is then increased, decreased, or held stable according to a set program, and the difference in temperature between the sample and the reference is measured. Each measurement is calibrated using an empty crucible, as this allows us to remove possible features caused by the crucible. The difference in temperature can then be converted to a heat flow. The heat flow describes the rate at which energy is removed from or added to the sample by endo-/exothermic reactions. If an endothermic reaction is occurring, like the evaporation of water, the sample will be colder than the reference, corresponding to an increased heat flow into the sample. Some phase transitions, like the glass transition, will cause a change in the heat capacity of the sample, and appear in the data as a step-like feature. Examples of what a glass transition, and endo- and exothermic peaks can look like can be found in Figure 4.

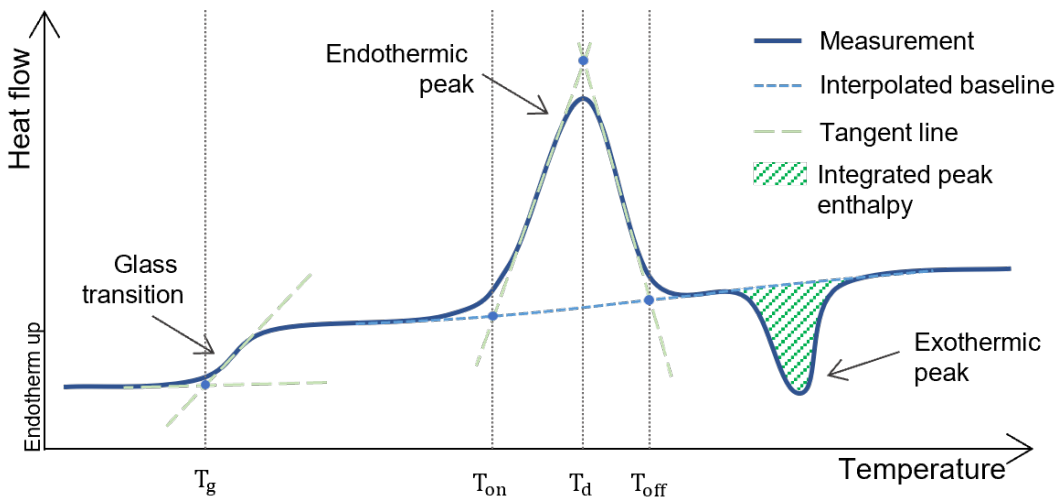


Figure 4: Example of what data treatment of a DSC curve with a glass transition and endo- and exothermic peaks could look like.

From the DSC curves, one can extract the on- and offset temperatures, T_{on} and T_{off} , of a transition by calculating the intersection of tangent lines with the base line. This method can also be used to extract the glass transition temperature, T_g . When a heat flow peak corresponds to protein denaturation, the maximum of that peak is named the denaturation temperature, T_d . The baseline of the measurement can be defined in different ways. When there is a clear difference in the heat capacity of the sample before and after the transition, a sigmoidal baseline is often used. Otherwise, a linear baseline is commonly used. The peak enthalpy, ΔH , can be extracted as the area between the peak and the baseline.

DSC is a technique which is fast and easy to perform. There are however some requirements for the samples. They must be able to fit in the small crucible, and they must maintain a good contact with the bottom of the crucible where the temperature is monitored. This means that this technique can mainly be used for liquid, pastes/gels and fine powders. The aluminium crucibles used for DSC measurements are hermetically sealed using either a solid lid or a punched lid which has a tiny hole to allow gasses to escape. It is important to consider which lid to use. If gasses, like water vapor, are evolved during the experiment, a great pressure can build up in the crucible. If the pressure becomes too great, the lid can violently pop off, putting the instrument at risk. However, some samples, like proteins, are particularly sensitive to moisture and allowing it to escape the crucible makes it impossible to study the effects of water.

The DSC heat flow is directly proportional to the heating rate, which means that some small or obscured signals can only be detected at a greater heating rate. However, a fast heating rate will also lead to broader data peaks. It is therefore important to carefully consider the heating rate to best suit the sample. Figure 5 shows the effects of heating rate, heat of transition, and thermal conductance on the DSC signal.

3.2 Thermogravimetric analysis with evolved gas analysis

Thermogravimetric analysis or TGA is, as the name suggests, a method where a sample's mass is monitored as the temperature is varied or held constant. The sample is placed in an open crucible on a very precise scale. The scale along with the sample is then lowered into a furnace where the temperature can be controlled. The furnace is then heated at a set heating rate until the desired temperature. The resulting plot of sample weight (after the crucible mass is subtracted) as a function of time or furnace temperature will reveal the points at which the sample gains or loses mass due to thermally induced processes. As an example, the presence of water in a sample will manifest as an increasing mass loss as we heat towards its boiling point. The shape of the TGA curve is determined by

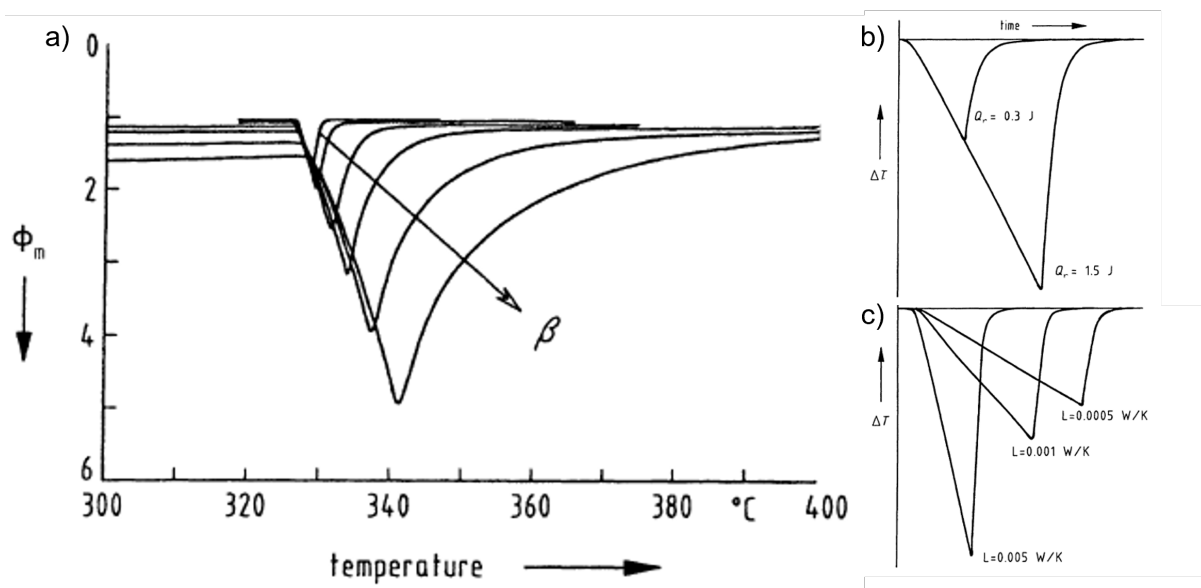


Figure 5: a) Measured heat flow vs temperature of lead, showing the effect of increasing the heating rate β from 5 to 50 K/min. The heating rate affects both the size, width, and position of the peak. Simulated data showing the effects of b) heat of transition Q_r , and c) thermal conductance L of the sample on temperature difference between sample and reference as a function of time.³⁹

many factors, including:

- Heating rate.** As with DSC, the heating rate will affect the shape of the observed features. When increasing the heating rate, the mass loss steps of the TGA curve will shift towards higher temperatures, but the amount of mass lost at each step will remain the same. This is illustrated in Figure 6 with calcium oxalate which has three well defined mass loss steps, and is therefore often used for instrument calibration. In this study, all TGA measurements have been carried out using a heating rate of 10 K/min. This heating rate offers a good compromise between the sharpness of the mass loss steps and data acquisition time. It is also commonly used in literature, which allows for more direct comparison with previously reported TGA curves of similar systems.
- Thermal conductance.** The thermal conductance of the sample will also influence the mass loss steps. If a sample has a high thermal conductance, the sample will quickly adjust to the temperature of the furnace. If the sample has a low thermal conductance, the temperature of the sample will be slower to adjust to that of the furnace. This is called 'thermal lag'. Further, the outer parts of the sample which are in contact with the crucible might be higher in temperature than the middle of the sample, as it will take time for the

thermal energy to propagate through the sample. Inhomogeneities of the sample can also lead to uneven heating of the sample. Each of these effects will be especially pronounced when applying a high heating rate. The thermal conductance of the sample should therefore be considered when choosing the heating rate. A rate of 10 K/min is fine for the powder samples studied herein.

Lastly, there are two very important experimental considerations to make before performing a measurement, namely the temperature range and sample amount. It might be tempting to fill the sample crucible to the brim and heat it as high as the instrument goes. However, many samples will rapidly expand, combust, or both when heated beyond a certain point. This can cause pollution of the instrument, which could then in turn compromise future measurements. It is therefore wise to be conservative with both sample amounts and the temperature range, while still ensuring that there is enough sample to have good data quality and a great enough temperature range to observe the phenomena of interest.

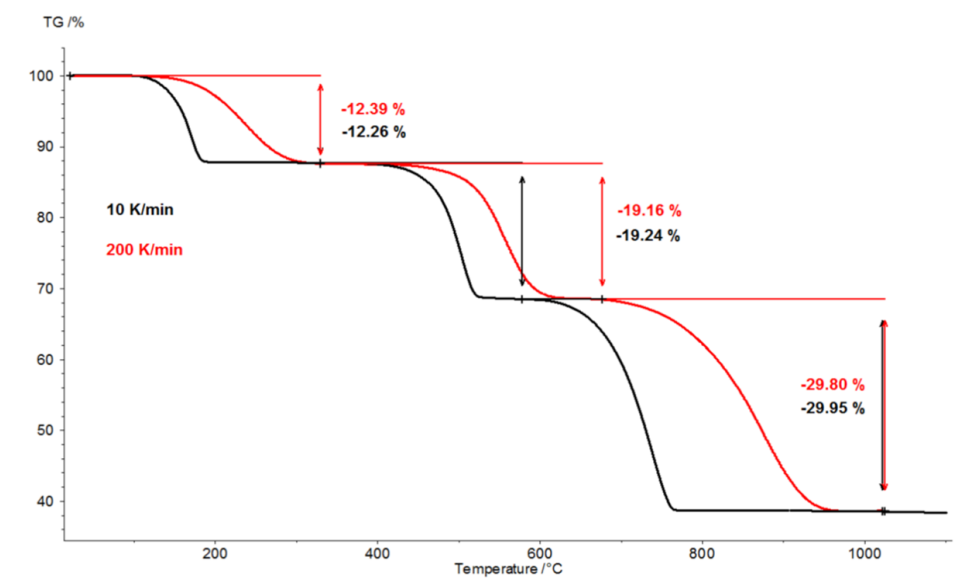


Figure 6: TGA measurements of calcium oxalate monohydrate at two different heating rates. The black curve is measured at 10 K/min, and the red curve at 200 K/min. We see how mass loss shifts towards higher temperatures when increasing the heating rate. Figure adapted from Füglein et al.⁴⁰

Evolved gas analysis with Mass Spectrometry and Infrared Spectroscopy

TGA is a very useful technique, as it requires no special preparation of samples, and is quick to measure. One of its limitations is that it does not tell us the reason for the mass

loss, only that it occurs. It can therefore be very beneficial to combine this method with evolved gas analysis (EGA). This way, we not only observe the mass loss, but we simultaneously measure the gasses evolved from the sample to determine their constituents. For the EGA performed in this project, we used a combination of mass spectrometry (MS) and Fourier transform infrared spectroscopy (FTIR).

From MS we learn the mass/charge relationship of each of the species in the gas, and their relative abundance. We therefore know the size of the molecules present in the gas, significantly limiting the number of possible species. Identification of the species is sometimes possible through comparison of the observed masses with a database like the one available from NIST.⁴¹ From FTIR we get a fingerprint of the gas. Infrared spectroscopy measures the energies absorbed by vibrations in the molecules, as illustrated in Figure 8. These vibrations are influenced both by the types of atoms in the molecule and each atoms surroundings. This allows us to determine precisely which species are present in the evolved gas. MS and FTIR compliment each other well, as MS gives us an idea of which species could be relevant so we do not need to look through millions of IR spectra to find a match. Also, some species are not IR-active, and can therefore only be detected by the very sensitive MS.

A relevant example of how the two methods compliment each other, is when both water and ammonia are present in the evolved gas. The two molecules have similar molecular weights, ~ 17 g/mol for ammonia and ~ 18 g/mol for water. They will therefore also show up at similar m/z values in the MS. The relative intensities of the MS signals for each of the two species can be seen in Figure 7. Here, we observe that the strongest signal for ammonia is at $m/z = 17$ as one would expect, but ammonia will also be detected clearly at $m/z = 16$ and slightly at $m/z = 14, 15,$ and 18 . Water shows up at $m/z = 18$, but also at $m/z = 17, 16, 19$ and 20 . When both species are present in the gas, the most intense signals from water will therefore contain signal from ammonia and vice versa. The common way of separating the two signals is to look at the ratios of the MS signals. If only water is present in the gas, the ratio of the signal at $m/z = 18$ to that at 17 will remain constant at around 100:21. If ammonia is then added to the gas, the signal at $m/z = 17$ will increase more than that at $m/z = 18$, and this ratio will therefore shift. However, when only a small amount of ammonia is introduced, this change in ratio can be difficult to detect, as we will later see. In this case, one cannot conclude whether ammonia is present in the evolved gas from the MS data alone. Luckily, ammonia is a very IR active molecule, which means that its vibrations at 960 cm^{-1} and 940 cm^{-1} will be visible even at low concentrations. FTIR analysis will therefore be able to tell us the temperatures at which ammonia is evolved, but not the amounts. MS analysis will reveal

whether the relative abundance of ammonia to water is small (undetectable through ratio analysis) or substantial (quantifiable through ratio analysis).

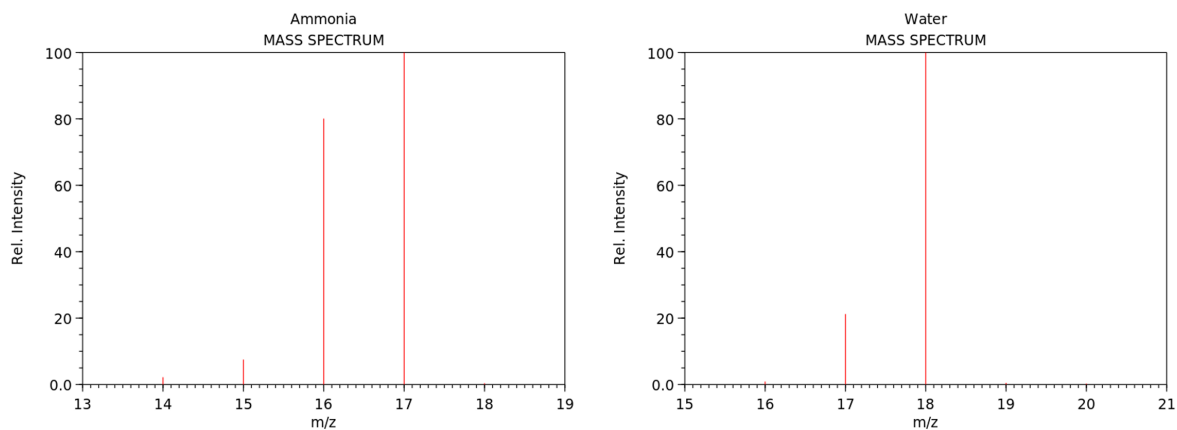


Figure 7: Mass spectra of water and ammonia gasses. Spectra reproduced from the NIST Chemistry WebBook.⁴¹

3.3 Imaging

Optical microscopy is a technique that allows us to directly observe the morphology of a sample. This was done using a inVia™ confocal Raman microscope. Confocal microscopes use different lenses to focus the light beam to a point, and thereby allow for great spatial resolution in all three dimensions. Furthermore, this particular microscope also has the capacity for Raman imaging.

Raman imaging relies on the Raman scattering process where a photon scatters off a molecule. As depicted in Figure 8, an electron in the molecule is temporarily excited to a virtual state before returning to the ground state. If the electron returns to a different vibrational mode, the energy of the scattered photon will change to conserve total energy. This energy shift, and therefore the energy of the vibrational modes, can be measured. Analogously to IR spectroscopy which also measures vibrational energies, Raman can be used for chemical fingerprinting. A great advantage of Raman scattering is that it can be incorporated in optical microscope since the relevant photon energies fall mostly within the visible light spectrum. However, this can also be a disadvantage as the Raman scattering process competes with fluorescence. If the sample fluoresces, this will create a background signal that can mask the weak Raman signal.

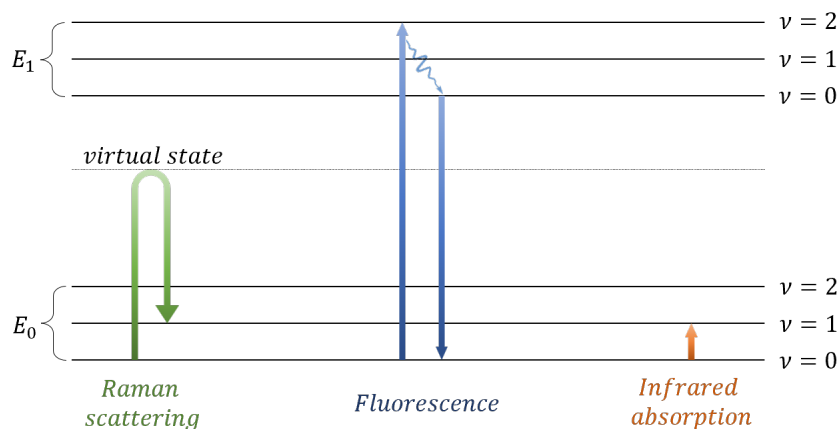


Figure 8: Representation of the concepts of Raman scattering, fluorescence, and infrared absorption. Raman and IR both give information on vibrational states, but using very different excitation energies. Raman and fluorescence have similar excitation energies, and are therefore competing phenomena.

3.4 X-ray powder diffraction

X-ray powder diffraction (XRPD) is a widely applied technique in the material sciences. It is mainly used to study crystalline material powders, and gives information on the degree of crystallinity, characteristic distances, constituent atoms, and particle size. In highly ordered crystals, XRPD can be used to solve the exact crystal structure, including the occurrence of different defects. XRPD is one of several techniques that rely on the concept of X-ray scattering. An incoming beam of X-rays is scattered from the atoms in the sample through interactions with the electrons. As the rays scatter, they create interference patterns due to their wave-like nature. These interference patterns, also known as the diffraction patterns, have positive interference at certain scattering angles. The angles then correspond to characteristic distances in the sample, like bond lengths or the distance between lattice planes. The scattering angle, usually denoted as 2Θ , is related to these distances, d , through Bragg's law:

$$n\lambda = 2d \cdot \sin(\Theta) \quad (1)$$

where n is the diffraction order ($n = 1, 2, 3, \dots$) and λ is the wavelength of the X-ray. The appearance of the wavelength, and thereby the energy, of the radiation in Bragg's law means, that the energy of the photon ray dictates the range of distances we can study. The energy of X-rays allows us to study distances on the Å (10^{-10} m) length scale, which is perfect for information about inter-atomic to inter-molecular distances. In a highly ordered sample, the diffraction pattern will display sharp peaks known as Bragg reflections

due to the characteristic distances present in the sample. In contrast, a disordered sample will not have characteristic distances to the same degree, and the diffraction pattern will show scattering at all angles, maybe with a few broad features.

In partially ordered samples, the degree of crystallinity can be determined by comparing the amounts of Bragg scattering to non-Bragg scattering. The relative crystallinity (RC) is calculated using the following formula.^{42–44}

$$RC = \frac{A_c}{A_c + A_a} \cdot 100\% \quad (2)$$

where A_c is the crystalline area found by integrating the Bragg reflections, and A_a is the amorphous area found by integrating the rest of the scattering signal corresponding to non-Bragg scattering. One very important note on this method, is that both the amorphous and crystalline areas are evaluated above a baseline. This baseline is defined as a line connecting the points of scattering signal at the lowest and highest scattering angles used in the RC evaluation. This is illustrated in Figure 9. This definition of a baseline makes the relative crystallinity very sensitive to the scattering intensities at the extremes of the dataset. Small variations in intensity at these points will have a great effect on the size of the amorphous area, and therefore the RC .

A way to avoid this is to evaluate the amorphous area all the way to the first axis without using a baseline. This will increase the size of A_a , and thereby decrease RC . This method is not commonly used in literature, but is much less sensitive to changes at the endpoints.^{45,46} Here, we will report both RC evaluated with a baseline and RC_{full} evaluated without a baseline.

3.5 Measurements and materials

All laboratory equipment was cleaned with 96% vol Ethanol before, between, and after each use. TA experiments were carried out The University of Copenhagen, Niels Bohr Institute.

PPI samples

To check for repeatability of the produced data, three samples of PPI were taken from bags of the same lot of Pisane™ C9* pea protein isolate stored at the Food Department at the University of Copenhagen..

- S1 or SA: surface PPI from Bag 1, which was opened on the side.
- S2: surface PPI from Bag 2, which had been opened but was rolled closed.

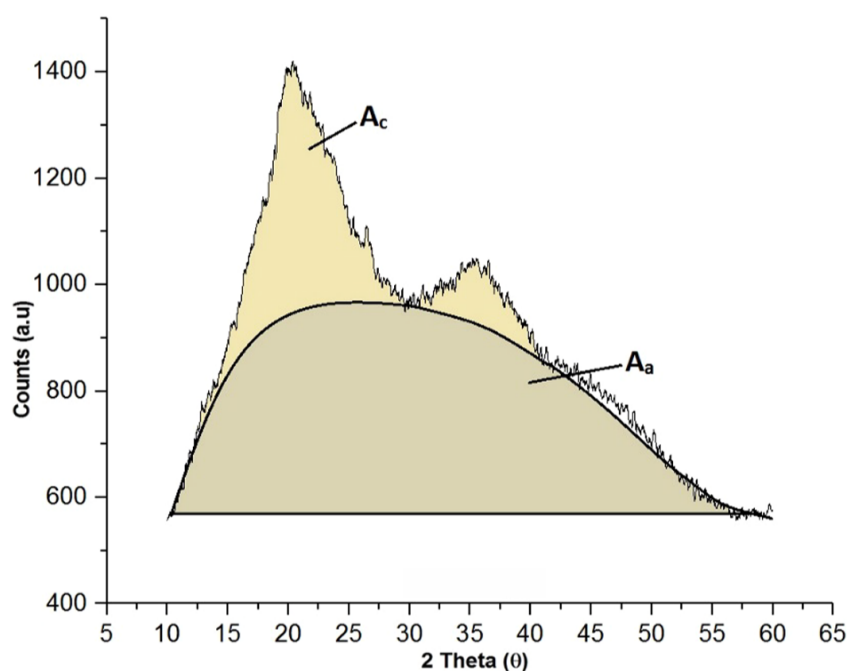


Figure 9: Representation of the crystalline and amorphous areas of a diffractogram. Figure reproduced from Kumar et al.⁴²

- S3: PPI from center of Bag 2.

Both Bag 1 and Bag 2 had been stored in a cupboard at room temperature for more than a year prior to sample collection.

Samples of PPI from other manufacturers were also tested.

- SB: NUTRALYS S85 XF from ROQUETTE
- SC: ProFam Pea 580 from ADM

All samples can be found in Figure 10. After sample collection, these samples were stored in closed containers in a drawer at ambient conditions and measured as is.

Reduction of PPI with DTT

The reduced PPI samples were prepared by adding sample SA (Pisane™ C9* pea protein isolate) to an aqueous solution of dithiothreitol (DTT) min. 99.5 % from ITW Reagents (molar mass 154.25 g/mol). The samples were then mixed in a tube rotator for two hours at room temperature. Hereafter, the samples were put in a freezer at -20 °C for a day, and then freeze-dried. After freeze-drying, the samples were put back in the freezer until the first measurement. Hereafter, the samples were kept at room temperature. After being kept at ambient temperature for four days, a small sample of DTT195 (named

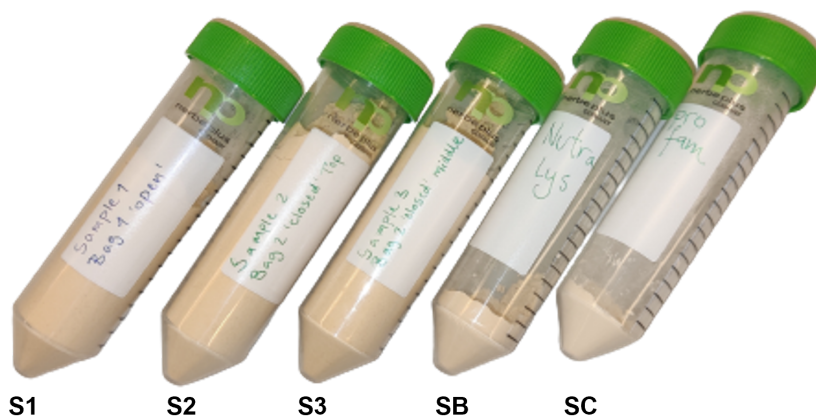


Figure 10: Image of all pea protein isolate samples in their containers. These are the dry samples as is, with no treatments applied. Sample S1 is also called SA.

rDTT195) was put in a refrigerator, to test whether the storing temperature would affect the sample. Table 3 summarizes the samples and their composition.

Table 3: Contents of each of the four PPI samples, treated by adding Pisane™ C9* pea protein isolate to aqueous solutions with varying concentrations of the reducing agent dithiothreitol.

	Control	DTT2	DTT20	DTT195
Milli-Q water	20 mL	20 mL	20 mL	20 mL
PPI mass [g]	1.0017	1.0034	1.0001	1.0028
DTT mass [mg]	0	6.1	60.5	600.2
DTT concentration	0	2 mM	20 mM	195 mM

TGA-FTIR-MS

TGA-FTIR-MS measurements were taken using a NETZSCH TG 209 F1 Libra coupled to FTIR from Bruker Optics Inc. and MS from NETZSCH. Samples were added to clean alumina crucibles and lightly pressed. A gas flow of 20 ml/min protective N₂ and 20 ml/min purge N₂ was used for all experiments. A heating rate of 10 K/min was used, with no isotherms. Most samples were heated from 20 °C to 220 °C as this was deemed a safe temperature range where the samples would not pollute the instrument, while still allowing for detection of the onset of thermal degradation. A sample mass of under 20 mg was used in all cases. One sample (SA) was heated to 255 °C with extra care taken to ensure that the measurement was safe for the instrument. The masses of crucibles and samples were measured by the instrument to µg precision. Table 4 gives the rounded mass of each sample. Absorption FTIR spectra were collected every 3 minutes in the

spectral range 650-4400 cm^{-1} . The MS ion current was measured every 0.005 s for whole values of m/z in the range 1-50.

Table 4: Mass of each sample measured using TGA-FTIR-MS. Values are rounded from five to two decimal places.

* Measured up to 230 °C

** Measured up to 255 °C

Sample	S11	S12	S21	S22	S31	S32
Mass [mg]	13.65	16.98	14.43	16.57	15.96	17.98
Sample	SA*	SA**	SB	SC		
Mass [mg]	12.04	9.63	12.73	12.83		
Sample	Control	DTT2	DTT20	DTT195	rDTT195	
Mass [mg]	2.85	2.91	2.85	3.02		Day 1
	3.34	3.01	3.19	3.05		Day 3
	3.03	3.14	3.16	2.88		Day 5
	3.08	3.28	3.08	2.90		Day 10
	3.02	2.84	3.35	3.19		Day 15
	2.75	3.02	3.06	3.04	3.16	Day 20

DSC

DSC measurements were taken on a NETZSCH DSC 214 Polyma machine. Samples were added to aluminium crucibles with punched lids. Punched lids were used to allow water vapor to escape and avoid a great gas pressure inside the crucible. Crucibles and samples were weighed on an analytical balance with mg precision. A gas flow of 40 ml/min protective N_2 and 60 ml/min purge N_2 was used. Each measurement has an initial isotherm of 15 min at 30 °C and no isotherms between scans. The initial isotherm helps minimize the buoyancy of the instrument when heating commences. Samples were then heated at 10 K/min up to 200 °C in the first scan unless otherwise stated. For some samples, a second heating scan was performed up to 120 °C. Liquid nitrogen was used for cooling the instrument.

Imaging

Microscopy was carried out on inViaTM Qontor confocal Raman microscope from Leica Microsystems CMS GmbH. Samples were added to a glass slide and gently pressed flat. The slide was mounted on the microscope stage and moved into focus. Lenses of 5x, 20x,

Table 5: Mass of each sample measured using DSC.

Sample	S11	S12	S21	S22	S31	S32
Mass [mg]	2.6	2.2	2.5	2.3	2.3	2.2
Sample	SA	SB	SC			
Mass [mg]	2.7	2.8	2.8			
Sample	Control	DTT2	DTT20	DTT195	rDTT195	
Mass [mg]	2.1	2.0	2.2	2.1		Day 1
	2.2	2.1	2.0	2.2		Day 4
	2.0	2.0	1.9	2.2		Day 13
	1.9	2.0	2.2	2.0	2.1	Day 20

and 50x magnification from Leica Microsystems CMS GmbH were used. Images were collected as single frames from a live feed. For the experiments with heating, samples were added to a round glass disc (~ 2 cm diameter) with a shallow edge and padded flat. For sample S2, a small indentation was made in the sample to create a thinner area. This sample holder was placed in a thermal stage from Linkam Scientific (serial number THMS600) which was mounted on the microscope stage. The temperature programmed to increase with 1 K/min with image acquisition every 5 °C.

XRPD

XRPD data was acquired at the Institute of Chemistry at the University of Copenhagen. The instrument used was a Bruker D8 Discover diffractometer. Samples were added to PMMA sample holders and patted flat. The sample holders were then added to an automatic sample changer. Each sample was measured over two hours with a wavelength of 1.5406 Å (Cu K_α) in the range 5-50° at room temperature.

4 Survey of sample heterogeneity and data reproducibility

The main goal of this chapter of the project is to test for reproducibility. A previous study by Rui Liu found significant discrepancies between two samples of the same batch of PPI.⁹ Before we conduct any further investigation of the thermal properties of PPI, we will therefore need to determine whether the results are reproducible. We will perform a thorough survey of three different samples, named S1, S2, and S3, from the same batch of PPI. The samples are described in the previous section. We will also test for variations within each sample by performing experiments in duplicates.

4.1 Results

Selected microscopy images can be found in Figure 11 and Figure 12. Microscopy was performed on four duplicates of all three samples (S1-S3) without any modification of the samples. This was done to observe if the morphologies of all areas of all samples were identical, or if there were some immediate differences. The images in Figure 11 are of samples S1 and S2, and are representative of all obtained images. The full set of images can be found in Appendix A, Figures A1, A2, and A3. The images show no clear morphological differences between the samples. We observe no color differences, and the grains appear to have similar shapes and sizes.

To investigate how the morphology of the PPI changes during heating, the samples were placed in a thermal microscope stage. The first sample measured was S1. After heating to 200°C, a clear difference in color between the top and bottom of the ~ 1 mm thick sample was observed, with the bottom being a darker orange indicating that it had received more heat. Therefore, S2 was prepared with a thick area of ~ 1 mm thickness (similar to that of S1) as well as a thinner area of < 0.5 mm thickness as to allow us to observe the difference with the microscope.

Figure 12 shows what happens when this sample is heated. The first row of images is of the thicker area, and we observe that the color turns yellow when heated, but the morphology appears to stay the same. The thin area as shown in the second row of images has a deeper color at 200°C compared with the thicker area. When heating to 210°C, the sample turns black and appears partially melted.

During heating, Raman spectra were recorded with intervals of 5 °C. As explained in the experimental section, fluorescence can sometimes outcompete Raman scattering,

as Raman scattering it is a relatively weak phenomenon. This is unfortunately the case for the PPI samples. The recorded spectra therefore mostly show the fluorescence background. However, one peak was observed at $\sim 1002\text{ cm}^{-1}$ in all samples. This peak stems from the breathing vibrations of the benzene ring in the amino acid phenylalanine (Phe), and has been reported in literature for various different proteins, including pea proteins.⁴⁷⁻⁵⁰ The intensity of this peak does not change in a meaningful or consistent way with increasing temperature. Plots summarizing the Raman data can be found in Appendix C.

Figure 13 summarizes the results of TGA and evolved gas MS. In the TGA data, we observe mass loss twice. First, at lower temperatures, with a maximum mass loss rate around 80°C . This temperature is often referred to as the dehydration temperature, T_{dehy} . After dehydration, at 150°C the moisture loss is 4.65% with a standard deviation of 0.09%. The second mass loss begins at around 175°C and corresponds to degradation of the protein. The total mass loss at 220°C is 6.43% with a similar standard deviation. In the evolved gas MS we observe that water is released at both events of mass loss, whereas hydrogen sulfide and carbon dioxide only appear when the protein degrades. Only tiny amounts of hydrogen sulfide are detected. Importantly, we note that all samples and duplicates appear to follow the same trends, meaning that our results are reproducible.

Complete TGA-FTIR-MS data for S31 can be found plotted in Figure 14. The biggest

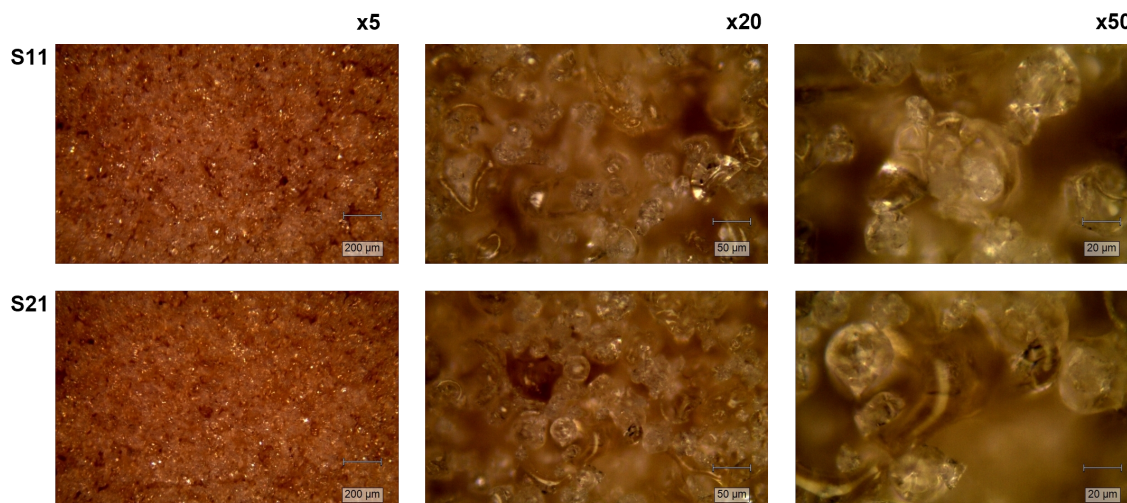


Figure 11: Optical microscopy with 5, 20, and 50 times magnification of samples S11 (sample 1 duplicate 1) in the top row and S21 (sample 2 duplicate 1) in the bottom row. These are representative of all samples and duplicates. The magnification and scale bars are shown on the individual images. Images were taken at room temperature.

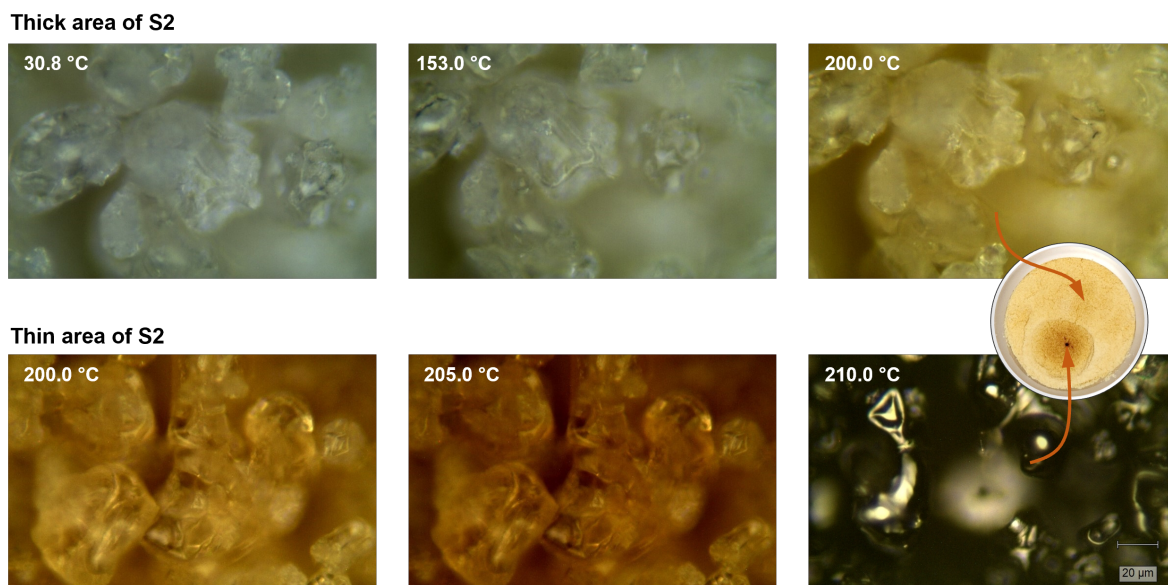


Figure 12: Optical microscopy of thicker area (top row) and thinner area (bottom row) of sample S2. The temperature at which the image was taken is given on the individual images. The scale bar is found on the last image and is the same for all images. The magnification is 50x. Insert is a picture of the sample after heating to 210 °C with thin and thick areas shown. Heating rate is 1 K/min with image acquisition every 5 °C below 200 °C, and every 1 °C above 200 °C.

difference between the results of the two techniques, is that it is possible to separate ammonia from water with FTIR. As discussed in the experimental section, we can apply ratio analysis to the signals at $m/z = 17$ and 18. From this, we find no clear indication of ammonia, meaning that MS alone indicates no or very small amounts of ammonia in the entire temperature range. However, ammonia is clearly present in the FTIR spectra at degradation temperatures, i.e. above 170 °C. The most prominent ammonia features are the twin peaks observed at 960 cm^{-1} and 940 cm^{-1} . The higher energy peak is first observed at 172 °C, while the lower energy peak is observed at 176 °C. We can therefore conclude that small amounts of ammonia are evolved at temperatures above 172 °C. The carbon dioxide peak around 2300 cm^{-1} is broader and therefore more difficult to precisely determine. It first appears around 150 °C and then more prominently from around 190 °C, which is in agreement with the MS data. The evolution of NH_3 and CO_2 are of great interest, as these are markers of thermal degradation of the proteins. These species are evolved when the amino acids that make up the proteins start breaking down.⁵²

In Figure 15 we have the DSC thermograms for all three samples and their duplicates. We observe a smaller feature around 70°C. This potentially correspond to a glass transition in the protein, as glass transitions have previously been reported by Ricci et al¹ in

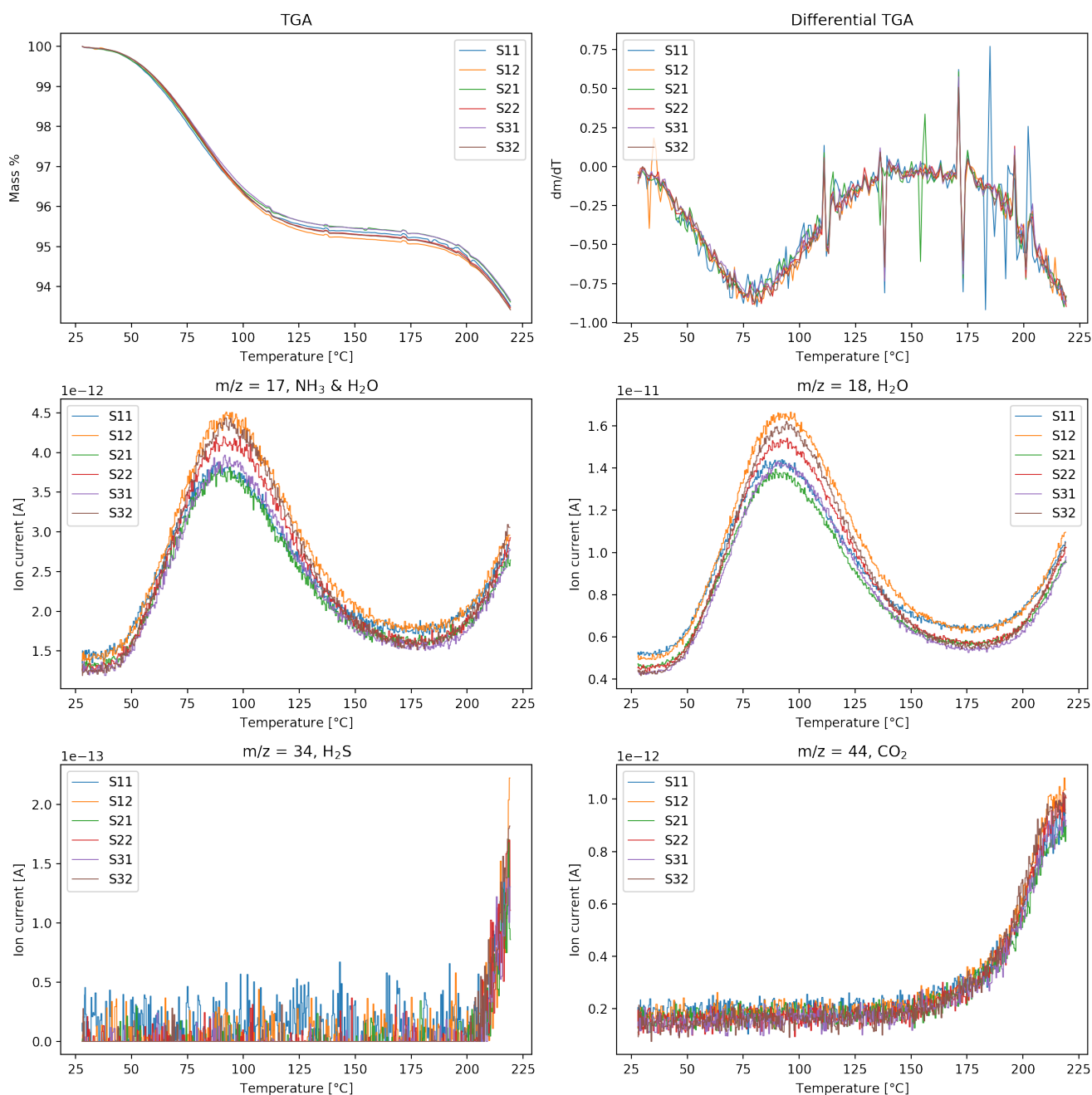


Figure 13: TGA and evolved gas MS of duplicated of samples S1-S3. Top row shows the TGA curves and their derivatives. Rows two and three contain plots of selected MS signals. The relevant species for each plotted m/z value is given in the plot titles. Heating rate is 10 K/min, and a gas flow of 20 ml/min protective N_2 and 20 ml/min purge N_2 was used. Sample masses can be found in Table 4.

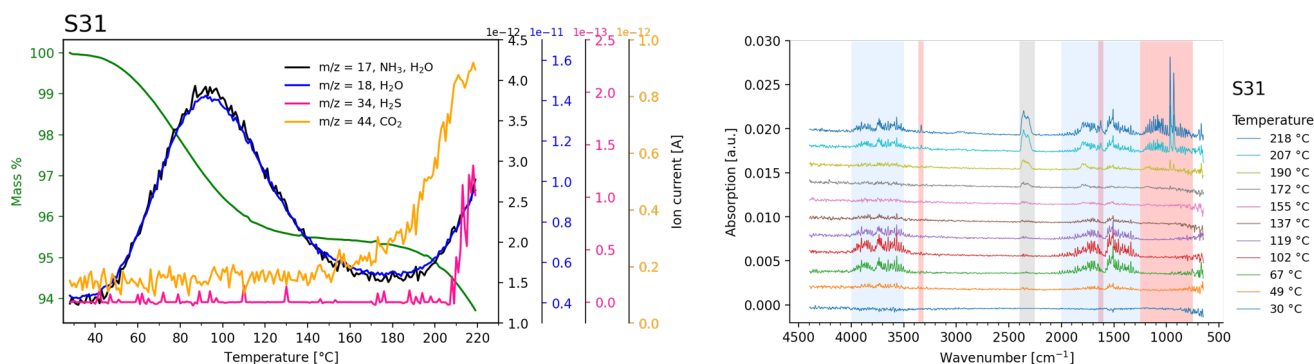


Figure 14: TGA-FTIR-MS data for sample S31. TGA and evolved gas MS can be found in the left graph. Evolved gas FTIR can be found to the right with spectra offset for better readability. Energies corresponding to vibrations in water have been highlighted in blue ($4000\text{-}3500\text{ cm}^{-1}$, $2000\text{-}1250\text{ cm}^{-1}$), ammonia in red ($3360\text{-}3310\text{ cm}^{-1}$, $1650\text{-}1600\text{ cm}^{-1}$, $1250\text{-}750\text{ cm}^{-1}$), and carbon dioxide in grey ($2400\text{-}2250\text{ cm}^{-1}$). No vibrations corresponding to hydrogen sulfide are observed. Signals from each of the species have been identified through comparison with spectra provided by the NIST Chemistry WebBook.⁵¹

pea protein concentrates of different purity levels. It could also be a different phase transition in the samples, or be related to the mass loss observed around this temperature. From the DSC curves we can extract the denaturation temperature, $T_d = 123 \pm 2^\circ\text{C}$, as the maximum of the main peak. The value for each sample, along with peak enthalpies, and onset and offset temperatures, can be found in Table 6. Here, T_d is in the range $120\text{-}123^\circ\text{C}$ for most samples, but a bit higher for S31 (127.5°C). This shift towards higher denaturation temperatures only happens for one of the duplicates of S3 and can therefore not be attributed to a significant difference between samples S1-S3. Interestingly, the enthalpy of the peak varies a lot between samples S1-S3, but not much between duplicates of the same sample. Though the enthalpy values of S31 and S32 are artificially low due to a shorter data range, this still holds true when comparing these two duplicates, and when comparing S1 with S2. This could be the first indication of a difference between the three collected samples.

Lastly, we measured powder diffraction on S1, S2, and S3. The resulting diffractograms can be found in Figure 16. The diffractograms of the three samples are nearly identical. These measurements were not done in duplicates, as a much larger amount of the PPI powder was used for XRPD than for DSC and TGA, and the measured sample can be assumed to be representative. Three peaks are present in all samples. The two main peaks at around 8.8° (peak 1) and 19° (peak 2) are reflections of α -helix and β -sheet structures respectively.^{53,54} The smaller peak at around 32° (peak 3) has previously been

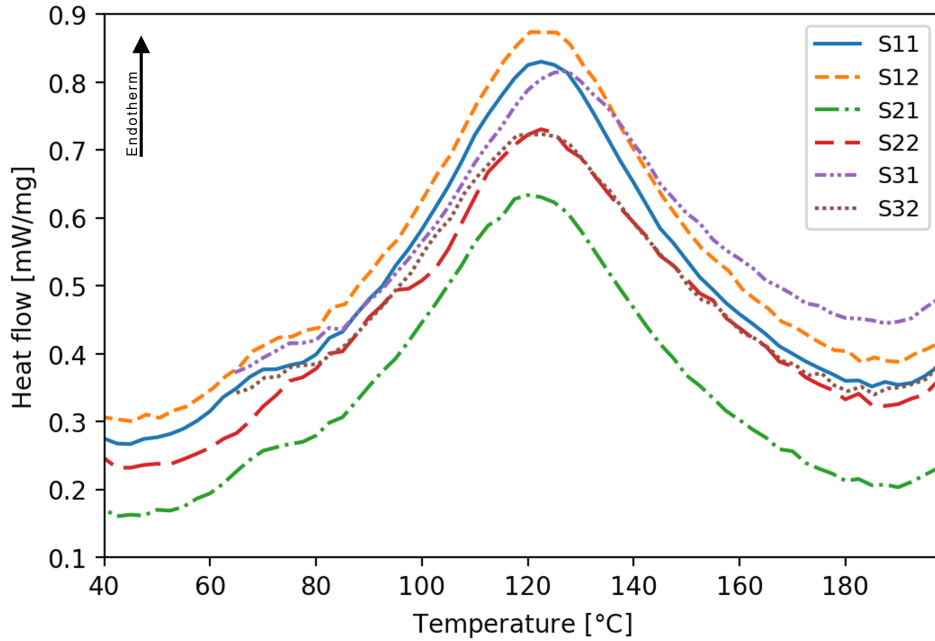


Figure 15: DSC thermograms for each of the three samples with duplicates. A limited temperature range is shown for S31 and S32 due to an instrument issue causing a non-constant heating rate at low temperatures for these samples. Endotherm processes are plotted at positive heat flow values, and the heating rate is 10 K/min. Gas flow is 40 ml/min protective N₂ and 60 ml/min purge N₂. Sample masses can be found in Table 5.

observed in pea and cotton seed protein.^{9,53} The relative crystallinity of the samples was found to be 64.5-65.6 % as summarized in Table 7. This is a much higher RC value than the 36.91 % which has previously been reported,⁹ and cannot be explained purely by the different ranges of scattering angles used for the calculation. As previously discussed, the method used to calculate *RC* is very sensitive to the scattering intensity at the extremes of the dataset. One should therefore take great caution when comparing *RC* values.

Table 6: Summary of values extracted from DSC for samples S11-S32. Onset, denaturation and offset temperatures are valid for the denaturation peaks of the samples, and not the feature at 70 °C.

* Samples evaluated based on a shorter data range from 65 °C. This mainly affects the enthalpy, but also the on- and offset temperatures due to changes in the baseline.

Sample	ΔH [J/g]	T_{on} [°C]	T_d [°C]	T_{off} [°C]
S11	170.1	77.3	122.5	164.3
S12	178.0	75.9	120.5	165.6
S21	152.0	69.6	120.0	166.0
S22	154.9	81.8	122.5	171.3
S31*	121.5	85.4	127.5	166.6
S32*	118.9	80.9	123.0	167.5
Average		78 ± 5	123 ± 2	167 ± 2

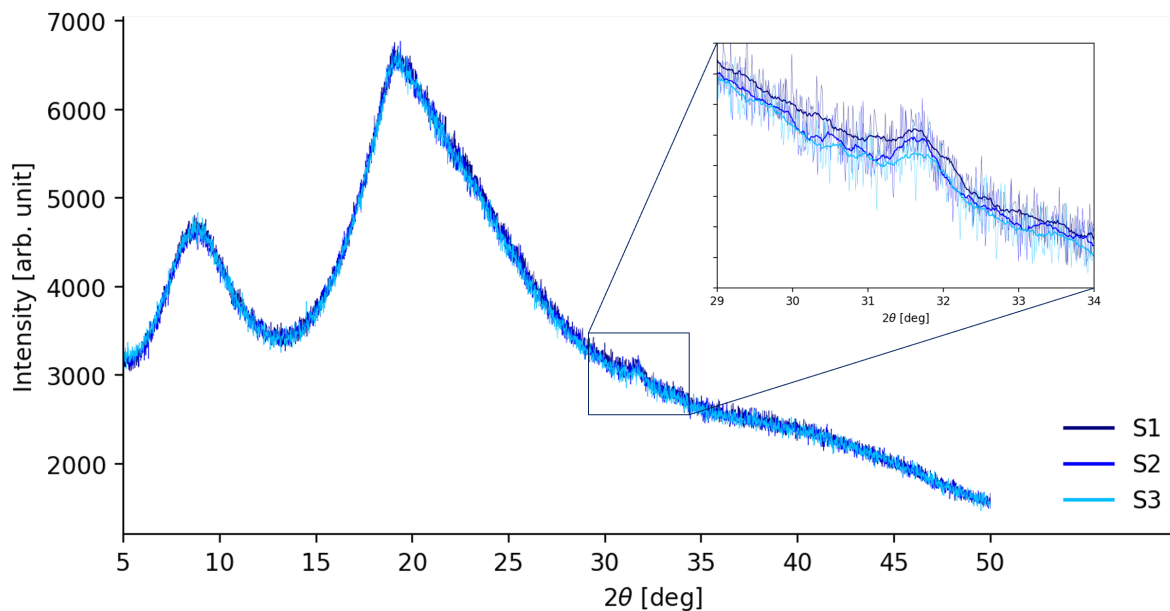


Figure 16: XRPD diffractograms of samples S1-S3. The insert contains a section of the data overlaid with a smoothed version of the same data.

Table 7: Comparison of values of RC , RC_{full} , and peak positions for samples S1-S3 and RC reported in literature. Relative crystallinities are calculated using equation 2 in the range 5 - 50°

* PPI 'Sample 2' as reported by Liu.⁹ RC calculated in range 5 - 55°.

Sample	RC	RC_{full}	Peak 1	Peak 2	Peak 3
S1	65.6 %	21.6 %	8.8° (10.0 Å)	19.1° (4.6 Å)	31.6° (2.8 Å)
S2	64.7 %	21.0 %	8.8° (10.0 Å)	19.2° (4.6 Å)	31.7° (2.8 Å)
S3	64.5 %	20.8 %	8.8° (10.0 Å)	19.1° (4.6 Å)	31.7° (2.8 Å)
PPI*	36.91 %		9.01° (9.80 Å)	19.28° (4.60 Å)	31.69° (2.82 Å)

4.2 Discussion

From the results of optical microscopy on sample S2 in Figure 12 we observe a clear change in color at temperatures above 150 °C, which corresponds to the temperatures of thermal degradation observed in TGA experiments. Furthermore, above 200 °C, the sample rapidly changes color and morphology, appearing black and partially melted at 210 °C. However, we also observed a clear difference in the amount of heat received by the parts of the sample which were in direct contact with the bottom of the sample holder, and those that were not. We can not know whether the temperature recorded by the thermal stage is the same as that of the imaged area of the sample. Therefore, we can only qualitatively conclude that the sample rapidly darkens at degradation temperatures.

The TGA curves reported in Figure 13 show two mass loss steps. These two steps have also previously been reported in literature at similar temperatures.^{1,9,55} Some small irregularities, or ‘bumps’, can be observed on the TGA curve and more prominently on the differential TGA. These are likely due to movement, like stomping or fast walking, in the vicinity of the instrument during the measurement. Those occurring in the exact same fashion across all samples are due to irregularities in the calibration measurement, again due to movement in the vicinity of the instrument. We also note, that while the MS curves appear to have the same shape, they vary in intensity. This is due to the fact that while the TGA curves are normalized to the sample mass, the MS signal is not. The MS signal directly represents the amount of material with a certain mass/charge relationship present in the evolved gas. Therefore, a larger sample mass will (loosely) correspond to a greater MS signal, as we find to be the case here.

Through IR spectroscopy, we can separate the signals related to water from the signals related to ammonia. Ammonia only appears at temperatures from 172 °C and up, whereas water signals appear at both events of mass loss. This is in agreeance with what we observed with MS, and allows us to conclude that the $m/z = 17$ signal in the MS spectrum is due only to water at the first mass loss event, and mostly due to water with a contribution from ammonia at the second. This contribution must be small, as the ratio of the $m/z = 17$ to $m/z = 18$ signal is near constant, as it would be for a pure water signal.

The DSC thermograms as found in Figure 15 have clear endothermic peaks related to denaturation of the protein. The denaturation temperature of a protein depends on its structure at all levels of complexity from primary to quaternary. It can be affected by both physical and chemical treatments, and importantly by plasticizers like water. The moisture content of the protein samples therefore very important to consider, as a higher water content would lower the denaturation temperature.⁵⁶ Moreover, it could

also affect the glass transition. The feature which we observe around 70°C could be a glass transition as observed by Ricci et al.¹ More measurements are needed to determine whether this is the case. Peak enthalpies were found to vary much more between samples S1-S3 than between duplicates of the same sample. This might be the only indication of a fundamental difference between the collected samples. It could therefore prove fruitful to investigate this further with more duplicates of the samples.

In general, our data is not perfectly repeatable, as is normal with biological samples. We find that there are small differences between the samples and between duplicates, and that these differences are expressed more in some measurements than others. However, we have overall shown good repeatability of our measurements, which is important for correct interpretation of further experimental data.

5 Comparing different PPIs

Now that we know that we can trust each measurement, we broaden our horizons. In this chapter, we will study the thermal characteristics of PPI from three different producers. These are PISANE™, NUTRALYS, and ProFam, but in the following we will refer to them by the sample names SA, SB, and SC respectively. From the perspective of a food scientist, it is very interesting to know whether different brands of PPI have different thermal properties, as this might influence how they should be treated to achieve the desired product. If we can use easy and quick techniques like TGA and DSC to narrow down how the PPI should be treated, this could save both time and money. Here, we have chosen to compare PPI from different manufacturers, but the same process could be applied to samples of different batches or storage conditions from one manufacturer.

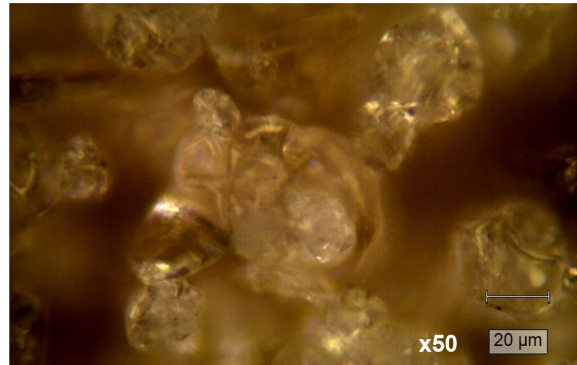
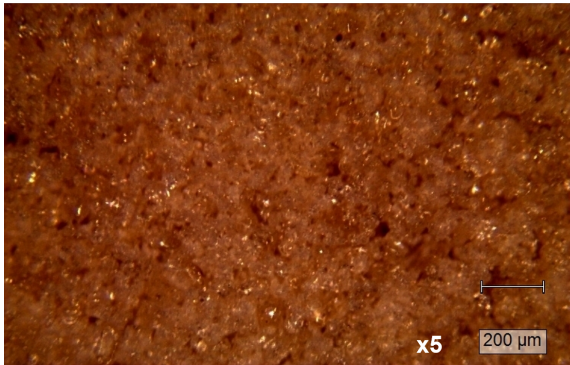
5.1 Results

Figure 17 shows microscopy images of samples SA-SC at two different magnifications. The images at five times magnification show that all three samples appear to be homogeneous with even distributions of particle sizes. When zooming in to fifty times magnification, we can distinguish the individual particles of protein. We observe a clear difference between the granule sizes of the samples. SA has larger particles of around 40-60 μm , whereas SB and SC have particles of around 20-30 μm . As previously discussed, this difference could be a result of the milling process used by the producer, or could relate to the extraction process and storage conditions.⁵⁷

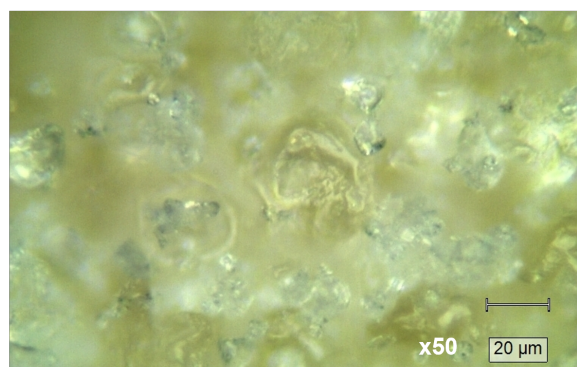
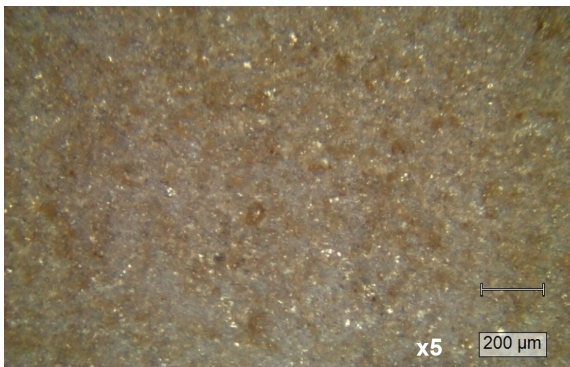
A comparison of the three different TGA curves can be found in Figure 18. Here, we again have two mass loss events, the first related to moisture loss and the second to protein degradation. Sample SA loses moisture at a higher rate and over a greater range of temperatures than the other two. By evaluating the percentage of mass lost at 150 °C, we find that SA contains 4.22 % moisture, which is more than SB at 3.58 % and SC at 3.76 %. The mass lost by each sample in the temperature range 150 °C to 220 °C has also been evaluated, and corresponds to the mass loss caused by protein degradation. Sample SC degrades the fastest, with 2.73 % mass lost to degradation at 220 °C followed by SB with 2.20 % and lastly SA with 1.87 %. Overall, SC has lost the largest percentage of its mass at 220 °C, and this is mostly due to its rapid degradation.

We gain further insight by studying the EGA data in Figure 19. Here, we make several interesting observations. The MS signal of CO₂ in SC is 67 % greater than that of SA and 28 % greater than that of SB at 220 °C. This confirms that thermal degradation

SA



SB



SC

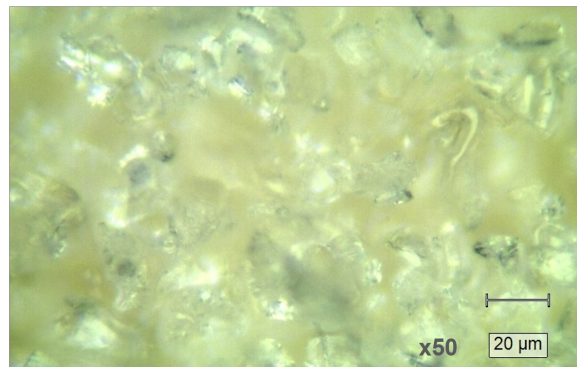


Figure 17: Optical microscopy with 5, and 50 times magnification of samples SA, SB, and SC. The magnification and scale bars are shown on the individual images. Images were taken at room temperature.

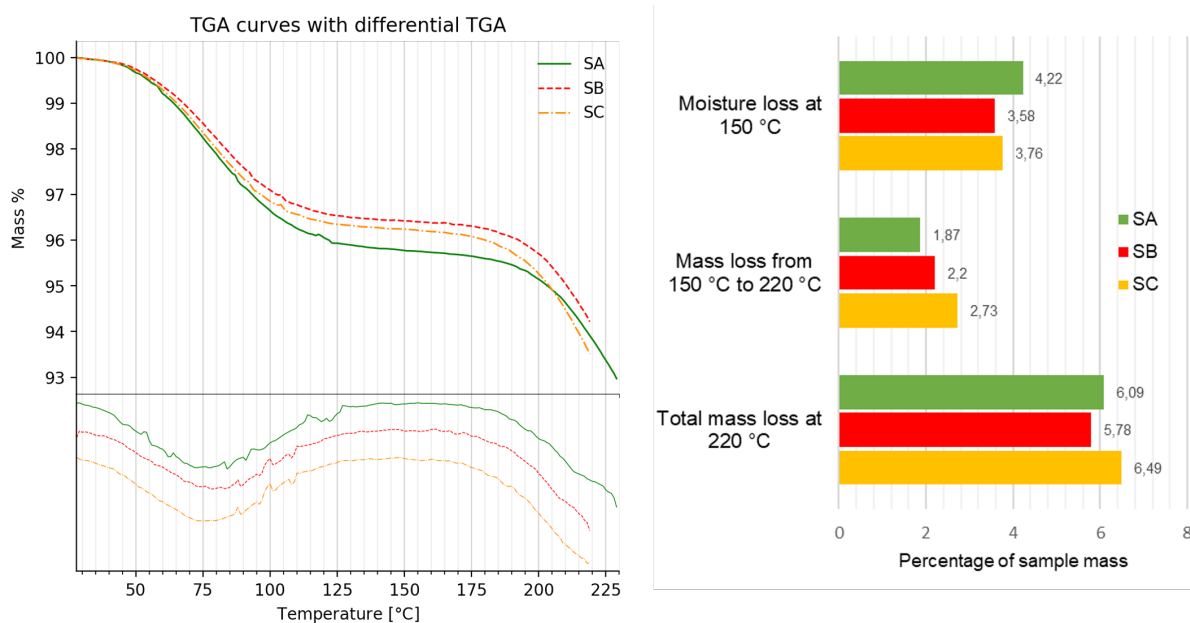


Figure 18: TGA curves with their derivatives (bottom) of samples SA, SB, and SC. SA was measured from 28 °C to 230 °C, while samples SB and SC were measured from 28 °C to 220 °C. Heating rate is 10 K/min, and a gas flow of 20 ml/min protective N₂ and 20 ml/min purge N₂ was used. Selected values have been extracted from these curves and can be found in the diagram to the right. Samples masses can be found in Table 4.

of SC is faster than that of the other samples. This is true even when we account for the mass of each sample which will influence signal intensity. A direct comparison of MS signals corrected for the sample mass can be found in Figure A4 in Appendix B.

We also observe that the CO₂ signals of the samples have a small plateau beginning at 205 °C for SC and 210 °C for SA and SB. In sample SA, we also observe a decrease in the signal of H₂S at temperatures above 220 °C. This 'pause' in thermal degradation is also reflected in the differential TGA curves (Figure 18) of especially SA and SB.

Evolved gas FTIR spectra of the samples are very similar. The spectra of SA are interesting, as a new peak starts to form in the frequency range 3000-2800 cm⁻¹ at temperatures above 220 °C. This peak has also been reported in evolved gas FTIR studies of whey protein films and soy protein films and correspond to the C-H vibration in saturated carbohydrates.^{58,59} This is confirmed by the MS data in Figure 20, where we observe an increase in MS signals above m/z=42 for high temperatures. These m/z values are characteristic for a number of small alkanes and carbohydrates which would display C-H vibrations.⁴¹

DSC thermograms can be found in Figure 21. The three samples show widely different

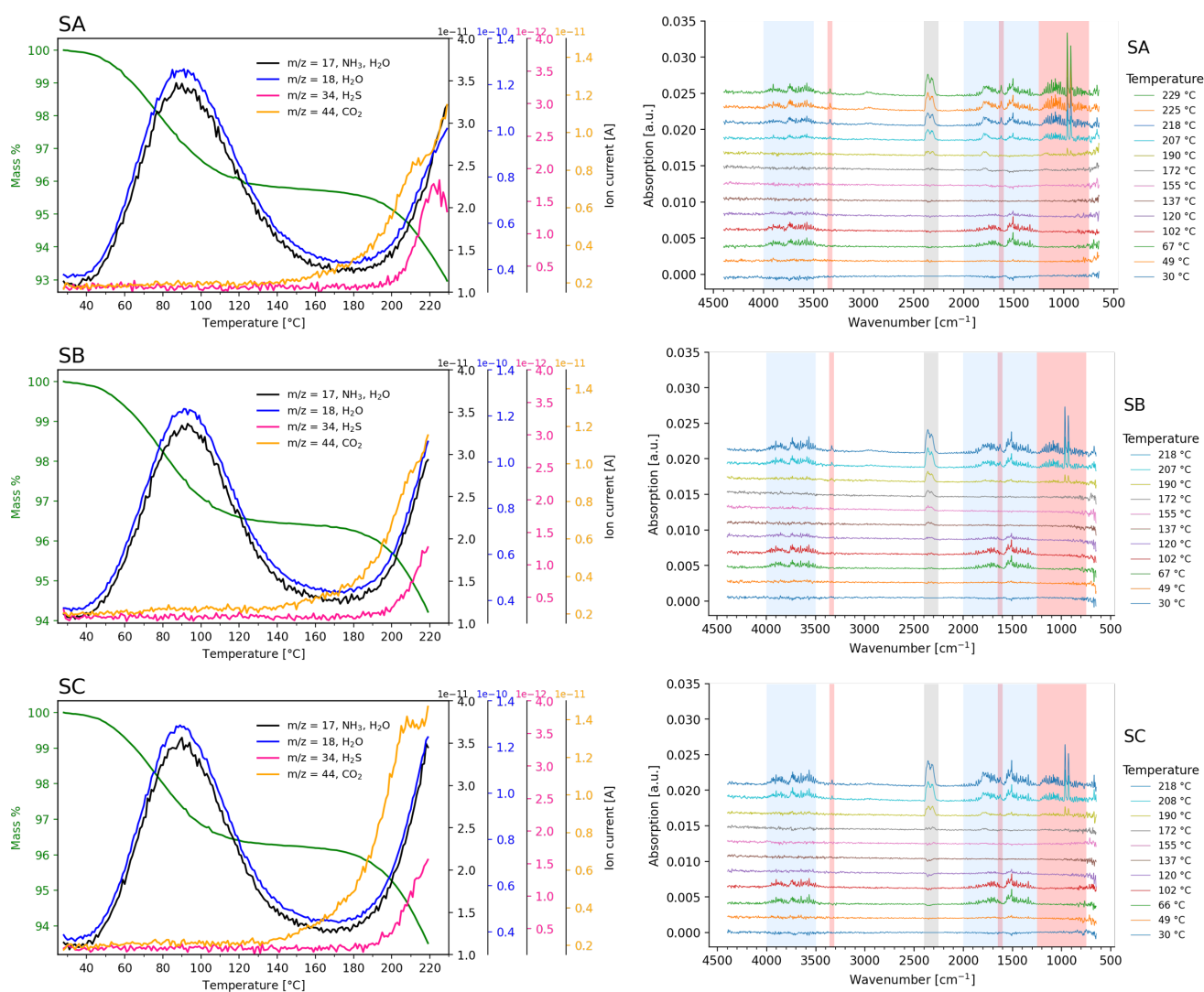


Figure 19: Full TGA-FTIR-MS data of samples SA-SC. The left column contains TGA curves alongside selected evolved gas MS signals. The relevant species for each plotted m/z value is given in the legend. The right column contains selected evolved gas IR spectra from each sample. Energies corresponding to vibrations in water have been highlighted in blue (4000-3500 cm^{-1} , 2000-1250 cm^{-1}), ammonia in red (3360-3310 cm^{-1} , 1650-1600 cm^{-1} , 1250-750 cm^{-1}), and carbon dioxide in grey (2400-2250 cm^{-1}). The MS and FTIR signals are plotted on the same scales across samples.

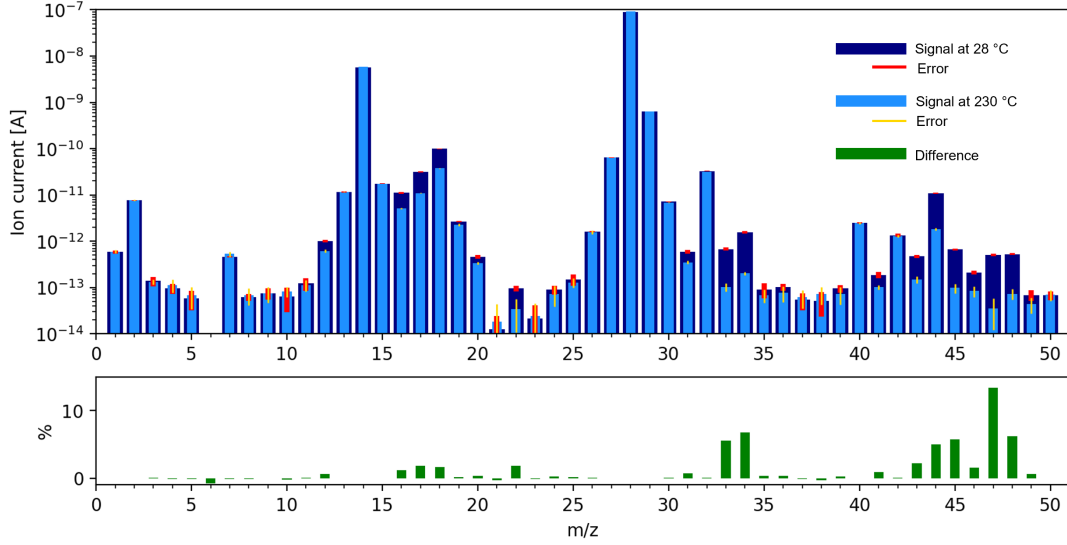


Figure 20: Summary of MS data for SA at the beginning and end of the measurement. The height of each bar in the top plot corresponds to the signal intensity of that m/z value at the beginning (28 °C) and end (230 °C) of the heating scan. These values are obtained as an average of the first and last 50 data points corresponding to a very narrow temperature range to mean out the data noise. The standard deviation of these data points is given as the error. Note the logarithmic y-scale. The bottom plot shows this change in intensity as a percentage.

behaviors. The denaturation temperatures are 124.7 °C for SA, 133.1 °C for SB, and 128.5 °C for SC. The difference between these values of T_d are greater than the standard deviation of ± 2 °C obtained from samples S11-S32. The feature which we have previously observed around 70 °C is present in all samples (SA: 75 °C, SB: 74 °C, SC: 77 °C). However, in SC it is very pronounced and is clearly a peak and not a glass transition, see Figure 4. The second heating scans show no features.

Table 8: Summary of values extracted from the first DSC heating scan for samples SA-SC. Onset, denaturation and offset temperatures are valid for the denaturation peaks of the samples, and not the feature at 70 °C.

Sample	ΔH [J/g]	T_{on} [°C]	T_d [°C]	T_{off} [°C]
SA	159.7	76.4	124.7	168.1
SB	102.1	83.8	133.1	175.1
SC	121.6	72.9	128.5	171.9

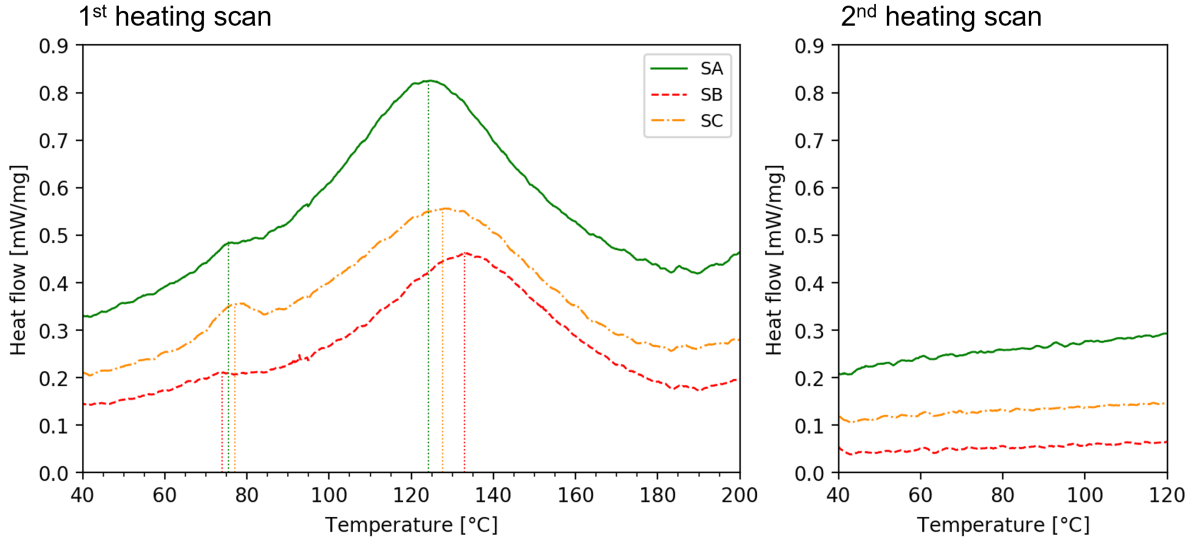


Figure 21: DSC thermograms for each of samples SA, SB, and SC. First and second heating scans are shown. Endotherm processes are plotted at positive heat flow values, and the heating rate is 10 K/min. Gas flow is 40 ml/min protective N₂ and 60 ml/min purge N₂. Sample masses can be found in Table 5.

5.2 Discussion

The data presented above indicates significant differences between the three samples in every measurement. Sample SA stood out by having a larger particle size and a greater moisture content. Lan et al.⁶⁰ have previously used scanning electron microscopy to look at different preparations of pea proteins. They found particles with a structure resembling what we observed here. They also found that the PPI preparation method had a significant impact on its properties. The difference in size observed here is therefore worthy of note.

The moisture content is a central modifier of protein properties and food characteristics and longevity in general. Through TGA-MS analysis, we find that SA loses more water than the other two samples. From DSC, we observe that SA has a lower denaturation temperature. This indicates that SA has more water, but that the water is less bound to the proteins, as bound and hydration water requires more energy to evaporate. SA also showed a slower onset degradation, meaning that this sample has the best thermal stability at degradation temperatures. This could possibly be linked to the larger granule size of this sample. By measuring TGA-FTIR-MS of this sample to 230 °C, we discovered what appears to be a 'pause' in thermal degradation. This means that degradation of PPI is likely not a single step process, but might involve multiple steps. Ricci et al. observed a similar phenomenon in lentils.¹ A multi step degradation process

is entirely plausible, as PPIs contain not only a mix of different types of protein but also other components like starches and fats. Each component will contribute differently to the thermal properties of the samples.

We also observed a new IR peak in the frequency range 3000-2800 cm^{-1} at temperatures above 220 °C. This is a sign of a more pervasive protein degradation, as FTIR and MS suggest the presence of small alkanes or carbohydrates in the evolved gas.

To study the thermal degradation further, we measured TGA-FTIR-MS of SA over a greater temperature range (28-255 °C). The result can be found in Appendix G. Here, we observe that thermal degradation is a two-step process. It appears that the release of CO_2 , NH_3 , and water is momentarily stalled at around 215 °C while H_2S is released. The release of H_2S stops at around 240 °C. This is likely because there is no more sulfur left in the sample, as pea proteins only contain very small amounts of sulfur-containing amino acids.

Based on optical microscopy, the morphologies of SB and SC are almost identical at room temperature. Sample SC behaved comparably to SB in the first mass loss step. However, at degradation temperatures, SC decomposed rapidly compared to SB and even more so compared to SA. This was reflected in the CO_2 signals of EGA which were significantly stronger.

DSC measurements show a relationship between moisture content (from TGA) and denaturation temperature. A higher moisture content is related to a lower denaturation temperature. Water molecules interact with both inter- and intramolecular bonds. In some proteins, the presence of water serves to stabilize the unfolded protein state, thereby reducing T_d . This relationship has been documented in literature in various different protein systems.⁶¹⁻⁶³

Interestingly, DSC of SC shows a distinct peak at 77 °C which cannot be a glass transition. Based on the initial reproducibility measurements, we have theorized that the feature was a glass transition, because a glass transitions have previously been reported in literature at similar temperatures.¹ These glass transitions were observed in a second heating scan and in sealed crucibles. In this work, we do not observe any transitions in the second heating scan. This could be due to two effects. Firstly, our measurements were made using DSC crucibles with a punched lid. This means that the evaporated water can escape the crucible in the first heating scan. As we know, moisture works as a plasticizer and removing it can cause the glass transition temperature to increase beyond the measured temperature range. Secondly, it could be the case that our samples

do not have a glass transition and that both peaks are features of entirely irreversible processes. The peak around 75 °C could therefore either be a sum of a glass transition and an irreversible phase transition, or purely an irreversible phase transition. Either way, we have a phase transition, the nature of which is yet to be determined. There are several possible causes of this transition, some of which are listed below.

- **Denaturation of individual pea protein fractions.** Pea proteins can be divided into many different protein fractions. Each type of protein has distinct thermal behaviors, including denaturation temperatures. The most abundant of the fractions are legumin (11S globulin) and vicilin (7S globulin). Denaturation temperatures of 82.2 °C and 90.4 °C have recently been reported in literature for purified pea vicilin and legumin respectively, at unknown moisture contents.⁶⁴ However, a study of legumin and vicilin in soybean protein isolates found that such low denaturation temperatures could be obtained only at hydration levels above 80 % w/w. When decreasing the moisture content, the denaturation temperatures increased dramatically.⁶⁵ This means that even though soy and pea protein isolates have different thermal behaviors, it is unlikely that the denaturation of vicilin or legumin is the cause of the transition observed around 75 °C.
- **Evaporation of different water domains.** As previously discussed, water can associate with proteins in three different ways, as bulk water, hydration water, and bound water. It is possible that this initial feature is caused by evaporation of bulk water. Bulk water does not associate with the proteins, and we would therefore expect it to be released at lower temperatures than hydration water.
- **Phase transition in non-protein components of the PPI.** The PPIs in question contain around 80 % protein, meaning that the remaining 20 % is made up of primarily starch and water with some fiber and fats. These components again have their own thermal behaviors. One possibility is that the peaks around 75 °C are due to gelatinization of the small fraction of pea starch present in the PPIs. DSC peaks at comparable temperatures have been reported in literature for soy and pea starches.^{66–68}

Due to the complex nature of the PPI samples, it is difficult to determine the exact cause of the phase transition at 75 °C. This would likely be an interesting future study.

6 PPI reduced with DTT

In this chapter, we will take a detailed look at pea protein isolates treated with the reducing agent dithiothreitol (DTT). DTT is a powerful reducing agent that reduces the disulfide bridges in proteins in a two-step redox reaction seen in Figure 22. The products of the redox reaction are a reduced disulfide bond and a cyclic form of oxidized DTT.⁶⁹ Disulfide bridges form between residues of the sulfur containing amino acid cysteine. The formation of disulfide bridges is important for the tertiary and quaternary structures of proteins, and thereby also for protein functionality. Reducing these bonds can lead to partial or complete unraveling of the protein. This can in turn affect many properties of the protein that are essential for food applications, like gelling and emulsion properties, texture, and taste. There is therefore a need to better understand the reduction of pea proteins. Here, we apply thermal analysis to gain new insight into the weakly studied system of reduced pea protein.

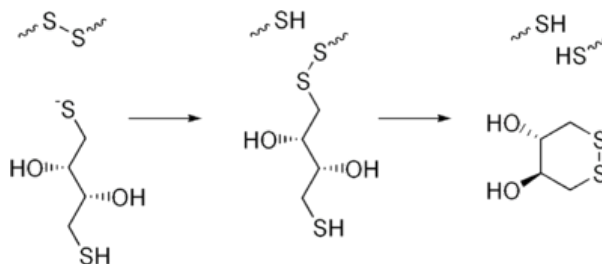


Figure 22: Two-step redox reaction between dithiothreitol (DTT) and a disulfide bond, producing a reduced disulfide bond and a cyclic form of oxidized DTT. Adapted from AG Scientific.⁶⁹

The effectiveness of DTT is in some cases limited by poor access to the disulfide bridges of the protein. Most pea proteins are globular proteins, meaning that in aqueous solutions, the proteins are wound up into a sphere-like shape with a hydrophobic center and a hydrophilic shell. Cysteine residues tend towards the hydrophobic part of the protein, meaning that its disulfide bridges will be hard to reach for DTT, especially in larger protein structures.⁷⁰ Strong concentrations of DTT (50-100 mM) should therefore be used for complete reduction. If one wishes to maintain the reduced proteins in solution, concentrations of 1-10 mM should be applied.⁷¹ Reduction of disulfide bridges is reversible over time, meaning that there is a small chance for the disulfide to reform after reduction.

Here, we have tested a low (2 mM), medium (20 mM), and high (195 mM) concentration of DTT. The samples have been named accordingly as DTT2, DTT20, and DTT195.

The samples have been measured over the course of 20 days to track the evolution of the samples over time. To test the effects of storage temperature, a small sample of DTT195 was put in the fridge on day 4 and not measured again until day 20. This sample is named rDTT195, r as in refrigerated. The reduction process includes dissolving the pea proteins in aqueous DTT solution and freeze-drying the samples after treatment. To account for the possible effects of these steps, a control sample was also measured. This sample has gone through the same processing as the reduced samples, just without DTT.

6.1 Results

Table 9: Summary of extrapolated onset temperatures of each mass loss step observed with TGA. Values are given for days 1 and 20 of all samples treated with DTT. The onset temperatures were calculated as the intersection of a line tangent to the region of low mass loss before T_{on} with a line tangent to the region of greatest mass loss after T_{on} .

Sample	Day	T_{on} [$^{\circ}$ C], 1 st mass loss step	T_{on} [$^{\circ}$ C], 2 nd mass loss step	Total mass loss [%] at 220 $^{\circ}$ C
Control	1	51.8	197.9	4.43
	20	55.4	201.5	4.85
DTT2	1	50.8	193.4	4.94
	20	53.6	200.0	4.52
DTT20	1	51.9	193.4	7.44
	20	54.9	188.3	8.06
DTT195	1	44.9	144.9	38.84
	20	52.2	146.1	36.69
rDTT195	20	54.9	145.8	35.88

Figure 23 shows TGA curves of all treated samples at day 1 and day 20, and the onset temperatures and total mass loss are summarized in Table 9. All samples display two mass loss steps, though the first step is less well defined for sample DTT20, and very subtle for sample DTT195. All samples display differences between the first and last measurement. Samples Control and DTT2 show similar behaviors. For both samples, an increase in water loss was observed over the course of the 20 days (0.30 % and 0.35 % at 150 $^{\circ}$ C respectively). We also observe that the onset of both mass loss steps shifts towards higher temperatures for these samples. The onset temperatures of Control are a bit higher than those of DTT2 on both day 1 and 20, indicating that this sample is slightly more thermally stable. As the only sample, DTT20 shows a decrease in water loss at the first mass loss event and a decrease in thermal stability at degradation tem-

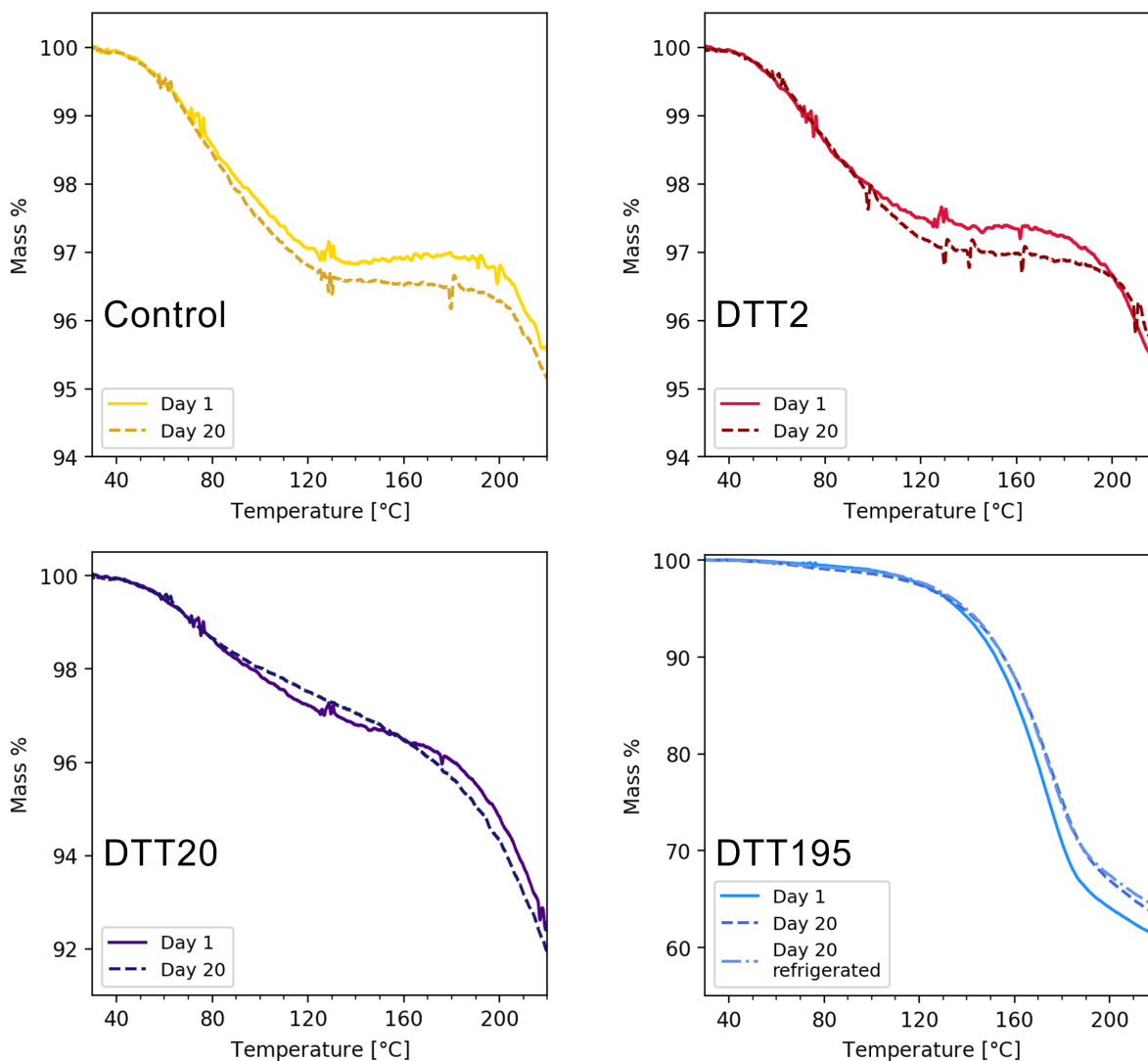


Figure 23: TGA curves for all treated samples on days 1 and 20. Samples were measured in the temperature range 28-220 °C at 10 K/min with a gas flow of 20 ml/min protective and 20 ml/min purge N₂. Sample masses can be found in Table 4.

peratures after 20 days. The shape of the TGA curve also changes significantly after 20 days. On day 20, it becomes quite difficult to determine where the first mass loss step ends and the second begins. DTT195 has by far the greatest total mass loss with up to 38.84 % at 220 °C. The first mass loss event for this sample has an early onset on day 1 (44.9 °C), but on day 20 the onset is similar to the other samples. The second mass loss step of this sample begins as early as 145 °C, more than 40 °C lower than for any other sample. TGA curves from all samples at all days can be found in Appendix E.

To determine the nature of the mass loss for each sample, we first turn to the MS

data as depicted in Figure 24. Here, we observe the greatest water loss from sample Control, followed by DTT2, DTT20, and lastly DTT195 and rDTT195. This is true for both days 1 and 20. Based purely on the water signal at $m/z = 18$, we would infer that the non-bound water contents of samples Control, DTT195, and rDTT195 increase over the 20 days, whereas it decreases slightly for DTT2 and DTT20. This is not what we observed through TGA. Interestingly, it appears that sample rDTT195 has its maximum water loss in the first mass loss step at 70 °C. This is the same as for sample DTT195 on day 1, and not day 20 where the maximum water loss is closer to 80 °C. All versions of sample DTT195 have significant signal at $m/z = 34$ from 100 °C. The onset of this signal is around 175 °C for DTT20, 190 °C for DTT2, and 200 °C for Control. Very high signals at $m/z = 44$ have been measured for all samples of DTT195. The signal has a peak at 183 °C for DTT195 day 1, at 182 °C for rDTT195 day 20, and at 180 °C for DTT195 day 20. The rest of the samples show similar behavior to that of the untreated samples at this m/z value.

Selected FTIR datasets can be found in Figure 25. We observe three new peaks, indicated in the figure, which we have not observed in the untreated samples. The Control sample has a new peak at 1800 cm^{-1} which can be observed at temperatures above 190 °C. This peak is due to carbonyl C=O stretching vibrations.⁷²⁻⁷⁴ For DTT195, two new peaks are observed. These peaks first appear at 155 °C, and are most intense at 172 °C. The peak at 2930 cm^{-1} is due to C-H stretching vibrations.⁵⁹ The peak at 1050 cm^{-1} is likely due to S=O stretching vibrations.⁷⁵ Full FTIR data from all days can be found in Appendix D. The characteristic signals of thermal protein degradation (from NH_3 and CO_2) which show up at 190 °C or later, are observed in all samples. The main differences between samples and over time are observed in the temperature region below thermal degradation, meaning 30-172 °C. Analysis of this temperature region is summarized in Table 10. From FTIR, we find that no samples show the same behavior, and that all samples evolve over time. Unfortunately, some of the datasets from the treated samples have over subtraction of atmospheric carbon dioxide and water. Therefore, these specific datasets (given in the table) can not be analyzed.

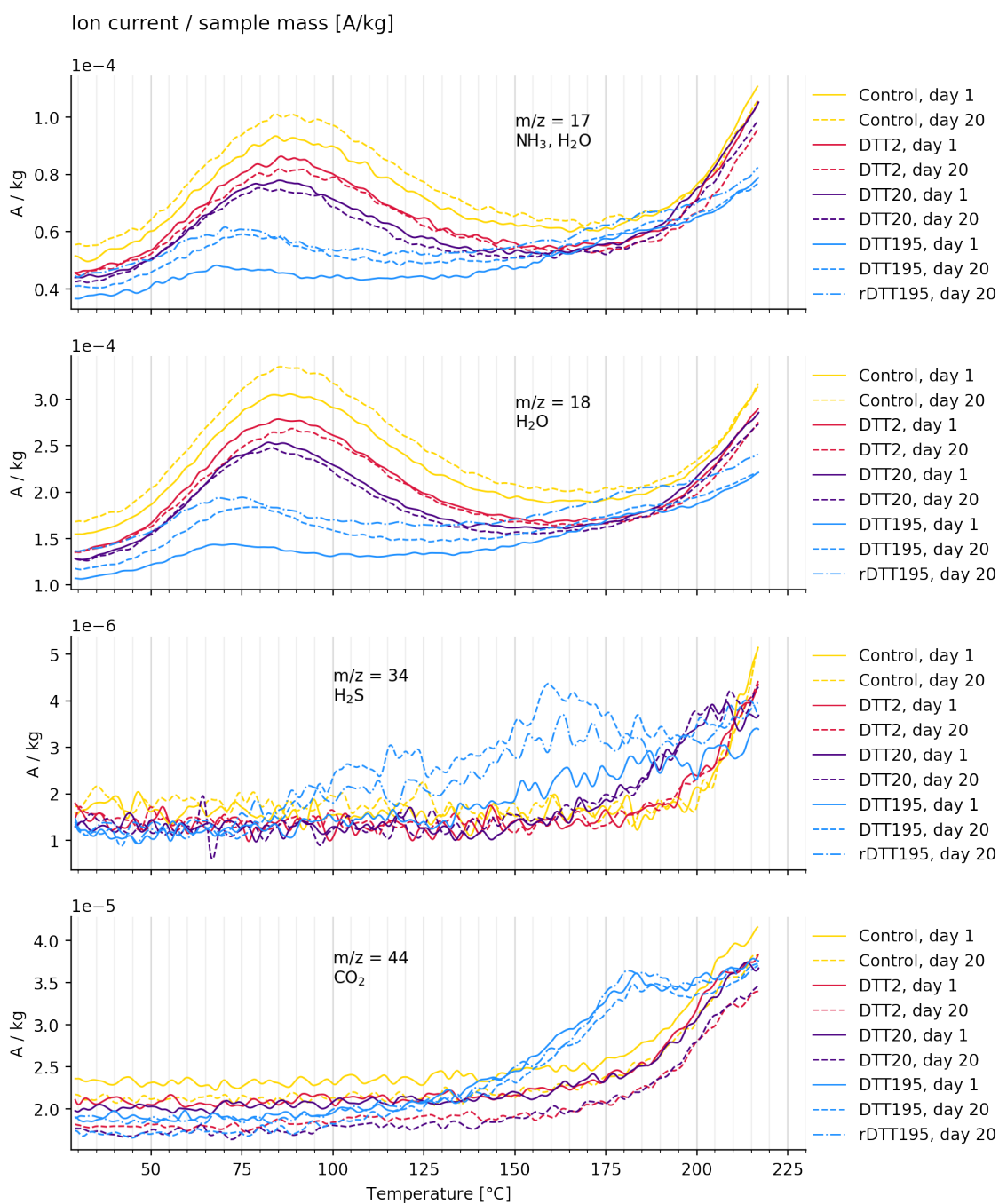


Figure 24: Selected MS signals for all treated samples on days 1 and 20. Signals have been divided by the sample mass to better be able to compare signal intensity between samples, and smoothed for better visibility. The plotted m/z value as well as the relevant species are shown on each plot. Heating rate is 10 K/min and measurements were taken in a nitrogen atmosphere. Sample masses can be found in Table 4.

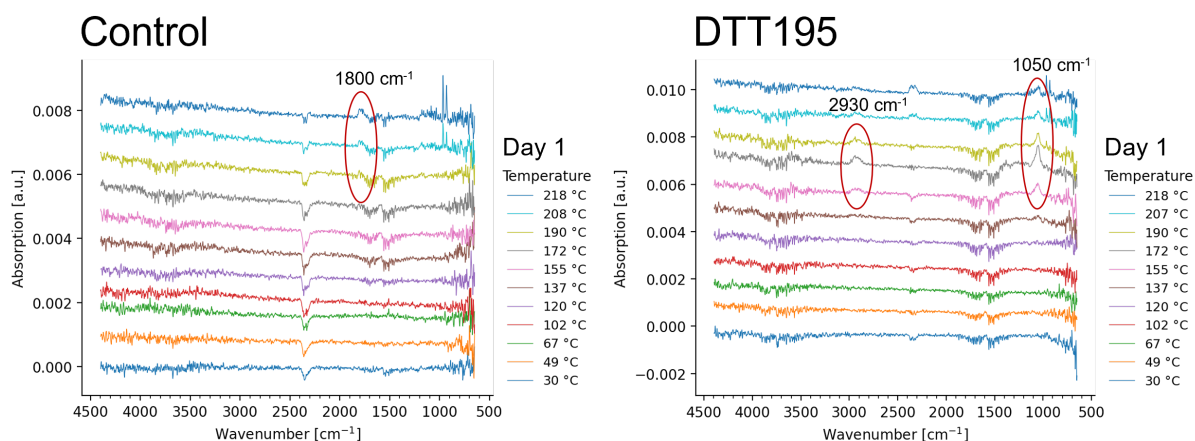


Figure 25: Selected FTIR datasets from samples Control and DTT195 on day 1. Both samples have an over subtraction of atmospheric water and Control has over subtraction of carbon dioxide. The presence of these species can therefore not be determined from the above spectra. However, three new peaks can be observed at 1800 cm^{-1} , 2930 cm^{-1} , and 1050 cm^{-1} as indicated by the red circles.

Table 10: Summary of FTIR data in the temperature region below thermal degradation of the proteins (30-172 °C). A molecule is noted below if its characteristic IR absorption pattern is present in the FTIR spectra from the given day in this temperature range. The color indicates the relative intensity of the signal.

Sample	Day 1	Day 3	Day 5	Day 10	Day 15	Day 20
Control	*	H ₂ O	CO ₂	H ₂ O	H ₂ O	H ₂ O
DTT2	*	CO ₂ , H ₂ O	H ₂ O		H ₂ O	CO ₂
DTT20		*	H ₂ O, CO ₂	CO ₂ , H ₂ O		
DTT195				*		CO ₂ , H ₂ O

Light gray: low signal intensity. Gray: moderate signal intensity. Black: high signal intensity.

* spectra could not be analyzed.

DSC thermograms for all treated samples on day 1 and day 20 can be found in Figure 26. All samples have an increase in overall heat flow from day 1 to day 20. Samples Control, DTT2, and DTT20 show similar behaviors with comparable denaturation temperatures, see Table 11. The denaturation temperatures, onset temperatures, and offset temperatures of these samples all decrease after 20 days. Samples DTT195 have very different signals to those of the other samples. The main peak sits at around 100-110 °C, which is significantly lower than any other samples measured. The shape of this peak is also different, as it is much sharper than the broad peaks observed so far, and has a less well-defined 'shoulder' at 120-140 °C. The shape of the thermogram of rDTT195 is more like that of DTT195 at day 1 than day 20.

Table 11: Summary of values extracted from DSC for all treated samples on days 1 and 20. Onset, denaturation and offset temperatures as well as peak enthalpy are given.

Sample	Day	ΔH [J/g]	T_{on} [°C]	T_d [°C]	T_{off} [°C]
Control	1	220.5	71.9	128.3	182.3
	20	246.5	67.2	121.5	179.7
DTT2	1	153.7	80.7	135.9	182.6
	20	211.6	73.2	127.3	180.6
DTT20	1	159.9	70.5	125.6	174.8
	20	143.2	67.4	123.0	172.5
DTT195	1	130.1	53.1	98.0	121.9
	20	163.0	63.4	111.8	124.6
rDTT195	20	150.2	60.2	101.3	127.3

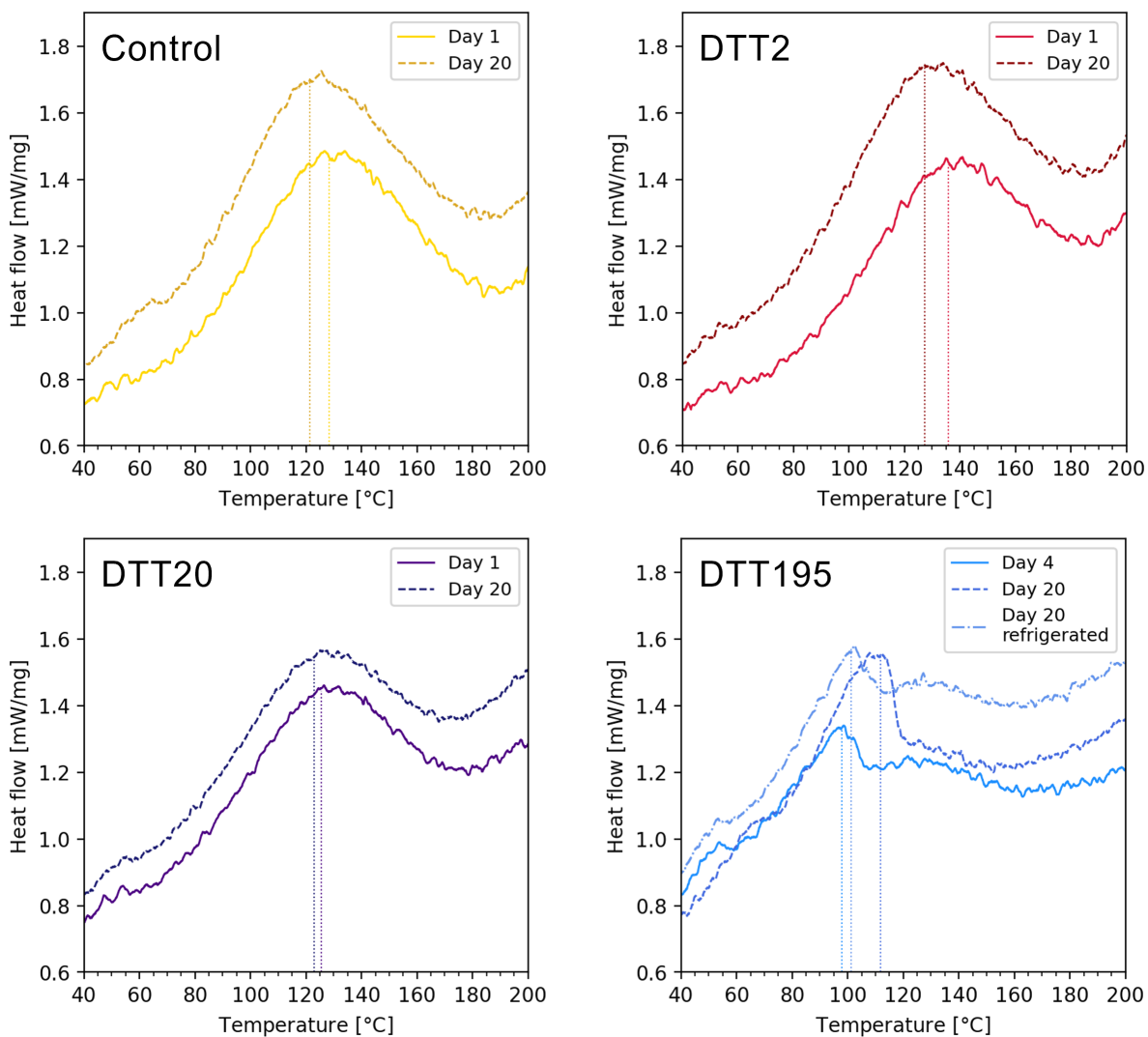


Figure 26: DSC thermograms for all treated samples on days 1 and 20. Samples were measured in the temperature range 30-200 °C at 10 K/min with a gas flow of 40 ml/min protective and 60 ml/min purge N₂. Endotherm processes at positive heat flow values. Sample masses can be found in Table 5

6.2 Discussion

The effect of DTT at varying concentrations

Based on the presented data, we conclude that the addition of DTT changes the properties of the samples, and that the degree of change is correlated with the DTT concentration. Across all measurements, the samples Control and DTT2 are the most similar. Through TGA, we learn that Control has slightly higher onset temperature at both mass loss events. This indicates higher thermal stability for the sample without DTT. When increasing the DTT concentration beyond 2 mM, we observe an increase in mass loss. This is likely due to pyrolysis of DTT in addition to the protein. For sample DTT2, DTT accounts for 0.6 wt% of the sample. For DTT20 it is 5.7 wt% and for DTT195 it is 37.4 wt%. From MS, we know that DTT195 releases great amounts of H₂S and CO₂ at temperatures well below 190 °C where we expect to observe thermal degradation of the proteins. FTIR analysis confirms that the proteins do not degrade until 190 °C, as ammonia is not observed before this point. We can therefore conclude that for DTT195, the mass lost before 190 °C, which is around 30-34 %, is mainly due to vaporization of water and DTT.

The MS of sample DTT20 also shows an earlier release of H₂S, beginning around 160 °C. For the same reason as above, we know that this is from DTT, as it cannot be from the protein. This raises the question of why the breakdown of DTT occurs at such high temperatures in DTT20 compared to DTT195. One possible answer is that in DTT195, DTT was added in such great excess that it is still largely present in its native non-oxidized form. In DTT20, we expect most of the DTT to be in the oxidized cyclic form. It is very possible that the oxidized and non-oxidized forms have different thermal stabilities. One indication of this is that the melting point of the non-oxidized DTT (41-44 °C) is much lower than that of the oxidized form of DTT (130-132 °C).⁷⁶

Through DSC analysis, we find that the samples containing DTT generally have a higher endothermic heat flow above 160 °C. This could be due to the breakdown of DTT. All samples show an increase in heat flow at high temperatures (above T_d). The onset of this peak is around 190 °C for Control and DTT2, 175 °C for DTT20, and 160 °C for DTT195. This corresponds well with the gasses evolved from each sample as observed through MS.

Two heat flow peaks can be observed for DTT195 below protein degradation temperatures. The first peak (100-110 °C) is sharp and drops off quickly, whereas the second (120-140 °C) is broad and subtle. From MS, we know that the only evolved gas at these temperatures is water. One possible explanation for these peaks, is that they correspond to evaporation of different domains of water. DTT is hygroscopic and might therefore

cause some of the bulk and hydration water in the samples to rearrange. This would create two different domains of water in the sample, one which is associated with the protein, and one which is associated with DTT. Since DTT is less thermally stable than the proteins, the water associated with it might require less energy to be evaporated and lead to the first endothermic peak. The second broad peak would then be the evaporation of the protein-associated water domain. This corresponds well with what we observe with MS, where the initial water loss happens at lower temperatures for DTT195 than the rest of the samples. Another possibility is that the first peak is indicative of a phase transition, like melting, in DTT itself.

Overall, it is difficult to separate the thermal properties of proteins reduced by DTT from those of DTT itself. This would be an interesting future area of study.

The effect of time

Across all the above presented thermal analysis data, comprising TGA, MS, FTIR, and DSC, no sample is the same from one measurement day to the next. From TGA, we find an increase in onset temperatures for both events of mass loss for all samples, with the exception being the second mass loss step of DTT20. The shapes of the TGA curves also vary over the 20 days, which is evident when looking at the full sets of TGA data in Appendix E. The nature of this change is non-linear and varies with DTT concentration. The same observation is made when tracking DSC curves over time as in Appendix F. This is supported by the FTIR analysis summarized in Table 10. Here, we observe that the samples release substantial amounts of CO₂, H₂O, or both in the pre-degradation temperature range at certain days throughout the experiment. There is no clear pattern for this behavior, but it does appear that this release of gaseous water and carbon dioxide happens later in time when the DTT concentration is increased. The refrigerated sample rDTT195 shows characteristics of both DTT195 on day 1 and on day 20. The TGA curve of rDTT195 is most like the last measurement of DTT195. Through MS analysis, we find that rDTT195 releases water at a temperature which is closer to that of the first DTT195 measurement. The shape of its DSC curve is closer to that of the first DTT195 measurement, but its enthalpy is more like the last measurement. We can thereby conclude that refrigerating the sample does affect the time evolution, but does not stop it completely.

There are many factors which could cause the samples to evolve over time. One of these is water, which as always plays a central role in determining the thermal properties of proteins. After freeze-drying, samples can lose so much water that they become hygroscopic. Though the samples are stored in a closed container, the air in those containers is replaced every time the container is opened to take a sample for measurements.

the uptake of atmospheric can therefore play a role, albeit a small one. Another possible contributor is the rearranging of water between domains of the sample as discussed above. In the beginning of this chapter, we also discussed how disulfide bridges in the proteins which have been reduced by DTT can reform over time. The disulfide bridges can either reform in the original location, or through interactions with neighboring cysteines. Lastly, DTT can interact with proteins in ways that are unrelated to reduction of disulfide bridges. In a study by M. C. Alliegro,⁷⁷ the thiol groups of DTT were found to inhibit the binding activity of a specific protein which had been mutated to not contain cysteine residues. It is therefore not a far leap to say that there is a possibility that the interaction of DTT with protein domains could influence the thermal properties of the proteins. Such an interaction could evolve over time and with rearrangements of water. All of the above-mentioned processes might also be affected by storage temperature.

The effect of freeze-drying

Another important point to notice, is that the sample Control, which is the PPI sample SA that has been hydrated and then freeze-dried in the same manner as the reduced samples, does not have the same thermal properties as SA. The main difference between SA and Control, is that SA is stable, whereas Control is not. On day 1, the TGA onset temperatures of Control are similar to those of SA, but this is not the case on day 20. The DSC thermograms of the two samples are different on every measured parameter. This is true no matter which measurement day we compare SA to. The instability of Control compared do SA is at least partially due to the high porosity of the freeze-dried sample, which can negatively affect its shelf-life.⁷⁸

Freeze-drying is a harsh process, which can significantly disturb the protein samples. This is evident in the Control sample. However, the effects of freeze-drying are not only limited to this sample, but also apply to the rest of the treated samples. This is another factor which should be considered when assessing the effects of DTT and time in the above data.

7 Conclusions

The first part of this work surveyed three samples of the same PPI to determine the reproducibility of thermal and structural measurements. Good reproducibility was achieved for TGA-FTIR-MS and XRPD. Optical microscopy showed no differences in the sample morphologies. DSC measurements showed a greater variance in curve shapes and heat flow. The denaturation temperature, T_d , of the samples was determined to be 123 ± 2 °C with an onset temperature of 78 ± 5 °C, and an offset temperature of 167 ± 2 °C. The peak enthalpy was found to vary a lot between samples S1-S3, and less between duplicates of the same sample. This indicates some fundamental difference between the three samples which is not otherwise reflected in the TGA and structural analysis.

TGA showed two mass loss events relating to moisture loss and thermal degradation. Through FTIR analysis, peaks related to ammonia, water, and carbon dioxide were identified. This was confirmed by MS which also showed trace amounts of a species likely to be hydrogen sulfide. Ammonia and carbon dioxide were used to identify thermal degradation, as these species are evolved during pyrolysis of amino acids. XRPD showed three peaks with the two main reflections being associated with α -helices and β -sheets in the protein structure. The relative crystallinity was determined to be 64.5-65.6 % which is much greater than previously reported values for the same PPI.⁹

In the second part of this work, we compared PPIs from three different manufacturers. The work done in the first part allowed us to determine that the observed variations in the data were due to differences in the samples. We conclude that the three samples overall display the same behavior, but at different temperatures. Sample SA (from PisaneTM) had the highest moisture content at 4.22 % and the slowest thermal degradation. Sample SC (from ProFam) had the fastest thermal degradation. MS of CO₂ and H₂S at temperatures above 200 °C reveals a two-step degradation process. DSC measurements showed denaturation temperatures 124.2 °C for SA, 132.9 °C for SB, and 127.6 °C for SC, with a lower T_d related with a higher moisture content. Comparing the moisture loss observed with TGA to the shape of the DSC curve of SA allowed us to conclude that the water molecules in this sample associate more weakly with the proteins.

The last part of this work surveyed PPIs reduced with DTT over time. The TGA-FTIR-MS data showed that increasing the DTT concentration lowered the thermal stability of the samples. We also found that for medium (DTT20) and high (DTT195) concentrations of the reducing agent, a significant portion of the mass loss was due to degradation of DTT itself. When comparing MS data of DTT20 and DTT195, we find

that DTT is degraded at significantly higher temperatures in DTT20, and that this is likely due to the DTT mainly being in the oxidized cyclic form in this sample. DSC thermograms of DTT195 showed two peaks below thermal degradation temperatures. This could possibly be due to evaporation from different water domains in the sample.

The treated samples Control, DTT2, DTT20, and DTT195 were shown to evolve in a non-linear fashion throughout the 20 days in which they were monitored. This was evident in all thermal analyses. The shapes of the TGA and DSC curves varied over time, and FTIR analysis at temperatures below thermal degradation showed significant release of CO₂ and water only on some days. The fact that the sample Control also evolved over time allowed us to conclude that the hydration and freeze-drying process destabilizes the proteins. By refrigerating a sample of DTT195, we found that the storage temperature also plays a role in how the sample evolves over time. The refrigerated sample was measured on day 20 and showed characteristics from both the first (day 1) and last (day 20) measurements of DTT195.

7.1 Future Perspectives

The work presented herein is intended as an initial survey of the thermal properties of pea protein isolates. Even though the applications of PPIs are many, only very few studies of their thermal properties have previously been published. This work therefore serves as a much-needed step towards a better understanding of this useful food material. Several new and interesting areas of research arise from the questions left unanswered by this work.

- When surveying PPIs from different manufacturers, we found clear differences in their thermal properties. But what exactly is the cause of these differences? To answer this question, a deep dive into the exact compositions of each of the samples is necessary. The samples from different manufacturers will likely be different on more than one parameter. Knowing the effects and significance of each of these parameters would be useful for intelligent design of food applications.
- We also observed a phase transition in the samples at around 75 °C in the DSC thermograms. Some theories as to the origin of this peak have been presented, but further experiments are needed to determine it.
- In our study of reduced PPIs, we were unable to separate the effects of DTT on the proteins from the effects of having DTT itself in the samples. If one could somehow remove DTT from the samples, or otherwise account for it, It would be possible to observe the thermal properties of reduced PPIs directly.

- Time (aging) was also shown to be an important factor for the treated samples. The non-linear evolution of the samples indicate that multiple processes play a role. Since chemical and physical treatments of food products are commonplace, deconvoluting these processes might allow one to either avoid them by taking the necessary precautions or utilize them in the product development.

References

- [1] L. Ricci et al. “On the thermal behavior of protein isolated from different legumes investigated by DSC and TGA”. en. In: *Journal of the Science of Food and Agriculture* 98.14 (2018), pp. 5368–5377. DOI: [10.1002/jsfa.9078](https://doi.org/10.1002/jsfa.9078).
- [2] Y. Zhang and J. Han. “Sorption Isotherm and Plasticization Effect of Moisture and Plasticizers in Pea Starch Film”. en. In: *Journal of Food Science* 73.7 (2008), E313–E324. DOI: [10.1111/j.1750-3841.2008.00867.x](https://doi.org/10.1111/j.1750-3841.2008.00867.x).
- [3] P. Shanthakumar et al. “The Current Situation of Pea Protein and Its Application in the Food Industry”. p. 5354. DOI: [10.3390/molecules27165354](https://doi.org/10.3390/molecules27165354).
- [4] M. C. Tulbek, R. S. H. Lam, Y. C. Wang, P. Asavajaru, and A. Lam. “Chapter 9 - Pea: A Sustainable Vegetable Protein Crop”. en. In: *Sustainable Protein Sources*. Ed. by S. R. Nadathur, J. P. D. Wanasundara, and L. Scanlin. San Diego: Academic Press, Jan. 2017, pp. 145–164. DOI: [10.1016/B978-0-12-802778-3.00009-3](https://doi.org/10.1016/B978-0-12-802778-3.00009-3).
- [5] W. S. Ratnayake, R. Hoover, and T. Warkentin. “Pea Starch: Composition, Structure and Properties — A Review”. en. In: *Starch - Stärke* 54.6 (2002), pp. 217–234. DOI: [10.1002/1521-379X\(200206\)54:6<217::AID-STAR217>3.0.CO;2-R](https://doi.org/10.1002/1521-379X(200206)54:6<217::AID-STAR217>3.0.CO;2-R).
- [6] A. C. Y. Lam, A. Can Karaca, R. T. Tyler, and M. T. Nickerson. “Pea protein isolates: Structure, extraction, and functionality”. In: *Food Reviews International* 34.2 (Feb. 2018), pp. 126–147. DOI: [10.1080/87559129.2016.1242135](https://doi.org/10.1080/87559129.2016.1242135).
- [7] L. Day. “Proteins from land plants – Potential resources for human nutrition and food security”. en. In: *Trends in Food Science & Technology* 32.1 (July 2013), pp. 25–42. DOI: [10.1016/j.tifs.2013.05.005](https://doi.org/10.1016/j.tifs.2013.05.005).
- [8] B. M. Bohrer. “Review: Nutrient density and nutritional value of meat products and non-meat foods high in protein”. en. In: *Trends in Food Science & Technology* 65 (July 2017), pp. 103–112. DOI: [10.1016/j.tifs.2017.04.016](https://doi.org/10.1016/j.tifs.2017.04.016).
- [9] R. Liu. “The role of water in pea protein hydration/dehydration, denaturation and degradation”. MA thesis. University of Copenhagen.
- [10] T. E. Creighton. *Proteins: structures and molecular properties*. eng. 2. ed., [Nachdr.] New York: Freeman, 2002.
- [11] Y. Levy and J. N. Onuchic. “Water and proteins: A love–hate relationship”. In: *Proceedings of the National Academy of Sciences* 101.10 (Mar. 2004), pp. 3325–3326. DOI: [10.1073/pnas.0400157101](https://doi.org/10.1073/pnas.0400157101).

- [12] X. Chen, I. Weber, and R. W. Harrison. “Hydration Water and Bulk Water in Proteins Have Distinct Properties in Radial Distributions Calculated from 105 Atomic Resolution Crystal Structures”. In: *The Journal of Physical Chemistry B* 112.38 (Sept. 2008), pp. 12073–12080. DOI: [10.1021/jp802795a](https://doi.org/10.1021/jp802795a).
- [13] Y. I. Matveev, V. Y. Grinberg, and V. B. Tolstoguzov. “The plasticizing effect of water on proteins, polysaccharides and their mixtures. Glassy state of biopolymers, food and seeds”. en. In: *Food Hydrocolloids* 14.5 (Sept. 2000), pp. 425–437. DOI: [10.1016/S0268-005X\(00\)00020-5](https://doi.org/10.1016/S0268-005X(00)00020-5).
- [14] J. Ahmed, Y. H. Roos, and S. Rahman, eds. *Glass transition and phase transitions in food and biological materials*. Chichester, West Sussex ; Hoboken, NJ: John Wiley & Sons Ltd, 2017.
- [15] L. Slade and H. Levine. “Glass Transitions and Water-Food Structure Interactions”. en. In: *Advances in Food and Nutrition Research*. Ed. by J. E. Kinsella and S. L. Taylor. Vol. 38. Academic Press, Jan. 1995, pp. 103–269. DOI: [10.1016/S1043-4526\(08\)60084-4](https://doi.org/10.1016/S1043-4526(08)60084-4).
- [16] S. Ikeda and K. Nishinari. “On solid-like rheological behaviors of globular protein solutions”. en. In: *Food Hydrocolloids*. 5th International Hydrocolloids Conference 15.4 (July 2001), pp. 401–406. DOI: [10.1016/S0268-005X\(01\)00052-2](https://doi.org/10.1016/S0268-005X(01)00052-2).
- [17] P. J. Shand, H. Ya, Z. Pietrasik, and P. K. J. P. D. Wanasundara. “Physicochemical and textural properties of heat-induced pea protein isolate gels”. en. In: *Food Chemistry* 102.4 (Jan. 2007), pp. 1119–1130. DOI: [10.1016/j.foodchem.2006.06.060](https://doi.org/10.1016/j.foodchem.2006.06.060).
- [18] M. Assad Bustillos, C. Jonchère, C. Garnier, A. L. Réguerre, and G. Della Valle. “Rheological and microstructural characterization of batters and sponge cakes fortified with pea proteins”. en. In: *Food Hydrocolloids* 101 (Apr. 2020), p. 105553. DOI: [10.1016/j.foodhyd.2019.105553](https://doi.org/10.1016/j.foodhyd.2019.105553).
- [19] L. Linares-García, R. Repo-Carrasco-Valencia, P. Glorio Paulet, and R. Schoenlechner. “Development of gluten-free and egg-free pasta based on quinoa (*Chenopodium quinoa* Willd) with addition of lupine flour, vegetable proteins and the oxidizing enzyme POx”. en. In: *European Food Research and Technology* 245.10 (Oct. 2019), pp. 2147–2156. DOI: [10.1007/s00217-019-03320-1](https://doi.org/10.1007/s00217-019-03320-1).
- [20] A. Bourgeois, J. Lebesgue, F. Mansy, and E. Bosly. “Method for extracting pea proteins”. en. US10390548B2. Aug. 2019.
- [21] T. G. Burger and Y. Zhang. “Recent progress in the utilization of pea protein as an emulsifier for food applications”. en. In: *Trends in Food Science & Technology* 86 (Apr. 2019), pp. 25–33. DOI: [10.1016/j.tifs.2019.02.007](https://doi.org/10.1016/j.tifs.2019.02.007).

- [22] H.-N. Liang and C.-H. Tang. “pH-dependent emulsifying properties of pea [*Pisum sativum* (L.)] proteins”. en. In: *Food Hydrocolloids* 33.2 (Dec. 2013), pp. 309–319. DOI: [10.1016/j.foodhyd.2013.04.005](https://doi.org/10.1016/j.foodhyd.2013.04.005).
- [23] W. Peng et al. “Effects of heat treatment on the emulsifying properties of pea proteins”. en. In: *Food Hydrocolloids* 52 (Jan. 2016), pp. 301–310. DOI: [10.1016/j.foodhyd.2015.06.025](https://doi.org/10.1016/j.foodhyd.2015.06.025).
- [24] C. Masiá, P. E. Jensen, I. L. Petersen, and P. Buldo. “Design of a Functional Pea Protein Matrix for Fermented Plant-Based Cheese”. en. In: *Foods* 11.2 (Jan. 2022). Number: 2 Publisher: Multidisciplinary Digital Publishing Institute, p. 178. DOI: [10.3390/foods11020178](https://doi.org/10.3390/foods11020178).
- [25] P. Havea, P. Watkinson, and B. Kuhn-Sherlock. “Heat-Induced Whey Protein Gels: Protein-Protein Interactions and Functional Properties”. In: *Journal of Agricultural and Food Chemistry* 57.4 (Feb. 2009). Publisher: American Chemical Society, pp. 1506–1512. DOI: [10.1021/jf802559z](https://doi.org/10.1021/jf802559z).
- [26] K. S. Liu and F.-H. Hsieh. “Protein–Protein Interactions in High Moisture-Extruded Meat Analogs and Heat-Induced Soy Protein Gels”. en. In: *Journal of the American Oil Chemists’ Society* 84.8 (Aug. 2007), pp. 741–748. DOI: [10.1007/s11746-007-1095-8](https://doi.org/10.1007/s11746-007-1095-8).
- [27] C.-H. Tang. “Thermal denaturation and gelation of vicilin-rich protein isolates from three *Phaseolus* legumes: A comparative study”. en. In: *LWT - Food Science and Technology* 41.8 (Nov. 2008), pp. 1380–1388. DOI: [10.1016/j.lwt.2007.08.025](https://doi.org/10.1016/j.lwt.2007.08.025).
- [28] D. J. McClements and L. Grossmann. “The Rise of Plant-Based Foods”. en. In: *Next-Generation Plant-based Foods: Design, Production, and Properties*. Ed. by D. J. McClements and L. Grossmann. Cham: Springer International Publishing, 2022, pp. 1–21. DOI: [10.1007/978-3-030-96764-2_1](https://doi.org/10.1007/978-3-030-96764-2_1).
- [29] Good Food Institute. *Executive summary — 2021 State of the Industry Report: Plant-based meat, seafood, eggs, and dairy*. 2022.
- [30] D. J. McClements and L. Grossmann. “Nutritional and Health Aspects”. en. In: *Next-Generation Plant-based Foods: Design, Production, and Properties*. Ed. by D. J. McClements and L. Grossmann. Cham: Springer International Publishing, 2022, pp. 227–284. DOI: [10.1007/978-3-030-96764-2_5](https://doi.org/10.1007/978-3-030-96764-2_5).
- [31] C. Lefranc-Millot and V. Teichman-Dubois. “Protein from Vegetable Sources: A Focus on Pea Protein”. fr. In: *Novel Proteins for Food, Pharmaceuticals and Agriculture*. John Wiley & Sons, Ltd, 2018, pp. 197–216.

- [32] D. J. McClements and L. Grossmann. “Properties and Functionality of Plant-Based Ingredients”. en. In: *Next-Generation Plant-based Foods: Design, Production, and Properties*. Ed. by D. J. McClements and L. Grossmann. Cham: Springer International Publishing, 2022, pp. 23–88. DOI: [10.1007/978-3-030-96764-2_2](https://doi.org/10.1007/978-3-030-96764-2_2).
- [33] S. Tabatabaei, B. Kuspangaliyeva, R. L. Legge, and A. R. Rajabzadeh. “Air Classification of Plant Proteins”. en. In: *Green Protein Processing Technologies from Plants: Novel Extraction and Purification Methods for Product Development*. Ed. by A. J. Hernández-Álvarez, M. Mondor, and M. G. Nosworthy. Cham: Springer International Publishing, 2023, pp. 31–59. DOI: [10.1007/978-3-031-16968-7_2](https://doi.org/10.1007/978-3-031-16968-7_2).
- [34] M. Mondor and A. J. Hernández-Álvarez. “Processing Technologies to Produce Plant Protein Concentrates and Isolates”. en. In: *Plant Protein Foods*. Ed. by A. Manickavasagan, L.-T. Lim, and A. Ali. Cham: Springer International Publishing, 2022, pp. 61–108. DOI: [10.1007/978-3-030-91206-2_3](https://doi.org/10.1007/978-3-030-91206-2_3).
- [35] J. Yang, S. Zhang, Y. Chu, and L. Chen. “Effects of Extraction Technologies on the Functionalities and Applications of Plant Proteins”. en. In: *Green Protein Processing Technologies from Plants: Novel Extraction and Purification Methods for Product Development*. Ed. by A. J. Hernández-Álvarez, M. Mondor, and M. G. Nosworthy. Cham: Springer International Publishing, 2023, pp. 307–346. DOI: [10.1007/978-3-031-16968-7_13](https://doi.org/10.1007/978-3-031-16968-7_13).
- [36] P. J. M. Pelgrom, J. Wang, R. M. Boom, and M. A. I. Schutyser. “Pre- and post-treatment enhance the protein enrichment from milling and air classification of legumes”. en. In: *Journal of Food Engineering* 155 (June 2015), pp. 53–61. DOI: [10.1016/j.jfoodeng.2015.01.005](https://doi.org/10.1016/j.jfoodeng.2015.01.005).
- [37] Z. X. Lu, J. F. He, Y. C. Zhang, and D. J. Bing. “Composition, physicochemical properties of pea protein and its application in functional foods”. In: *Critical Reviews in Food Science and Nutrition* 60.15 (Aug. 2020), pp. 2593–2605. DOI: [10.1080/10408398.2019.1651248](https://doi.org/10.1080/10408398.2019.1651248).
- [38] S. Sharan et al. “Fava bean (*Vicia faba* L.) for food applications: From seed to ingredient processing and its effect on functional properties, antinutritional factors, flavor, and color”. en. In: *Comprehensive Reviews in Food Science and Food Safety* 20.1 (2021). eprint: <https://ift.onlinelibrary.wiley.com/doi/pdf/10.1111/1541-4337.12687>, pp. 401–428. DOI: [10.1111/1541-4337.12687](https://doi.org/10.1111/1541-4337.12687).
- [39] G. Höhne, W. Hemminger, H.-J. Flammersheim, W. F. Hemminger, and H.-J. Flammersheim. *Differential Scanning Calorimetry*. eng. 2., nd rev. a. enlarged ed. Softcover version of original hardcover edition 2003. Berlin: Springer Berlin, 2010.

- [40] Dr. Ekkehard Füglein and Dr. Stefan Schmölder. *TGA Measurements on Calcium Oxalate Monohydrate*. URL: <https://analyzing-testing.netzsch.com/en/media/application-literature>.
- [41] National Institute of Standards and Technology (NIST). *Chemical Formula Search*. <https://webbook.nist.gov/chemistry/form-ser/>.
- [42] L. Kumar, M. Brennan, C. Brennan, and H. Zheng. “Influence of whey protein isolate on pasting, thermal, and structural characteristics of oat starch”. en. In: *Journal of Dairy Science* 105.1 (Jan. 2022), pp. 56–71. DOI: [10.3168/jds.2021-20711](https://doi.org/10.3168/jds.2021-20711).
- [43] N. W. H. Cheetham and L. Tao. “Variation in crystalline type with amylose content in maize starch granules: an X-ray powder diffraction study”. en. In: *Carbohydrate Polymers* 36.4 (Aug. 1998), pp. 277–284. DOI: [10.1016/S0144-8617\(98\)00007-1](https://doi.org/10.1016/S0144-8617(98)00007-1).
- [44] N. Sozer, H. Dogan, and J. L. Kokini. “Textural Properties and Their Correlation to Cell Structure in Porous Food Materials”. In: *Journal of Agricultural and Food Chemistry* 59.5 (Mar. 2011). Publisher: American Chemical Society, pp. 1498–1507. DOI: [10.1021/jf103766x](https://doi.org/10.1021/jf103766x).
- [45] K. Frost, D. Kaminski, G. Kirwan, E. Lascaris, and R. Shanks. “Crystallinity and structure of starch using wide angle X-ray scattering”. en. In: *Carbohydrate Polymers* 78.3 (Oct. 2009), pp. 543–548. DOI: [10.1016/j.carbpol.2009.05.018](https://doi.org/10.1016/j.carbpol.2009.05.018).
- [46] A. G. Barroso, R. H. Garcia, and N. L. Del Mastro. “X-ray diffraction pattern and relative crystallinity of irradiated arrowroot starch”. In: *Brazilian Journal of Radiation Sciences* 7.2A (Feb. 2019). DOI: [10.15392/bjrs.v7i2A.645](https://doi.org/10.15392/bjrs.v7i2A.645).
- [47] M. Jeżewski. “Application of Raman spectroscopy to study the high pressure effect on the secondary structure of bean (*Phaseolus vulgaris*) and pea (*Pisum sativum*) proteins”. In: *Polish Journal of Food and Nutrition Sciences* 48.2 (June 1998). Publisher: Institute of Animal Reproduction and Food Research of Polish Academy Sciences, pp. 275–284.
- [48] B. Hernández, F. Pflüger, S. G. Kruglik, and M. Ghomi. “Characteristic Raman lines of phenylalanine analyzed by a multiconformational approach”. en. In: *Journal of Raman Spectroscopy* 44.6 (2013), pp. 827–833. DOI: [10.1002/jrs.4290](https://doi.org/10.1002/jrs.4290).
- [49] H. Zhao, C. Shen, Z. Wu, Z. Zhang, and C. Xu. “Comparison of wheat, soybean, rice, and pea protein properties for effective applications in food products”. en. In: *Journal of Food Biochemistry* 44.4 (2020), e13157. DOI: [10.1111/jfbc.13157](https://doi.org/10.1111/jfbc.13157).
- [50] N. Kuhar, S. Sil, and S. Umapathy. “Potential of Raman spectroscopic techniques to study proteins”. en. In: *Spectrochimica Acta Part A: Molecular and Biomolecular Spectroscopy* 258 (Sept. 2021), p. 119712. DOI: [10.1016/j.saa.2021.119712](https://doi.org/10.1016/j.saa.2021.119712).

- [51] N. O. o. D. a. Informatics. *NIST Chemistry WebBook*. en. Publisher: National Institute of Standards and Technology. DOI: [10.18434/T4D303](https://doi.org/10.18434/T4D303).
- [52] I. M. Weiss, C. Muth, R. Drumm, and H. O. K. Kirchner. “Thermal decomposition of the amino acids glycine, cysteine, aspartic acid, asparagine, glutamic acid, glutamine, arginine and histidine”. In: *BMC Biophysics* 11.1 (Feb. 2018), p. 2. DOI: [10.1186/s13628-018-0042-4](https://doi.org/10.1186/s13628-018-0042-4).
- [53] J. Chen et al. “Determination of the domain structure of the 7S and 11S globulins from soy proteins by XRD and FTIR”. en. In: *Journal of the Science of Food and Agriculture* 93.7 (2013), pp. 1687–1691. DOI: [10.1002/jsfa.5950](https://doi.org/10.1002/jsfa.5950).
- [54] Z. He et al. “Surface Characterization of Cottonseed Meal Products by SEM, SEM-EDS, XRD and XPS Analysis”. en. In: *Journal of Materials Science Research* 7.1 (Dec. 2017). Number: 1, p28. DOI: [10.5539/jmsr.v7n1p28](https://doi.org/10.5539/jmsr.v7n1p28).
- [55] M. Xu and M.-J. Dumont. “Evaluation of the stability of pea and canola protein-based hydrogels in simulated gastrointestinal fluids”. en. In: *Journal of Food Engineering* 165 (Nov. 2015), pp. 52–59. DOI: [10.1016/j.jfoodeng.2015.04.033](https://doi.org/10.1016/j.jfoodeng.2015.04.033).
- [56] P. Gabbott, ed. *Principles and applications of thermal analysis*. OCLC: ocn156994442. Oxford ; Ames, Iowa: Blackwell Pub, 2008.
- [57] R. Kornet et al. “Coacervation in pea protein solutions: The effect of pH, salt, and fractionation processing steps”. en. In: *Food Hydrocolloids* 125 (Apr. 2022), p. 107379. DOI: [10.1016/j.foodhyd.2021.107379](https://doi.org/10.1016/j.foodhyd.2021.107379).
- [58] P. L. M. Barreto, A. T. N. Pires, and V. Soldi. “Thermal degradation of edible films based on milk proteins and gelatin in inert atmosphere”. en. In: *Polymer Degradation and Stability* 79.1 (Jan. 2003), pp. 147–152. DOI: [10.1016/S0141-3910\(02\)00267-7](https://doi.org/10.1016/S0141-3910(02)00267-7).
- [59] V. Schmidt, C. Giacomelli, and V. Soldi. “Thermal stability of films formed by soy protein isolate–sodium dodecyl sulfate”. en. In: *Polymer Degradation and Stability* 87.1 (Jan. 2005), pp. 25–31. DOI: [10.1016/j.polymdegradstab.2004.07.003](https://doi.org/10.1016/j.polymdegradstab.2004.07.003).
- [60] Y. Lan, M. Xu, J.-B. Ohm, B. Chen, and J. Rao. “Solid dispersion-based spray-drying improves solubility and mitigates beany flavour of pea protein isolate”. en. In: *Food Chemistry* 278 (Apr. 2019), pp. 665–673. DOI: [10.1016/j.foodchem.2018.11.074](https://doi.org/10.1016/j.foodchem.2018.11.074).
- [61] P. Zhou and T. P. Labuza. “Effect of Water Content on Glass Transition and Protein Aggregation of Whey Protein Powders During Short-Term Storage”. en. In: *Food Biophysics* 2.2 (Sept. 2007), pp. 108–116. DOI: [10.1007/s11483-007-9037-4](https://doi.org/10.1007/s11483-007-9037-4).

- [62] L. N. Bell, M. J. Hageman, and J. M. Bauer. “Impact of moisture on thermally induced denaturation and decomposition of lyophilized bovine somatotropin”. en. In: *Biopolymers* 35.2 (1995), pp. 201–209. DOI: [10.1002/bip.360350208](https://doi.org/10.1002/bip.360350208).
- [63] Z. K. Zhong and X. S. Sun. “Thermal Behavior and Nonfreezing Water of Soybean Protein Components”. en. In: *Cereal Chemistry* 77.4 (2000), pp. 495–500. DOI: [10.1094/CCHEM.2000.77.4.495](https://doi.org/10.1094/CCHEM.2000.77.4.495).
- [64] A. A. Schneider, F. Bu, and B. P. Ismail. “Enhancement of pea protein solubility and thermal stability for acidic beverage applications via endogenous Maillard-induced glycation and chromatography purification”. en. In: *Current Research in Food Science* 6 (Jan. 2023), p. 100452. DOI: [10.1016/j.crfs.2023.100452](https://doi.org/10.1016/j.crfs.2023.100452).
- [65] N. Kitabatake, M. Tahara, and E. Doi. “Thermal Denaturation of Soybean Protein at Low Water Contents”. In: *Agricultural and Biological Chemistry* 54.9 (Sept. 1990), pp. 2205–2212. DOI: [10.1080/00021369.1990.10870318](https://doi.org/10.1080/00021369.1990.10870318).
- [66] S. Wang and L. Copeland. “Phase Transitions of Pea Starch over a Wide Range of Water Content”. In: *Journal of Agricultural and Food Chemistry* 60.25 (June 2012). Publisher: American Chemical Society, pp. 6439–6446. DOI: [10.1021/jf3011992](https://doi.org/10.1021/jf3011992).
- [67] F. A. Villanova and A. H.-M. Lin. “Modification of Pea Starch Digestibility through the Complexation with Gallic Acid via High-Pressure Homogenization”. In: *Polymers* 14.13 (June 2022), p. 2623. DOI: [10.3390/polym14132623](https://doi.org/10.3390/polym14132623).
- [68] S. Li, Y. Wei, Y. Fang, W. Zhang, and B. Zhang. “DSC study on the thermal properties of soybean protein isolates/corn starch mixture”. en. In: *Journal of Thermal Analysis and Calorimetry* 115.2 (Feb. 2014), pp. 1633–1638. DOI: [10.1007/s10973-013-3433-4](https://doi.org/10.1007/s10973-013-3433-4).
- [69] AG Scientific. *Dithiothreitol (DTT) Applications You Must Know*. <https://agscientific.com/blog/dithiothreitol-dtt-applications.html>.
- [70] N. Nagano, M. Ota, and K. Nishikawa. “Strong hydrophobic nature of cysteine residues in proteins”. en. In: *FEBS Letters* 458.1 (1999), pp. 69–71. DOI: [10.1016/S0014-5793\(99\)01122-9](https://doi.org/10.1016/S0014-5793(99)01122-9).
- [71] interchim. *DTT (DithioThreitol)*. <https://www.interchim.fr/ft/0/054721.pdf>.
- [72] X. Wei et al. “Comparative investigation between co-pyrolysis characteristics of protein and carbohydrate by TG-FTIR and Py-GC/MS”. en. In: *Journal of Analytical and Applied Pyrolysis* 135 (Oct. 2018), pp. 209–218. DOI: [10.1016/j.jaap.2018.08.031](https://doi.org/10.1016/j.jaap.2018.08.031).

- [73] N. S. Masite, S. Ncube, L. M. Madikizela, F. M. Mtunzi, and V. E. Pakade. “Trace Metals, Crude Protein, and TGA-FTIR Analysis of Evolved Gas Products in the Thermal Decomposition of Roasted *Mopane* Worms, Sweet Corn, and Peanuts”. en. In: *International Journal of Food Science* 2022 (Oct. 2022). Publisher: Hindawi, e1509569. DOI: [10.1155/2022/1509569](https://doi.org/10.1155/2022/1509569).
- [74] Z. Ma, D. Chen, J. Gu, B. Bao, and Q. Zhang. “Determination of pyrolysis characteristics and kinetics of palm kernel shell using TGA-FTIR and model-free integral methods”. en. In: *Energy Conversion and Management* 89 (Jan. 2015), pp. 251–259. DOI: [10.1016/j.enconman.2014.09.074](https://doi.org/10.1016/j.enconman.2014.09.074).
- [75] *Infrared Spectroscopy Absorption Table*. <https://chem.libretexts.org/@go/page/22645>. Nov. 2020.
- [76] *Sigma-Aldrich*. en. <https://www.sigmaaldrich.com/DK/en>.
- [77] M. C. Alliegro. “Effects of dithiothreitol on protein activity unrelated to thiol-disulfide exchange: for consideration in the analysis of protein function with Cleland’s reagent”. eng. In: *Analytical Biochemistry* 282.1 (June 2000), pp. 102–106. DOI: [10.1006/abio.2000.4557](https://doi.org/10.1006/abio.2000.4557).
- [78] A. Ciurzyńska and A. Lenart. “Freeze-Drying - Application in Food Processing and Biotechnology - a Review”. In: *Polish Journal of Food and Nutrition Sciences* 61.3 (Sept. 2011). Publisher: Institute of Animal Reproduction and Food Research of Polish Academy Sciences, pp. 165–171. DOI: [10.2478/v10222-011-0017-5](https://doi.org/10.2478/v10222-011-0017-5).

Appendix A

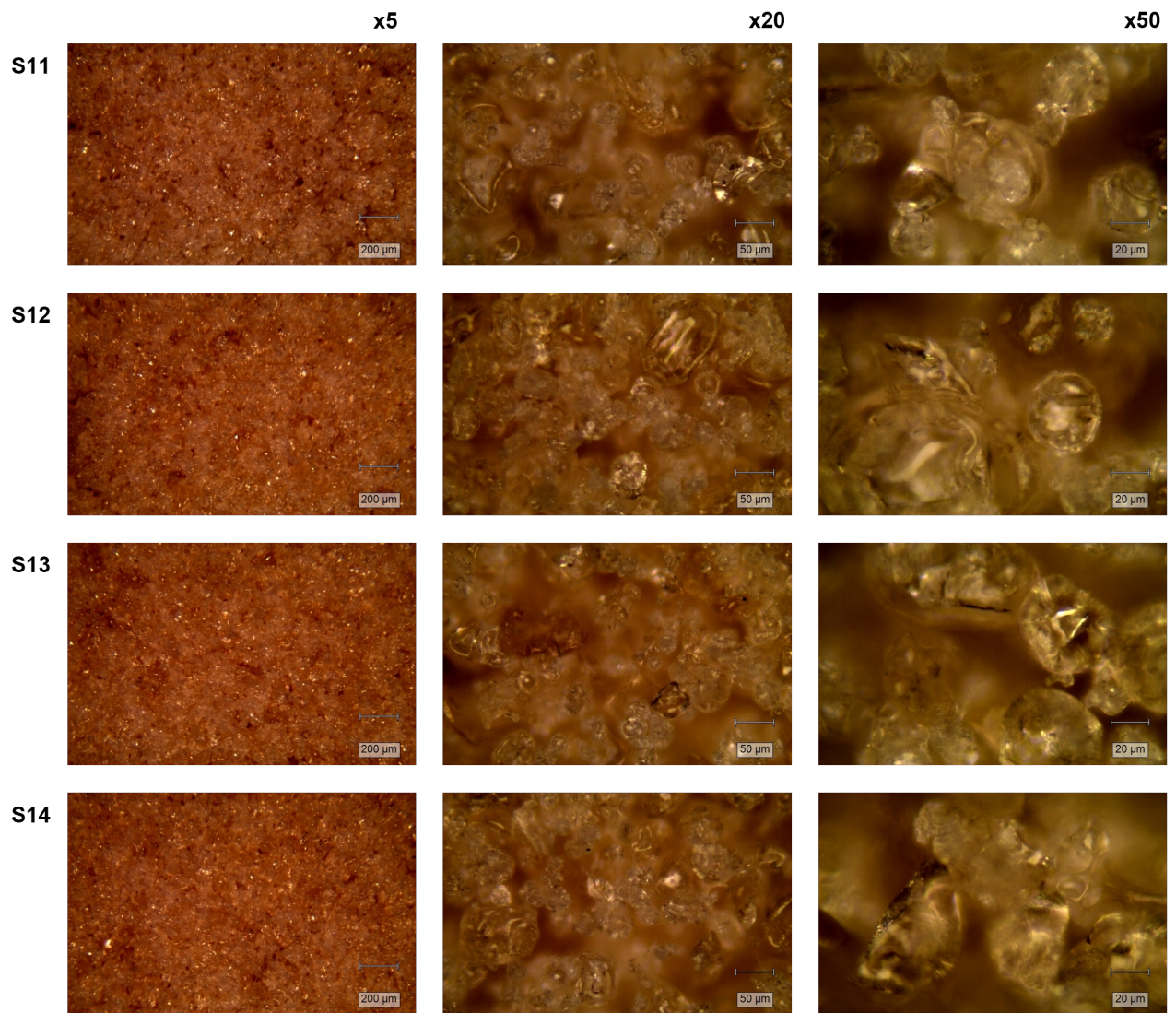


Figure A1: Optical microscopy of samples S11-S14 which are duplicates of S1. Images are shown at 5, 20 and 50 times magnification. Scale bars are shown on the individual images.

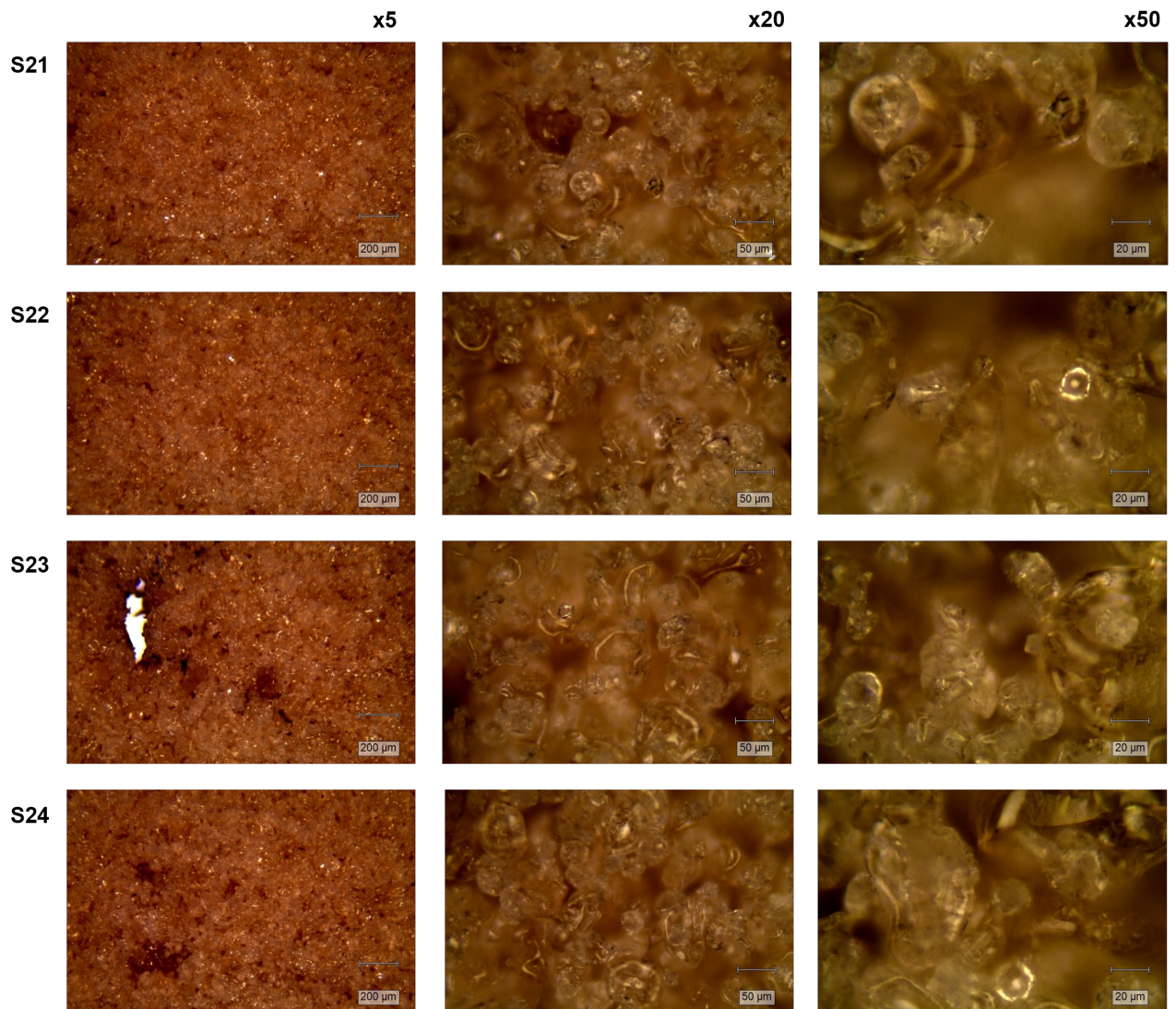


Figure A2: Optical microscopy of samples S21-S24 which are duplicates of S2. Images are shown at 5, 20 and 50 times magnification. Scale bars are shown on the individual images.

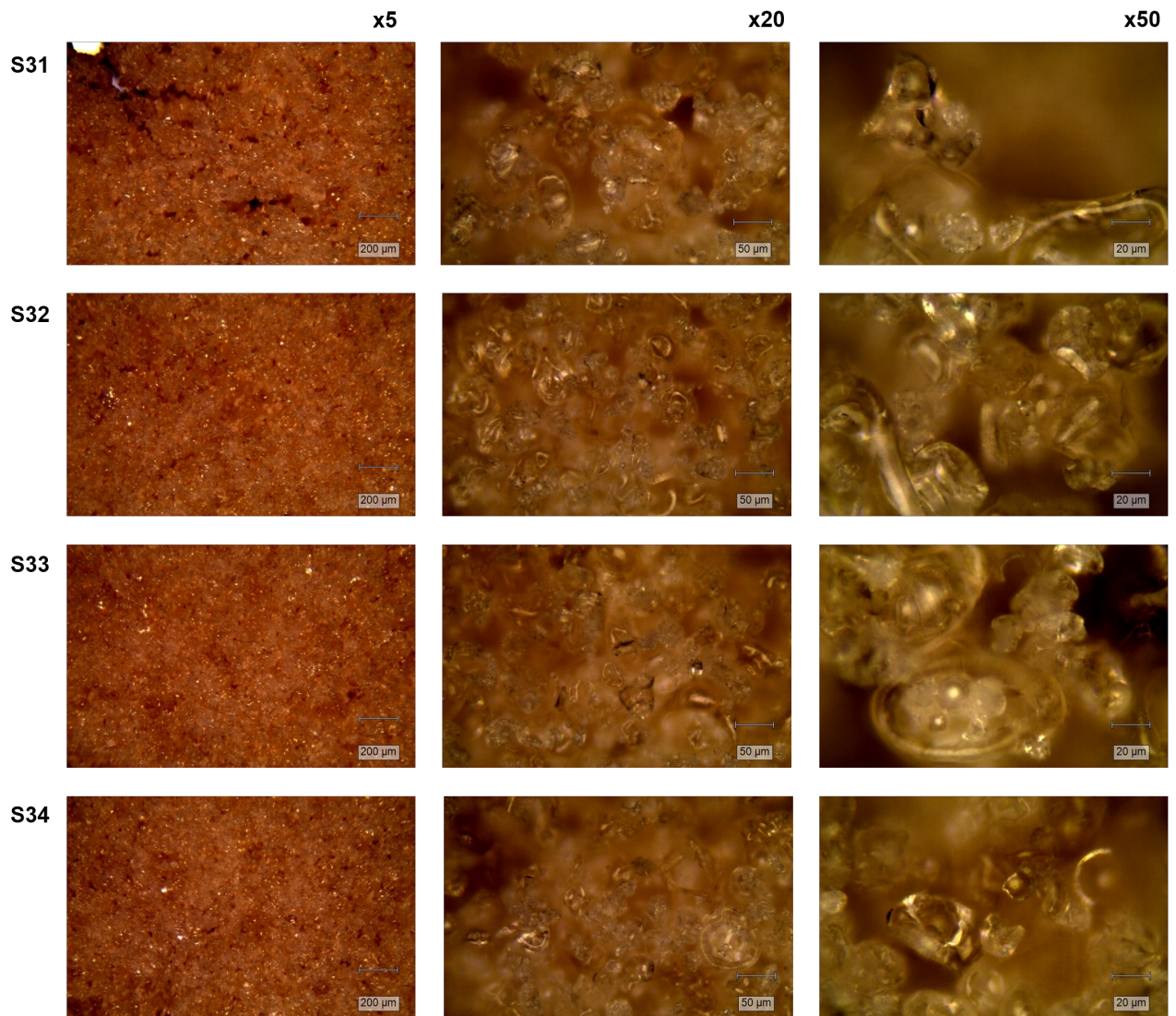


Figure A3: Optical microscopy of samples S31-S34 which are duplicates of S3. Images are shown at 5, 20 and 50 times magnification. Scale bars are shown on the individual images.

Appendix B

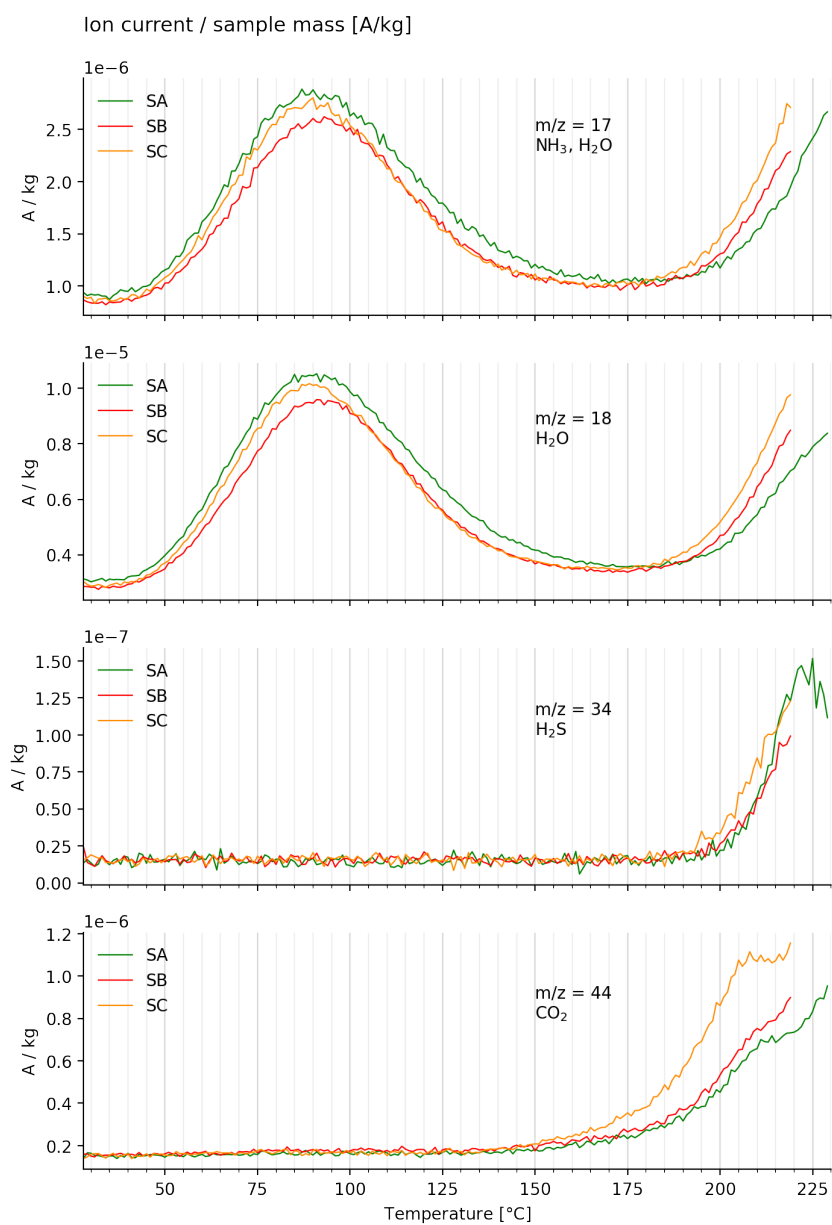


Figure A4: Selected MS signals from samples SA-SC divided by the mass of the individual samples. The plotted m/z value as well as the relevant species are shown on each plot. Heating rate is 10 K/min and measurements were taken in a nitrogen atmosphere. Sample masses can be found in Table 4.

Appendix C

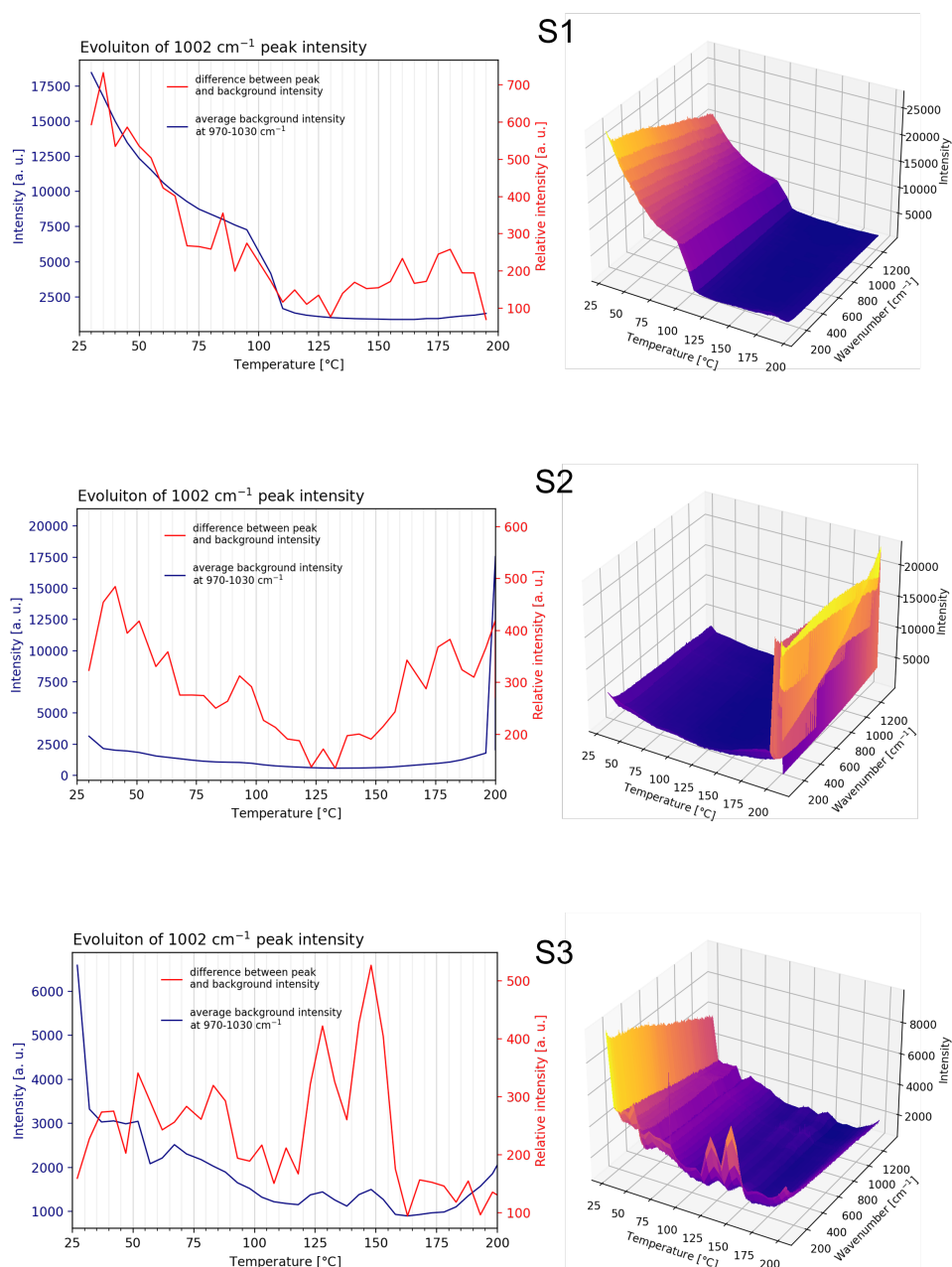


Figure A5: Raman data of samples S1-S3. The left plots show the intensity of the peak at 1002 cm^{-1} with the background intensity around the peak subtracted, compared to the intensity of this background. For sample S1, the peak intensity seems to follow the background intensity, but otherwise no clear trends are observed. The right 3D plots display the full datasets.

Appendix D

Control

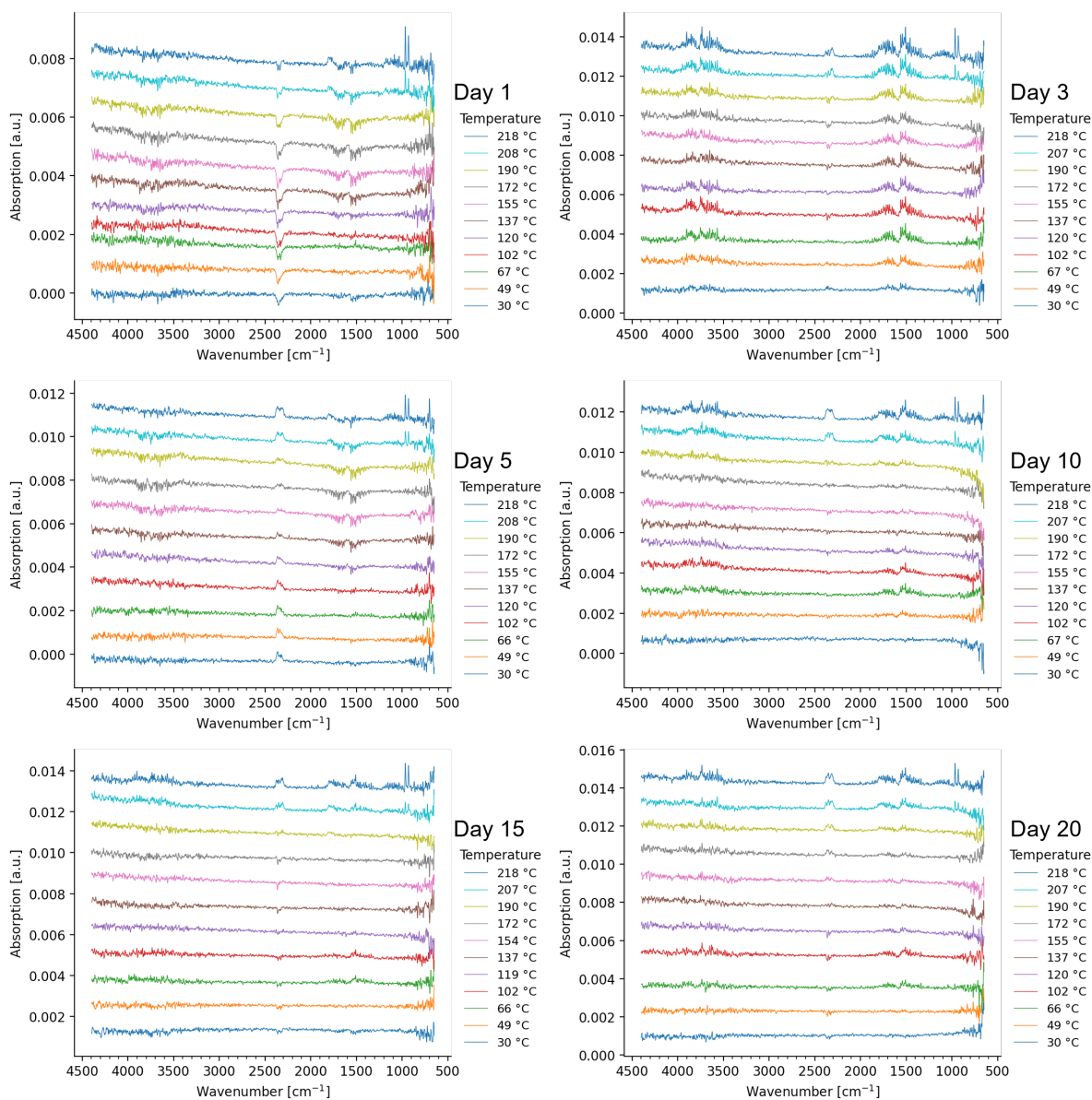


Figure A6: FTIR of sample Control on all days.

DTT2

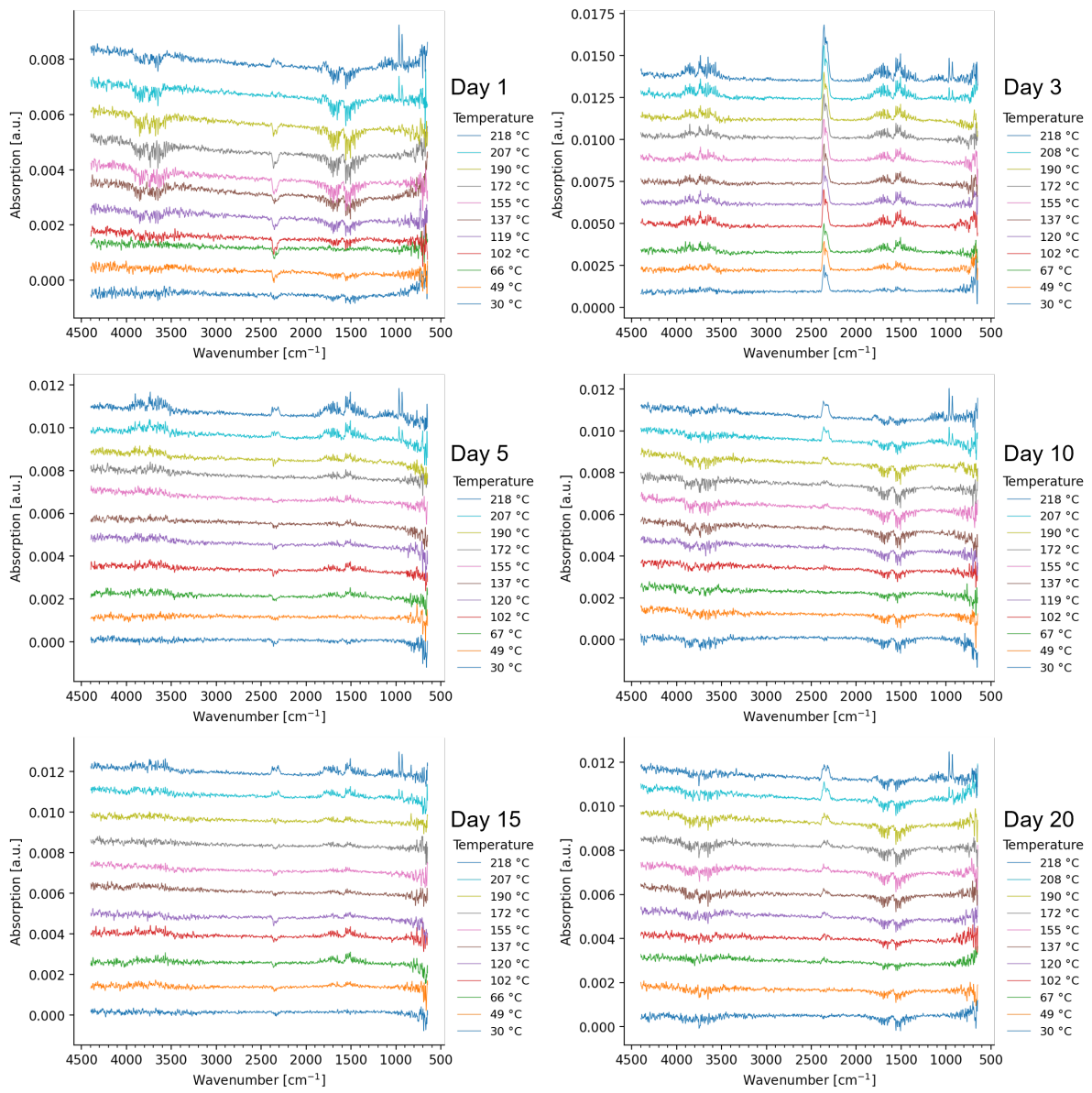


Figure A7: FTIR of sample DTT2 on all days.

DTT20

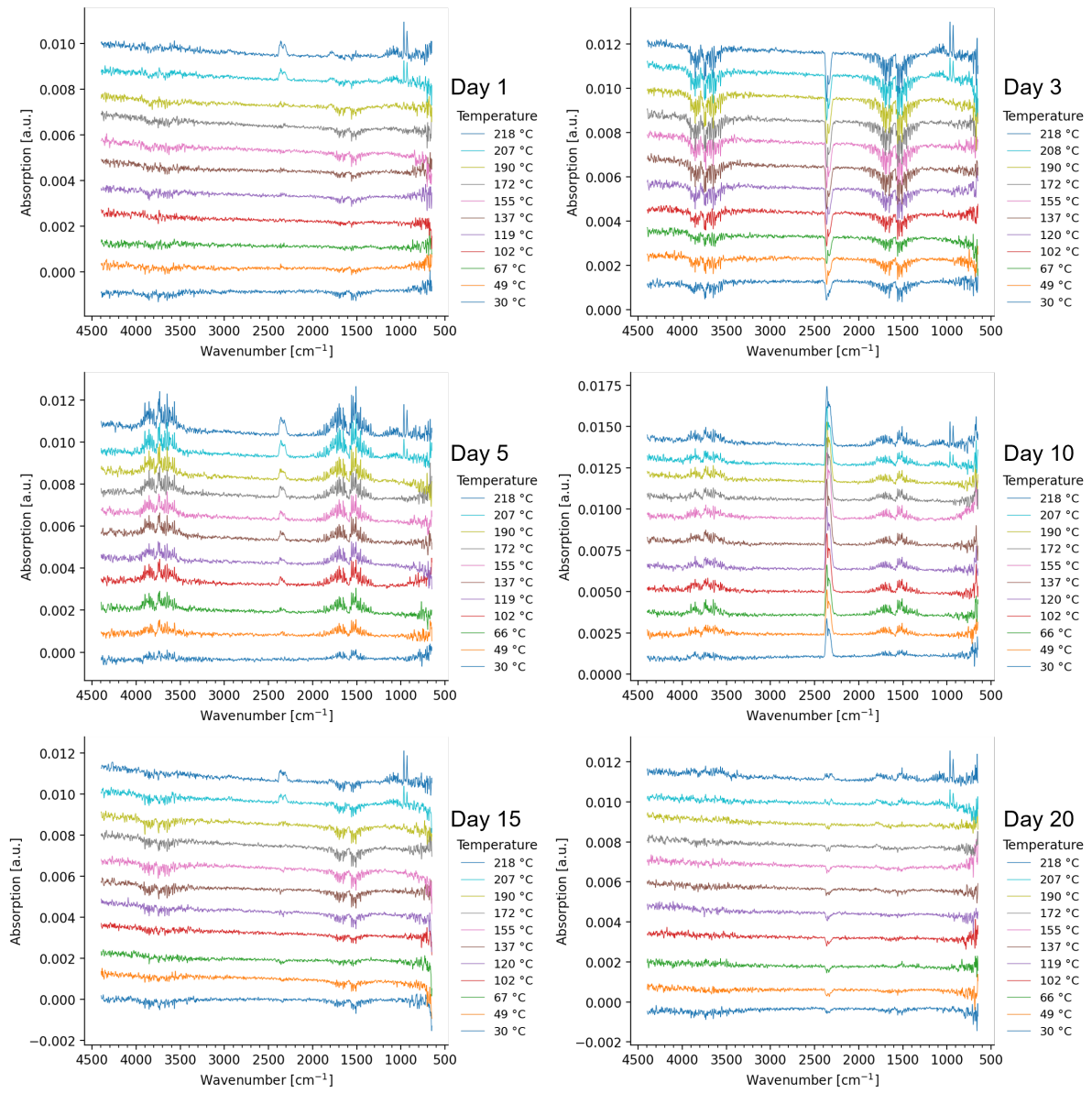


Figure A8: FTIR of sample DTT20 on all days.

DTT195

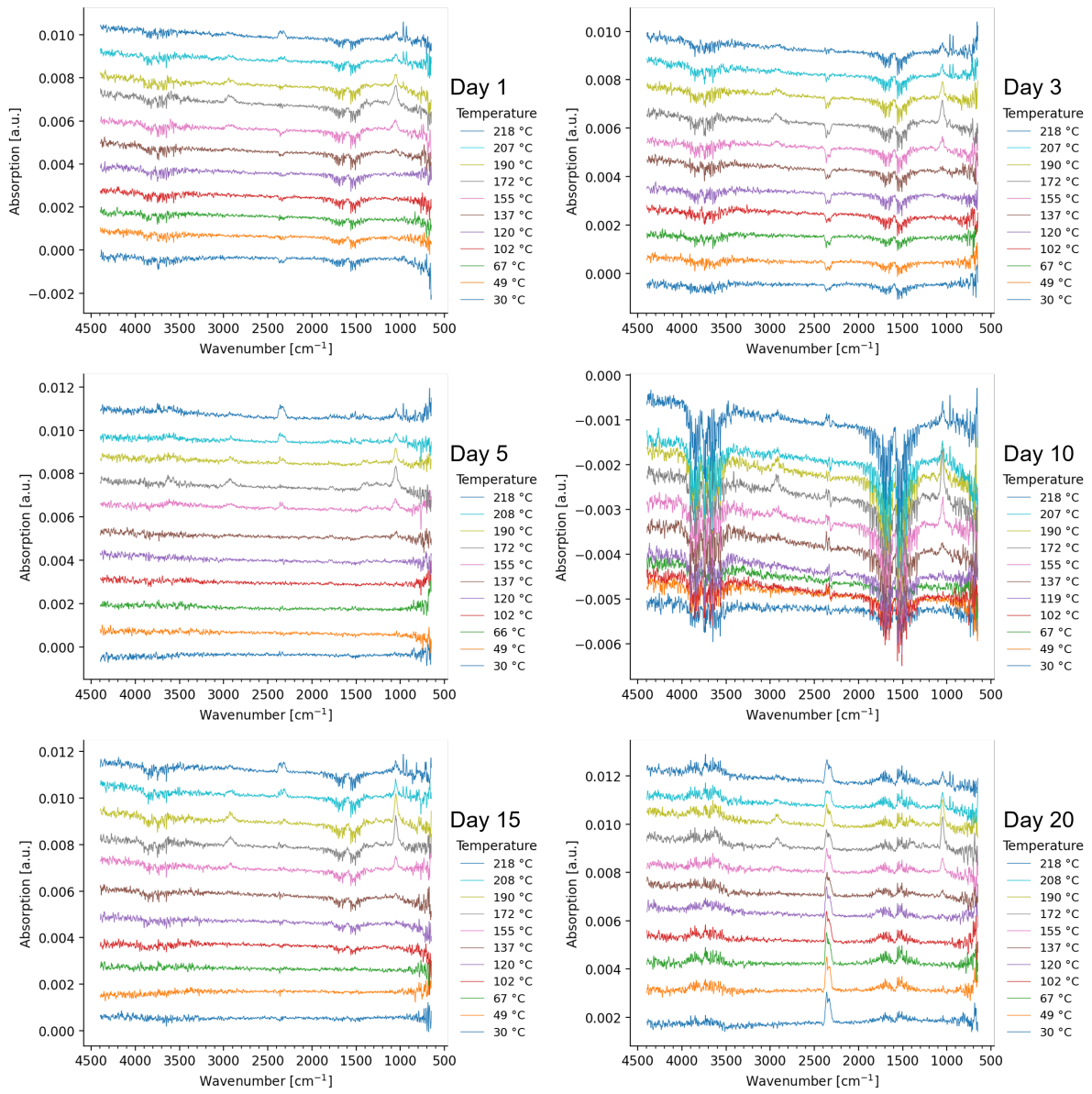


Figure A9: FTIR of sample DTT195 on all days.

Appendix E

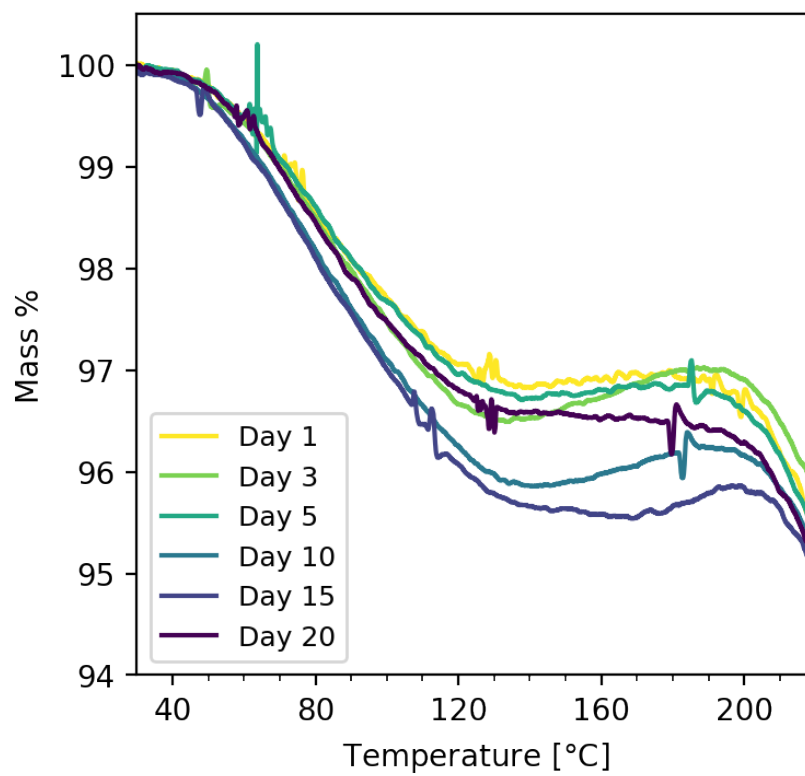


Figure A10: TGA curves of sample Control on all days.

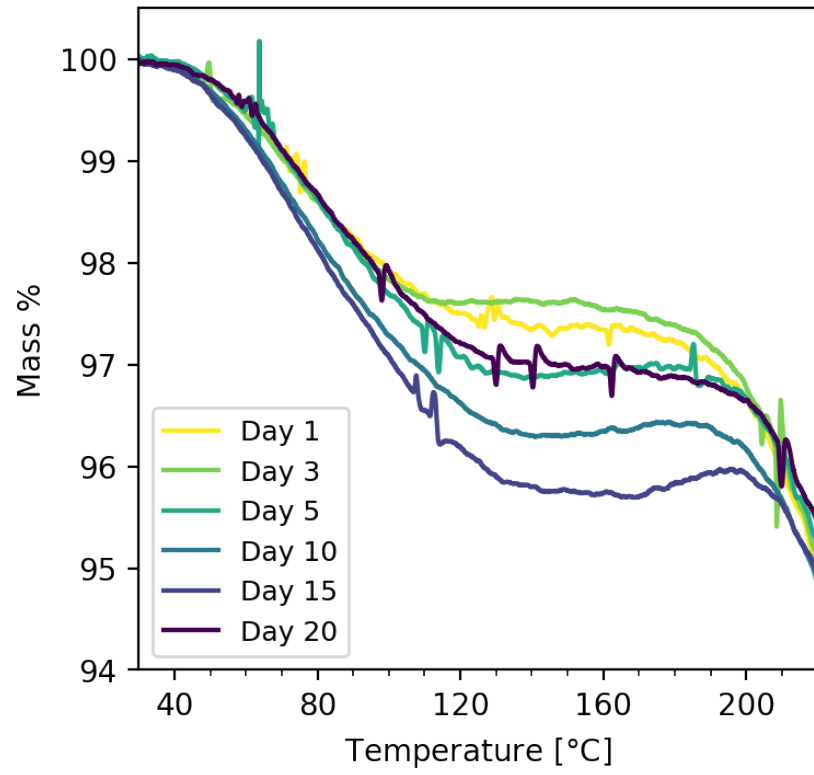


Figure A11: TGA curves of sample DTT2 on all days.

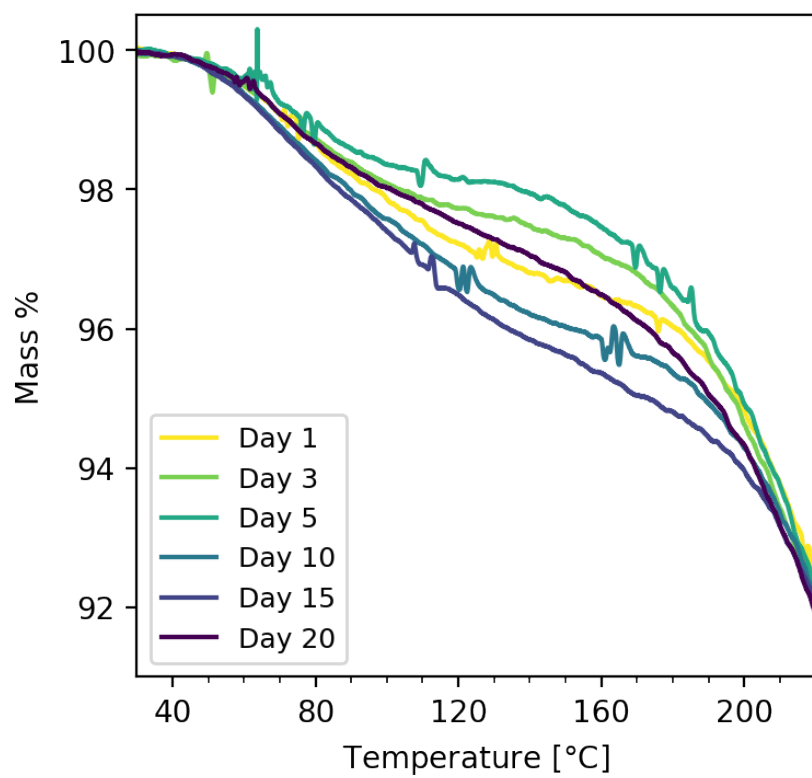


Figure A12: TGA curves of sample DTT20 on all days.

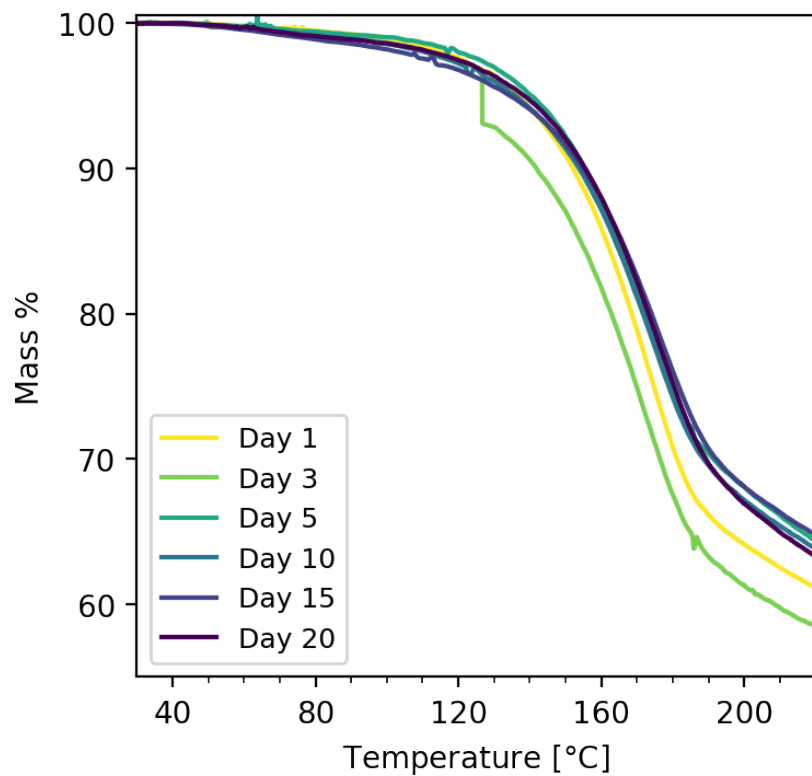


Figure A13: TGA curves of sample DTT195 on all days. The sudden mass loss observed on Day 3 at around 120 °C is likely due to a small grain of the sample jumping out of the crucible.

Appendix F

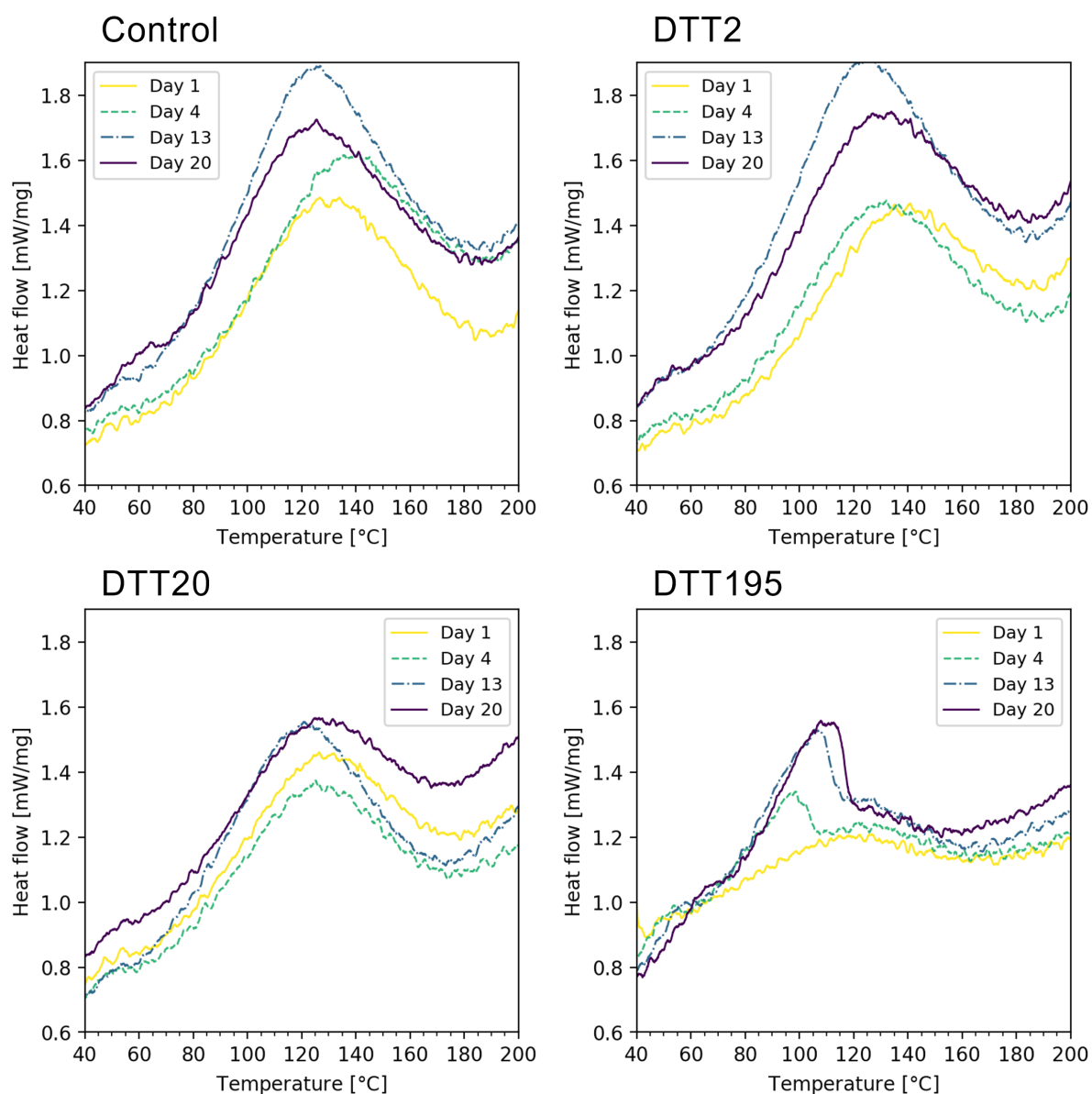


Figure A14: DSC thermograms of all treated samples on all measured days. Note that the measurement of DTT195 on day 1 should not be analyzed, as the crucible was not properly hermetically sealed. Samples were measured in the temperature range 30-200 °C at 10 K/min with a gas flow of 40 ml/min protective and 60 ml/min purge N₂. Endotherm processes at positive heat flow values. Sample masses can be found in Table 5

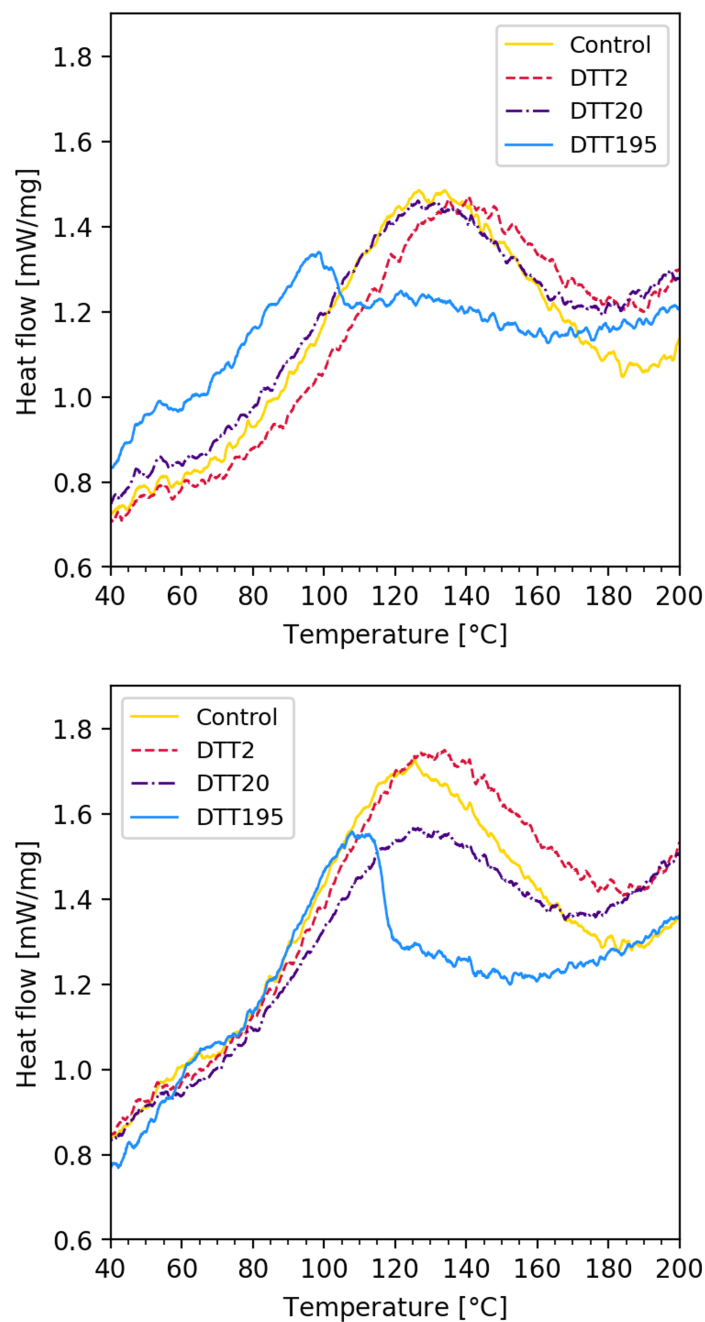


Figure A15: Direct comparison of first and last DSC thermograms from all four treated samples. Top: measurements from day 1 (Control, DTT2, DTT20) and day 4 (DTT195). Bottom: measurements from day 20 of all four samples. The measurement of DTT195 on day 1 was not used, as the crucible was not properly hermetically sealed. All samples were measured in the temperature range 30-200 °C at 10 K/min with a gas flow of 40 ml/min protective and 60 ml/min purge N₂. Endotherm processes at positive heat flow values. Sample masses can be found in Table 5

Appendix G

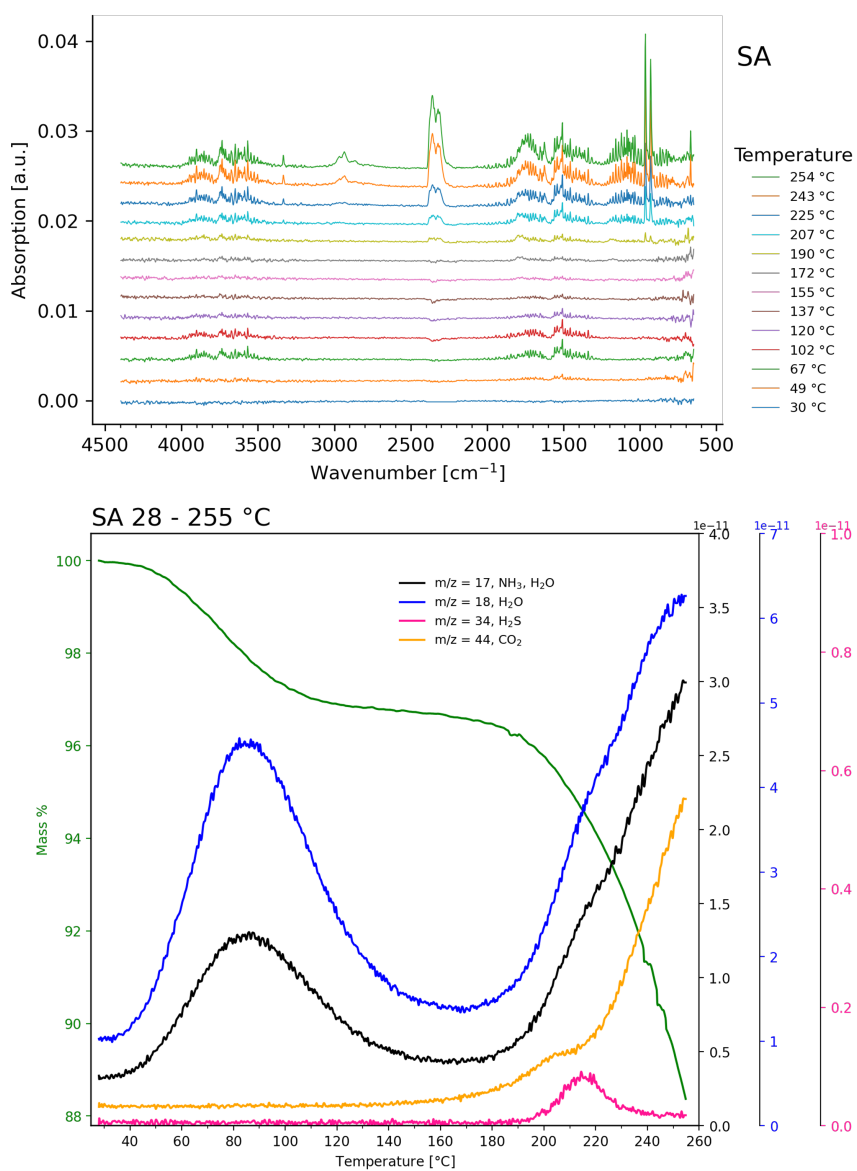


Figure A16: TGA-FTIR-MS data for SA at a greater temperature range (28-255 °C). Heating rate is 10 K/min, and a gas flow of 20 ml/min protective N₂ and 20 ml/min purge N₂ was used. Samples mass can be found in Table 4.